A Wind Profiler Assisted Case Study of a Nonprecipitating Warm Front

by
Steven M. London
Thomas B. McKee

Department of Atmospheric Science
Colorado State University
Fort Collins, Colorado

Colorado State University

Department of Atmospheric Science

Paper No. 526

A WIND PROFILER ASSISTED CASE STUDY OF A NONPRECIPITATING WARM FRONT

Steven M. London

Thomas B. McKee

Atmospheric Science Department
Colorado State University
Fort Collins, CO 80523

April 1993

Atmospheric Science Paper #526

A WIND PROFILER ASSISTED CASE STUDY OF A NONPRECIPITATING WARM FRONT

ABSTRACT

Wind profiler data collected during FIRE-II, in November, 1991, provided an opportunity for detailed observation of the passage of a warm front over Parsons, KS. Surface data, rawindsonde data and satellite observations were used to collaborate and understand the phenomena detected by the wind profiler. A quality-controlled set of wind profiler data were produced from the time-averaged spectra and the spectral moments derived from the time-averaged spectra. Using the wind profiler data set, the warm frontal zone was clearly identifiable as a low level, descending layer of veering winds over Parsons, KS. The warm frontal zone exhibited a relatively smooth surface, without the apparent height discontinuities observed by other researchers. Above the layer of warm advection, there was an abrupt transition to a layer of cold advection. The temperature gradient across this transition zone resulted in a layer of decreased stability. A study of the origin of the warm and cold advective zones found that the warm advection originated west-southwest of Parsons, in a region of warmer, but dry air, while the cold advection was from geostrophic flow around a strong cyclone far to the northeast of Parsons. The interaction between the northwesterly geostrophic flow and the southwesterly advective flow resulted in horizontal deformation, leading to frontogenesis.

ACKNOWLEDGEMENTS

The authors would like to thank Professor Stephen Cox and Professor Jon Peterka for their advice and suggestions. They would also like to thank Paul Hein, Research Associate, CSU Department of Atmospheric Science, who provided invaluable assistance in obtaining the wind profiler, surface and rawindsonde data from the FIRE-II field experiment supported by NASA Grant NAG-1-1146. Paul provided some of the software used in this study and spent a great deal of time patiently answering many questions about wind profilers. Professor Roger Pielke provided suggestions for studying warm fronts. Steve Finley, CSU Department of Atmospheric Science, helped use GEMPAK to analyze rawindsonde data and produce many of the figures in this paper.

Steve London would like to acknowledge that his graduate tuition was paid by AT&T Bell Laboratories, under the Special Enhanced Leave of Absence program. And special thanks goes to his wife, Kathy, who provided the continual support and encouragement to begin and persevere through this Master's program, despite the drastic change in our lifestyle.

TABLE OF CONTENTS

LIST OF FIGURES

1 INTRODUCTION

The overrunning of warm air over cold air prior to the passage of a surface warm front can result in large amounts of precipitation. Orographic enhancement of the precipitation can cause significant flooding, despite the innocuous appearance of the warm front on the synoptic scale (Hobbs, Locatelli 1987). Considering the potential economic impact of warm front-associated weather, there has been a surprising lack of observational studies of warm fronts. Compared to cold fronts, warm fronts are generally not as well defined and can be difficult to locate. In the past, this has led some meteorologists to doubt their existence.

The First ISCCP Regional Experiment - II (FIRE-II) provided an opportunity for the detailed observation of the passage of a warm front. From November 13, 1991 until December 7, 1992, the CSU wind profiler was in continuous operation and surface meteorological parameters were collected at Parsons, Kansas. In addition, rawindsondes were occasionally launched from Parsons during special study periods. Supplementing the standard NWS soundings at 0000 UTC and 1200 UTC, NWS rawindsondes were launched daily at 1800 UTC.

This thesis uses the data from FIRE-II to examine a warm front that passed through Parsons, Kansas on November 25, 1991. The CSU wind profiler was used as the primary instrument to study the front. Surface data and rawindsonde data were used to collaborate and understand the phenomena detected by the wind profiler. Section 2 provides a synoptic meteorological overview, incorporating upper air, surface and satellite observations. The processing and analysis of the wind profiler data, and study of the 25 November warm front are provided in Section 3. A comparison with other observational studies of warm fronts, and conclusions are presented in Section 4.

1.1 General Background

This section is subdivided into two sections. Section 1.1.1 describes the fundamental aspects of wind profiler operation. Commonly used procedures used to filter wind profiler data are presented. The computation of kinematic quantities from wind profiler data are described. Section 1.1.2 is a brief literature survey of warm fronts. Classical theories, numerical models, and previous observational studies are presented.

1.1.1 Wind Profilers

This section presents a brief overview of the principles and operation of wind profilers. For greater detail, the reader should consult other references (Van de Kamp 1988, Tycho 1988).

A wind profiler is a Doppler radar used to measure atmospheric winds above a site. Wind profilers depend upon the scattering of very high frequency (VHF) or ultra high frequency (UHF) electromagnetic radiation by minor irregularities in the index of refraction of air. These irregularities in the index of refraction are typically caused by turbulent eddies in the atmosphere. Since these turbulent eddies are carried by the wind, they are good "tracers" of the mean wind. The wind profiler transmits short pulses of electromagnetic radiation in a selected direction at a selected frequency. Echos are produced by the scattering of electromagnetic radiation. These echos are received from all heights within the range of operation of the profiler. The echos are sampled at selected times corresponding to distance and height from the profiler. The height associated with each sample is typically referred to as a "range gate" and corresponds to a volume of atmosphere illuminated by the electromagnetic radiation. By measuring the Doppler shift of the returned echo, the radial velocity of the turbulent eddies within the range gate can be deduced. Since there are turbulent eddies moving at various speeds

within the range gate (due to shear and turbulence), the echo is "spread out" in frequency. Several hundred samples are obtained and averaged to form a frequency spectra. The mean radial velocity is determined from the spectra by searching for a "spike" that contains the largest amount of power.

The radial velocity from a single wind profiler beam is clearly not sufficient to define the horizontal wind vector. In a typical wind profiler, three beams are used: one tilted to the east, one tilted to the north, and one vertical. The CSU wind profiler has two additional beams: one tilted to the south and one tilted to the west. The angle of the tilt is 75° from the horizon. For a three beam profiler, the wind vector is then calculated from

$$u = V_{east} \sec 75^{o} - w \tan 75^{o} \quad (1)$$

$$v = V_{north} \sec 75^{o} - w \tan 75^{o} \quad (2)$$

where V_{east} and V_{north} are the radial velocities determined from the east and north wind profiler beams. For the five-beam CSU wind profiler, equations (1) and (2) are also used, with appropriate modifications for the west and south beams.

A number of factors can affect the accuracy of wind profiler data and limit their applicability. These factors include:

- Radial wind velocities in excess of the Nyquist velocity (related to the pulse repetition frequency and number of samples used to derived the frequency spectra). For the CSU wind profiler, the Nyquist velocity is 28.9 m/s for when used in the low height mode, and 32.2 m/s when used in the high height mode.

- Nonuniform winds across the wind profiler beams, including nonuniformity caused by convection, lee waves and gravity waves. For example, the opposing beams of the CSU wind profiler, "illuminate" a volume of air separated by approximately 5400 m at a height of 10 km. During certain meteorological conditions, there can be a significant difference in wind velocity across a distance of 5400 m.
- An insufficient number of small scale eddies. As altitude increases, the density of the air decreases. As the density decreases, the Reynolds number of the atmosphere decreases. This decrease in Reynolds number with altitude places a lower limit on the size of the smallest eddies. This effectively limits the maximum height range of wind profilers.
- Low signal-to-noise ratio of received echo.
- Internally and externally generated electrical noise.
- Side lobes in the wind profiler antenna pattern.
- Hydrometeors, particularly liquid water.

A descriptive summary of wind profiler errors and limitations can be found in Van de Kamp (1988). Strauch, et al. (1987) discussed the effect of lee waves and gravity waves on horizontal wind accuracy. Wuertz, et al. (1988) discussed the effect of precipitation and Weber, et al. (1992) discussed the effect of nonuniform winds.

1.1.1.1 Quality Control of Wind Profiler Data

As discussed in the previous section, many factors can cause contamination of wind profiler data. Numerous methods have been devised to attempt to remove unrepresentative data from wind profiler data sets. Two methods have been used to provide quality control (QC) of wind profiler data from the NOAA demonstration

network. A third method has frequently been used to filter data obtained from the CSU wind profiler. In addition, the use of the CSU wind profiler to study this specific, synoptic scale event allows the use of unique quality control techniques which may not be generally applicable to other meteorological events or other wind profiler sites. These three methods, as well as others, were examined to determine their applicability to the 25 November, 1991 warm front case.

The first QC method was developed by Brewster and Schlatter (see Brewster (1989) and Brewster and Schlatter (1986, 1988)). The Brewster/Schlatter method uses the techniques of consensus averaging, median filter and shear checking. In the consensus averaging technique, an hourly average of the wind at a particular height level is derived from multiple 6-minute radial velocity samples. Each of the ten 6-minute radial velocity samples is examined to determine how many other radial velocity samples fall within a designated radial velocity "window" of the chosen 6-minute sample. The sample with the greatest number of other samples within the window is chosen. All of the samples within the window are then averaged to obtain the "consensus averaged" 1-hour average. If a consensus cannot be obtained (i.e. there are too few samples within the largest group of samples), the data for that hour, at that height, are flagged as bad.

The median filter and shear check are applied to consensus-averaged hourly data. In the median filter technique, data are gathered from adjacent hours and adjacent height levels. The median of this collection of data is computed for the two horizontal wind components. If the difference between the data and the median is greater than a threshold, then the median is recalculated using only data from the current hour and the previous hour. The data is flagged as bad if the observed data and the recalculated data differ by more than a threshold.

In the shear check technique, the vertical consistency between adjacent and nearby height levels is checked against a threshold. Three or four consecutive height levels are compared to determine if any of the wind vectors have an unacceptably large amount of shear between them.

The second QC method was developed by Wuertz and Weber (1989). The Wuertz/Weber method uses the techniques of continuity and pattern editing. The continuity technique is based on the expectation that wind measurements change smoothly from one height to another, and from one time to another. The "smoothness" is defined in terms of a maximum rotation between neighboring wind vectors. Greater rotation between neighboring wind vectors is permitted at lower wind velocities. The continuity technique also restricts the speed shear between neighboring wind vectors that have the same wind direction.

The pattern editing technique joins together those wind vectors in the neighborhood (i.e. nearby in time and space) that are continuous (as determined by the continuity technique) to form a pattern. A weight is assigned to each pattern, equal to the size of the pattern. By an iterative process, the pattern with the smallest weight is removed, removing that wind profiler data from the data set. Wind vector patterns and weights are recalculated. This process continues until all points are continuous.

The third QC method was developed at CSU by Hein (see Hein, et al. (1991)). The Hein method checks several characteristics of the radial velocity. If the variance of the radial velocity is less than a threshold, the data is marked as bad. If the echo signal power between the vertical, north and east beams deviates by more than a threshold, the data is marked as bad. A shear check is performed between adjacent height levels and time intervals for each radial velocity. If the percentage of spatial and temporal neighbors

that vary significantly from the subject radial velocity is greater than a threshold, the subject radial velocity is marked as bad.

The CSU wind profiler is a five beam profiler, rather than the more typical three beam profiler. By comparing the four wind velocities derived from the five beams, the uniformity of the derived wind field over the profiler can be tested. In nonconvective, nonprecipitating, synoptic scale events, far from a mountain barrier, the wind field should be uniform over the volume scanned by the wind profiler. Nonhomogeneous winds observed under these conditions are suggestive of bad data, and should be exploited as another quality control procedure. Quality control based on nonhomogeneous winds has not been used as a method of quality control in previous studies.

1.1.1.2 Calculation of Kinematic Quantities

Much of the earlier work using wind profilers studied the echo reflectivity strength in relation to atmospheric phenomena (Shapiro, et al. (1984), Rottger (1979), Larsen and Rottger (1983). More recent work has exploited the increased temporal resolution of the wind data provided by profilers to study the atmosphere.

The use of earlier technology, such as rawindsondes, provides high resolution wind data as a function of height. However, rawindsondes are typically launched only twice per day, and the geographic density of rawindsonde launch sites is fairly sparse. A single wind profiler provides the same high resolution data, but in a nearly continuous manner. From a single profiler, many kinematic quantities can be calculated. Neiman and Shapiro (1989) used a single wind profiler and the geostrophic form of the thermal wind equation to calculate the temperature gradient vector and temperature advection for an upper tropospheric front and jet stream passage. When the wind within the layer of interest is

not in geostrophic balance, the magnitude of the terms in the general form of the thermal wind equation must be considered (Forsythe, 1945).

A network of wind profilers expands the possibilities for calculation of kinematic quantities. Zamora, et al. (1987) used a network of three wind profilers to calculate upper tropospheric divergence and ageostrophic wind. The work by Zamora, et al. assumes that the wind field varies linearly throughout the region defined by the profiler network. They derived a method called the linear vector point function (LVPF) that allows the kinematic quantities of wind, divergence, vorticity and deformation at any point within a triangular wind profiler network to be calculated based on the three wind profiler observations, and the distance from the three wind profilers. Kuo, et al. (1987) simulated a network of wind profilers, each separated by 360 km, to calculate the temperature and geopotential fields using the divergence equation. They found that for synoptic situations with weak dynamic forcing, the retrieved fields are about as accurate as from the current rawindsonde network. For situations with strong dynamic forcing, the RMS errors can be approximately 50 % greater than the current rawindsonde network.

1.1.2 Warm Fronts

This section describes the classical theories of warm fronts, frontogenesis, numerical modelling of warm fronts based on the primitive equations, and previous observational studies.

1.1.2.1 Classical Theories

The origin of the classical theories of frontal development can be traced to work done by Bjerknes (1918) and Bjerknes and Solberg (1922). Bjerknes and Solberg were the first to present a detailed discussion of wave cyclones and their associated cold, warm and occluded fronts. Using a spatially dense network of surface data, Bjerknes (1918)

found zones of confluence associated with cold and warm fronts, and temperature gradients across these fronts. The well known patterns of clouds and precipitation associated with fronts was related to the adiabatic cooling of warm air lifted by the fronts. Bjerknes and Solberg (1922) were also the first to note the differences in vertical structure between cold and warm fronts. In particular, cold fronts are steeper and warm fronts can be difficult to locate at the surface.

Harrold (1973) introduced the concept of a "conveyor belt" of warm air, 100 to 1000 km wide, and several km in depth. The conveyor belt, is parallel to, and ahead of the surface cold front. As the air moves poleward, it rises up over the warm front. Most of the warm frontal precipitation is caused by condensation within the ascending portion of the conveyor belt.

There have been many papers discussing the banded nature of precipitation embedded within warm fronts (Herzegh and Hobbs (1980), Houze, et al. (1981), Rutledge and Hobbs (1983), Heymsfield (1979)). However, in general, there has been very little attention paid to the overall structure of warm fronts.

1.1.2.2 Warm Front Models Based on Primitive Equations

Hoskins and West (1979) and Hoskins and Heckley (1981) used semi-geostrophic theory to study frontogenesis. Semi-geostrophic theory combines the geostrophic momentum approximation form of the primitive equations, and a coordinate transformation. The result is a set of primitive equations in which the horizontal advection terms are the geostrophic wind. The ageostrophic flow is obtained by a coordinate transformation back to physical space. Semi-geostrophic theory is described more fully in Hoskins (1975).

Hoskins and West (1979) and Hoskins and Heckley (1981) modelled frontogenesis using a uniform Ertel potential vorticity model with a basic zonal jet flow $\bar{u}$, where $\bar{u} = 0$ at $Z = 0$ (surface). At $Z = H$ (top of troposphere), $\bar{u}$ varies sinusoidally in space from $1 - \mu$ to 1. Using typical synoptic values, they varied μ and studied frontogenesis as a function of time. They found that for small values of μ ($<= 0.1$), a warm front did not develop at all. For $\mu = 0.3$, a weak warm front develops between day 5.5 and day 6 east and southeast of the low center. For larger values of μ, the warm front develops later, and is weaker.

By using an inverted zonal jet flow (i.e. $\bar{u} = 0$ at $Z = H$, and $\bar{u}$ varying sinusoidally at $Z = 0$), a much stronger warm front develops south of the low, associated with the trailing edge of cold air ahead of the low. Further study showed that this warm front had many of the characteristics of a frontal occlusion. Both types of warm fronts (as well as the cold fronts obtained by the model), were very shallow in vertical extent.

1.1.2.3 **Previous Observational Studies**

In the past, there have been surprisingly few observational studies made of warm fronts. Heymsfield (1979) used the CHILL and NCAR CP-4 radars to study precipitation bands ahead of the surface warm front near Chicago, Illinois. From these observations, Heymsfield found a mesoscale vertical circulation superimposed on the larger scale frontogenetic vertical circulation. This mesoscale vertical circulation was hypothesized to be the cause of the horizontal periodicity in the precipitation bands.

Hobbs and Locatelli (1987) and Hertzman, Hobbs and Locatelli (1988) used doppler radars, rawindsondes, aircraft and surface observations to study a warm front approaching the Washington coast. They found that the warm frontal zone did not lower steadily in height as it approached a coastal location. Instead, there were periods when

the frontal zone was almost level, interspersed with periods when the height decreased sharply. They found that these "steps" in the frontal zone height may increase convergence, and intensify the precipitation bands. The airflow through the warm front was also studied. It was found that, contrary to the traditional view, the warm front was not a boundary through which air could not pass. In fact, airflow through the warm front provided the vorticity to maintain the frontal structure.

2 SYNOPTIC METEOROLOGICAL ANALYSIS

This section describes the synoptic scale meteorological situation prior to, and during the passage of the warm front through Parsons, KS on 25 November 1991. In general, the northeastern two-thirds of the United States was dominated by a strong cyclone located over eastern Canada. A weak intermountain anticyclone was located over the Great Basin (southern Idaho, Utah, Nevada). The cyclone strengthened with height, and the anticyclone weakened with height. These two pressure systems, the eastern Canada cyclone, and the intermountain anticyclone, are normal climatological features associated with the winter season in North America. A stationary front separated these two air masses and evolved into the warm front that was studied.

2.1 Upper Air

The axis of a longwave trough passed through eastern Kansas around 1200 UTC 23 November as shown in the 500 mb analysis (Figure 2.1). The cold air advection associated with this trough dropped the 500 mb temperature at Monett, MO from -13° C at 0000 UTC 22 November to -31° C at 0000 UTC 24 November. By 1200 UTC 23 November, a 500 mb low had formed and was centered near the northeast corner of Kansas. Over the next 36 hours, this 500 mb low moved northeastward to central Ontario, and the 500 mb temperature at Monett, MO rose to -20° C. By 0000 UTC 25 November,

nearly the entire United States was influenced by the geostrophic flow around the longwave trough and its associated low at 500 mb, as shown in Figure 2.2. From 0000 UTC 25 November to 0000 UTC 26 November, significant 500 mb cold air advection occurred over eastern Kansas, with the 500 mb temperature at Monett, MO falling to -26° C. The 310° K isentropic analyses for 25 November at 0000 UTC, 1200 UTC and 1800 UTC are shown in Figure 2.3, Figure 2.4 and Figure 2.5, respectively. These isentropic analyses show increasing heights with time over eastern Kansas, contrary to what would be expected for a warm front. Based on these isobaric and isentropic analyses, we conclude that no warm front occurred on 25 November at 500 mb and above. On 26 November, the 500 mb low moved rapidly northeastward. By 1200 UTC 26 November, the longwave trough no longer dominated the United States, as shown in Figure 2.6. During 26 November, warm air advection occurred over eastern Kansas at 500 mb in advance of a shortwave trough that formed in the east of the Rocky Mountains.

At 700 mb, very weak warm advection was evident at 0000 UTC 25 November, as shown in Figure 2.7. 24 hours later, at 0000 UTC 26 November, pronounced baroclinicity associated with the warm front is noted from eastern Oklahoma to the Canadian border, as shown in Figure 2.8

2.2 Surface

A strong surface cold front passed through eastern Kansas around 2100 UTC 22 November. A surface low formed along the front near Parsons, KS, moved rapidly northeastward along the front, and intensified. By 2100 UTC 23 November, the surface low was near Milwaukee, WI, and moved slowly northeastward thereafter. An arctic high moved southward, and was centered over Saskatchewan at 1200 UTC 24 November. By 2100 UTC 24 November, a well defined stationary front along the lee of the Rockies

separated the arctic air mass from the milder air associated with the intermountain high pressure, as shown in Figure 2.9. There was little movement in the stationary front until around 0600 UTC 25 November, when a weak low pressure trough formed over west Texas. The eastward movement of the intermountain high and the west Texas trough along with the formation of a surface low over Alberta caused the stationary front to evolve into an active warm front by 2100 UTC 25 November, as shown in Figure 2.10. The NWS analysis shows the surface warm front passing through Parsons, KS around 0000 UTC 26 November. The surface warm front moved slowly northeastward, as the surface low over west Texas moved rapidly eastward. By 1800 UTC 26 November, the surface warm front was north of Kansas, as shown in Figure 2.11.

A surface observing station was in continuous operation in Parsons, KS. A time series of the surface temperature for 25 November is shown in Figure 2.12. Observing Figure 2.12, it is not readily apparent when the surface warm front passed through Parsons. The warm frontal passage seems to be obscured by the diurnal temperature cycle. Similarly, the 25 November surface relative humidity shows only the normal diurnal variation. The wind direction time series for 25 November is shown in Figure 2.13. The wind gradually veered from north at 0400 UTC, to east at 1000 UTC, and southeast thereafter. After 1600 UTC, there were wind direction fluctuations between northeast and south. The downward infrared radiation (IR) time series for 25 November is shown in Figure 2.14. Between 0800 UTC and 1500 UTC, the downward IR was nearly constant. As discussed in Section 2.3, this constant downward IR was due to clouds caused by the overrunning of warm air over the cold air. After 1600 UTC, there was a significant decrease in IR as the warm front lowered over Parsons, and overrunning clouds moved north of Parsons.

2.3 Satellite Observations

Hourly infrared satellite images were available for the central United States. At 0300 UTC 25 November, low, broken clouds were observed over northern Oklahoma and southern Kansas, as shown in Figure 2.15. At 0900 UTC 25 November, a broad band of low clouds ran in a northwest-southeast direction from southeast Kansas to southwest South Dakota, as shown in Figure 2.16. This band of clouds was caused by the overrunning of warm air over the cold, arctic air. The southern edge of the cloud band coincides with the location of the surface warm front. Convective activity caused by intensification of the trough is clearly visible over northern New Mexico and Colorado. At 2100 UTC 25 November, the trough has moved eastward into Oklahoma, forcing the warm frontal cloudiness toward the northeastward to northeastern Kansas and Nebraska, as shown in Figure 2.17.

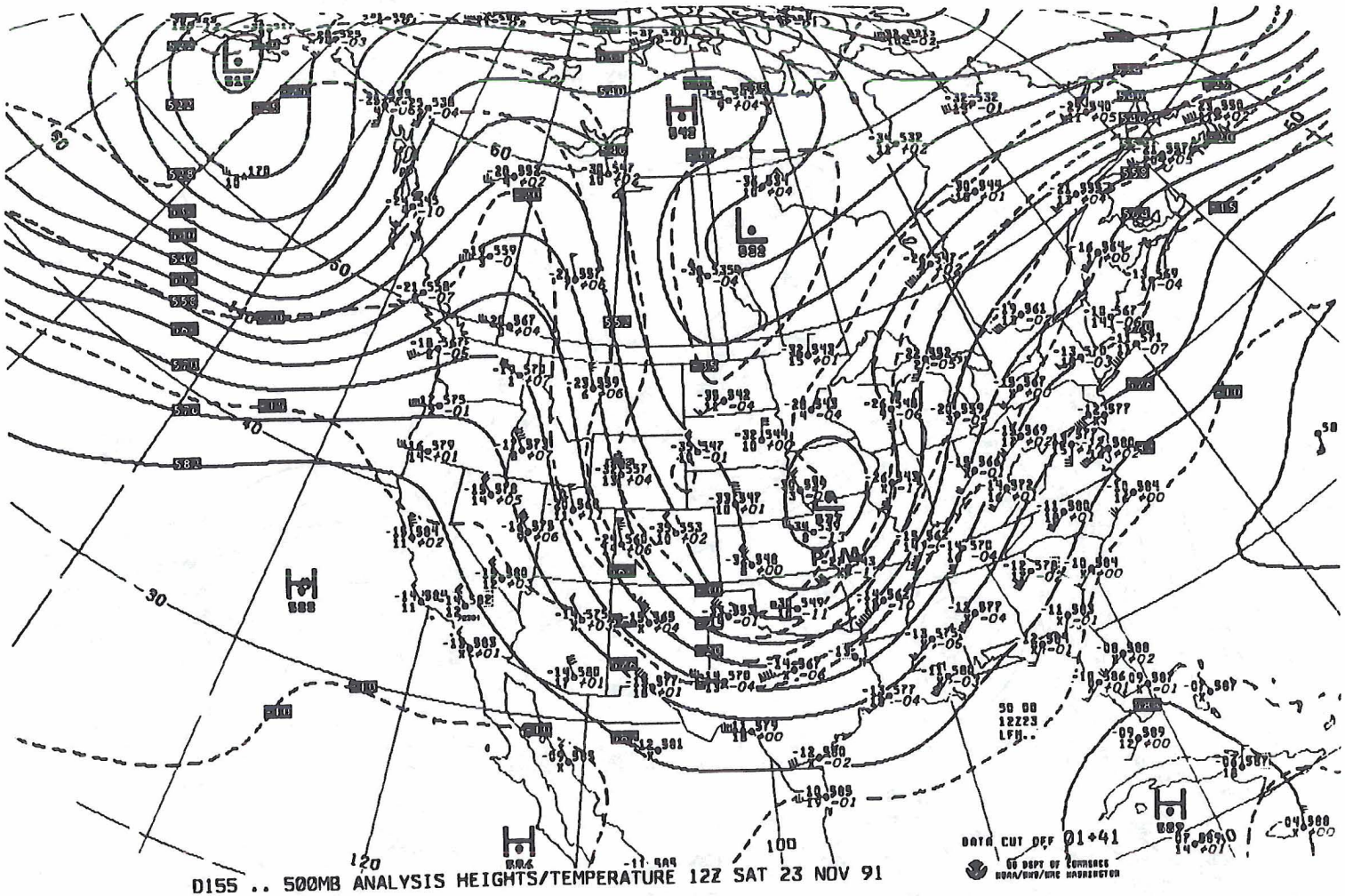

Figure 2.1 - 1200 UTC 23 November 500 mb Analysis. Point labeled "P" is Parsons, KS. Point labeled "M" is Monett, MO.

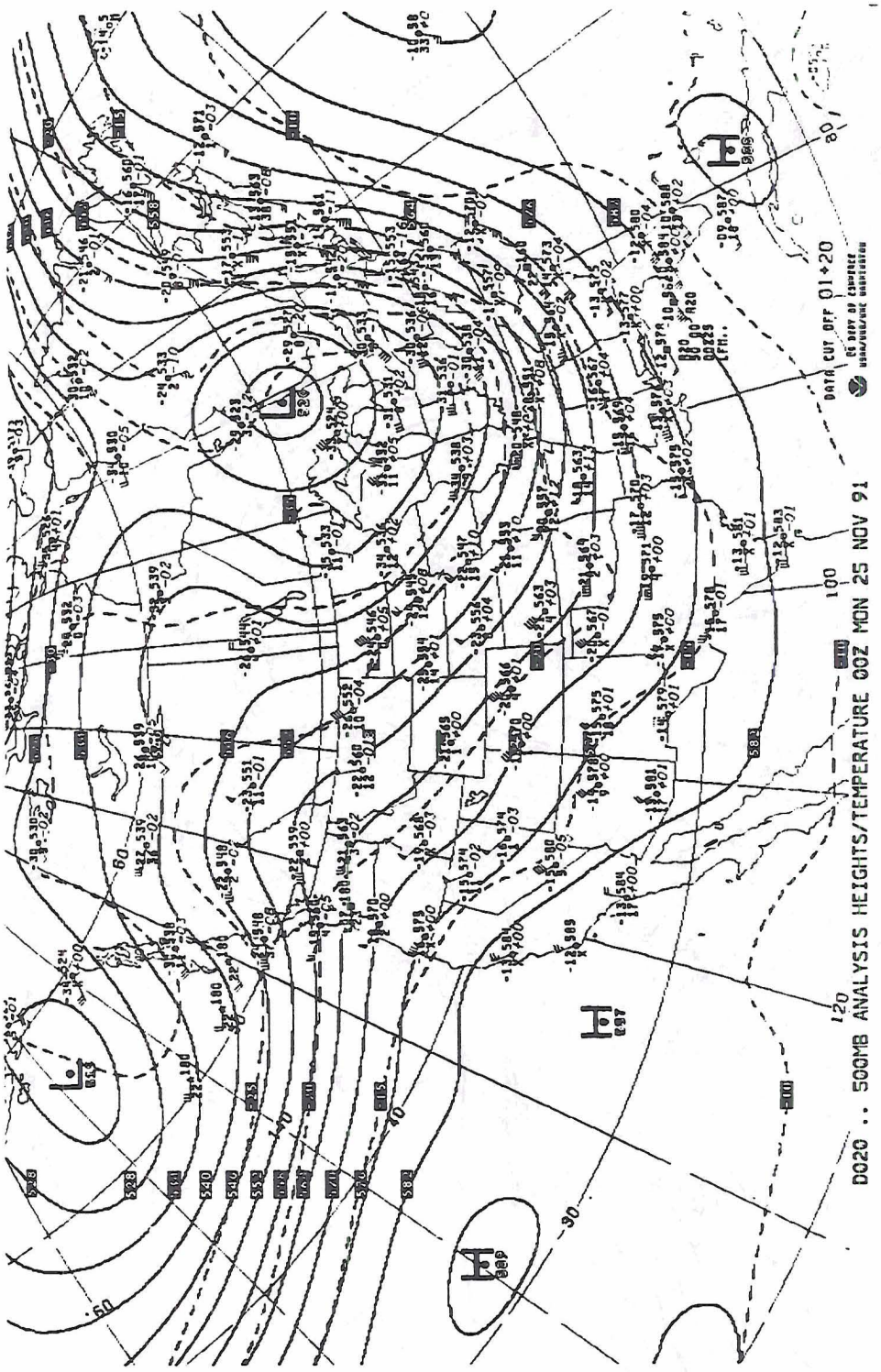

Figure 2.2 - 0000 UTC 25 November 500 mb Analysis

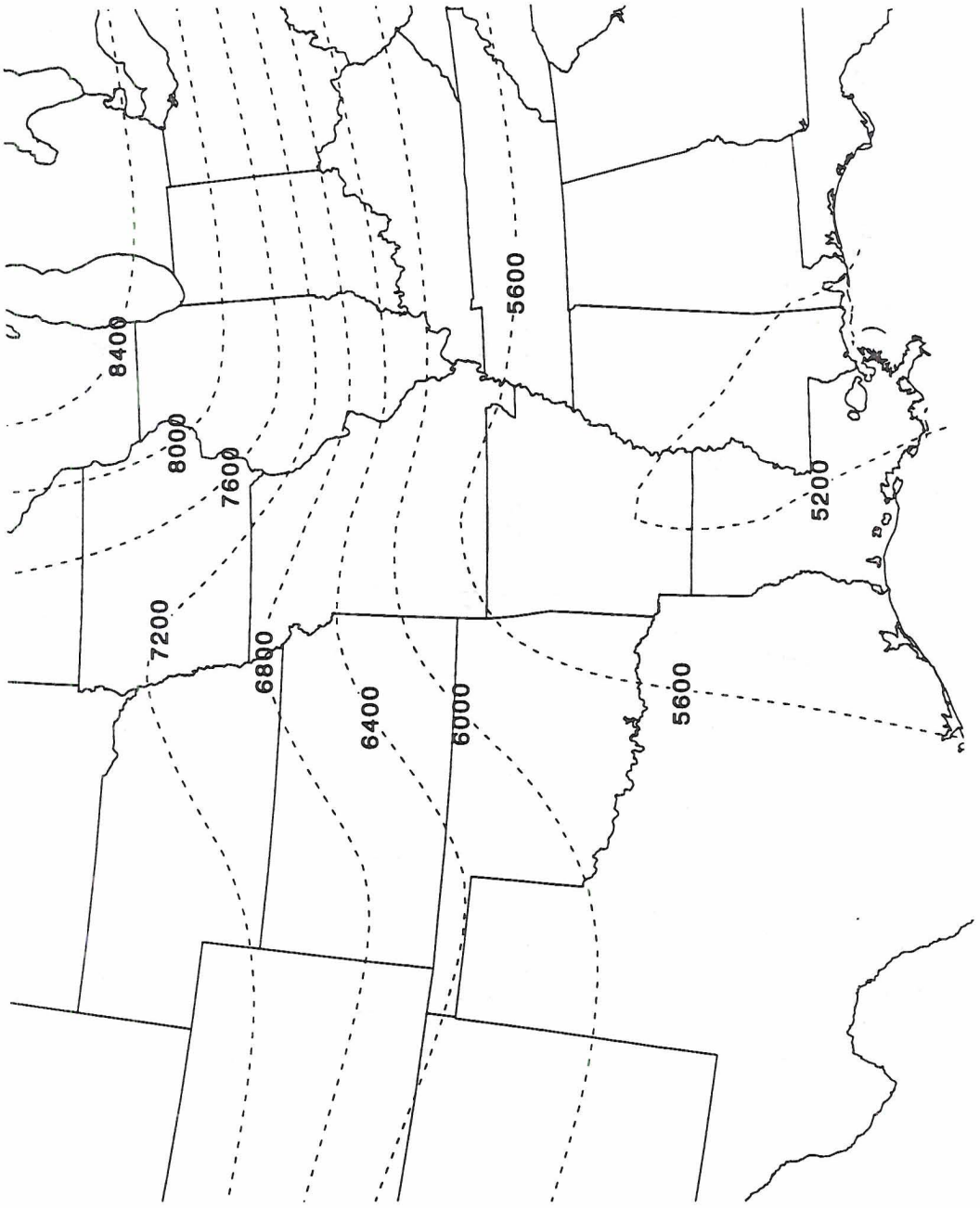

Figure 2.3 - 0000 UTC 25 November 310 Degree Isentropic Height (meters)

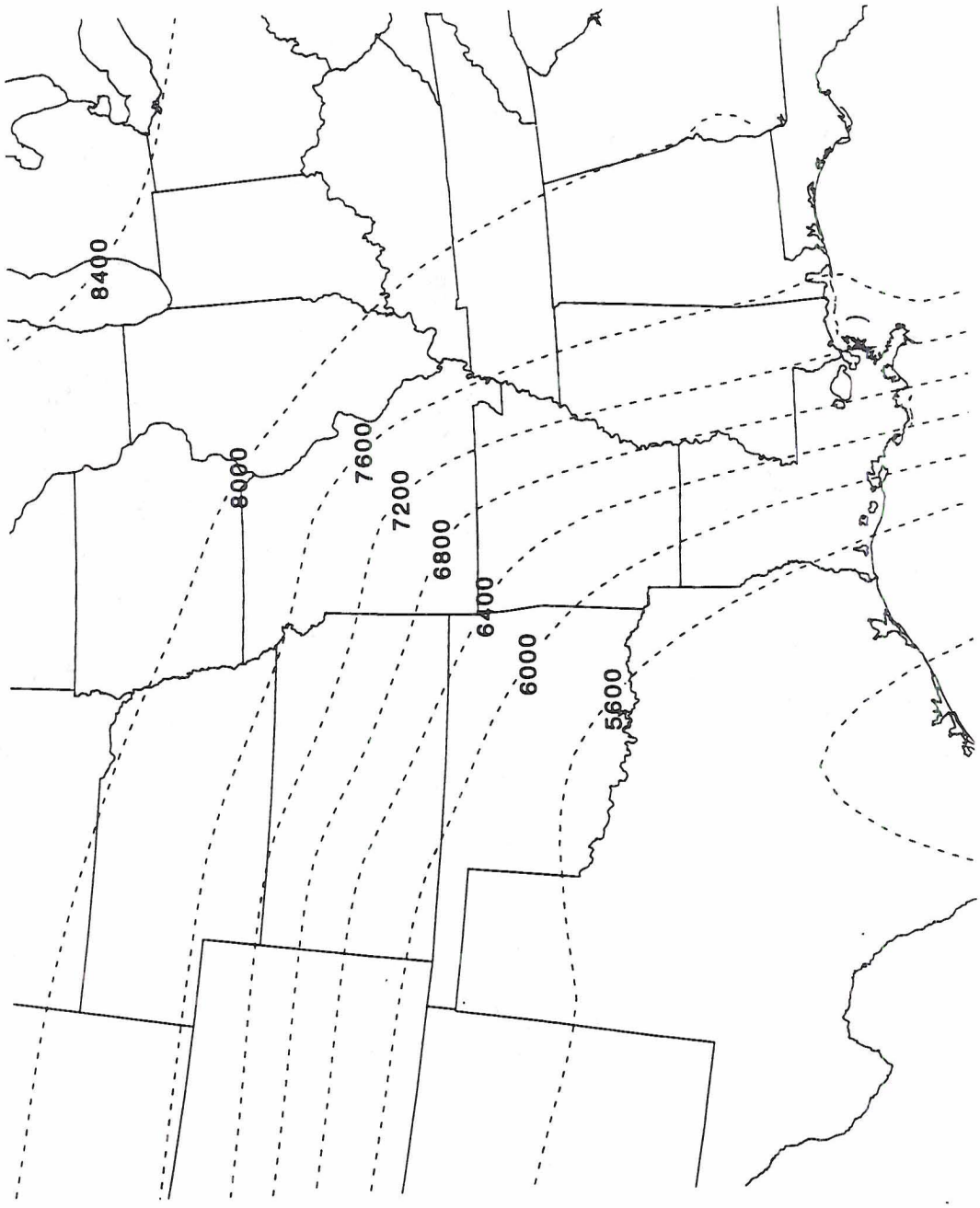

Figure 2.4 - 1200 UTC 25 November 310 Degree Isentropic Height (meters)

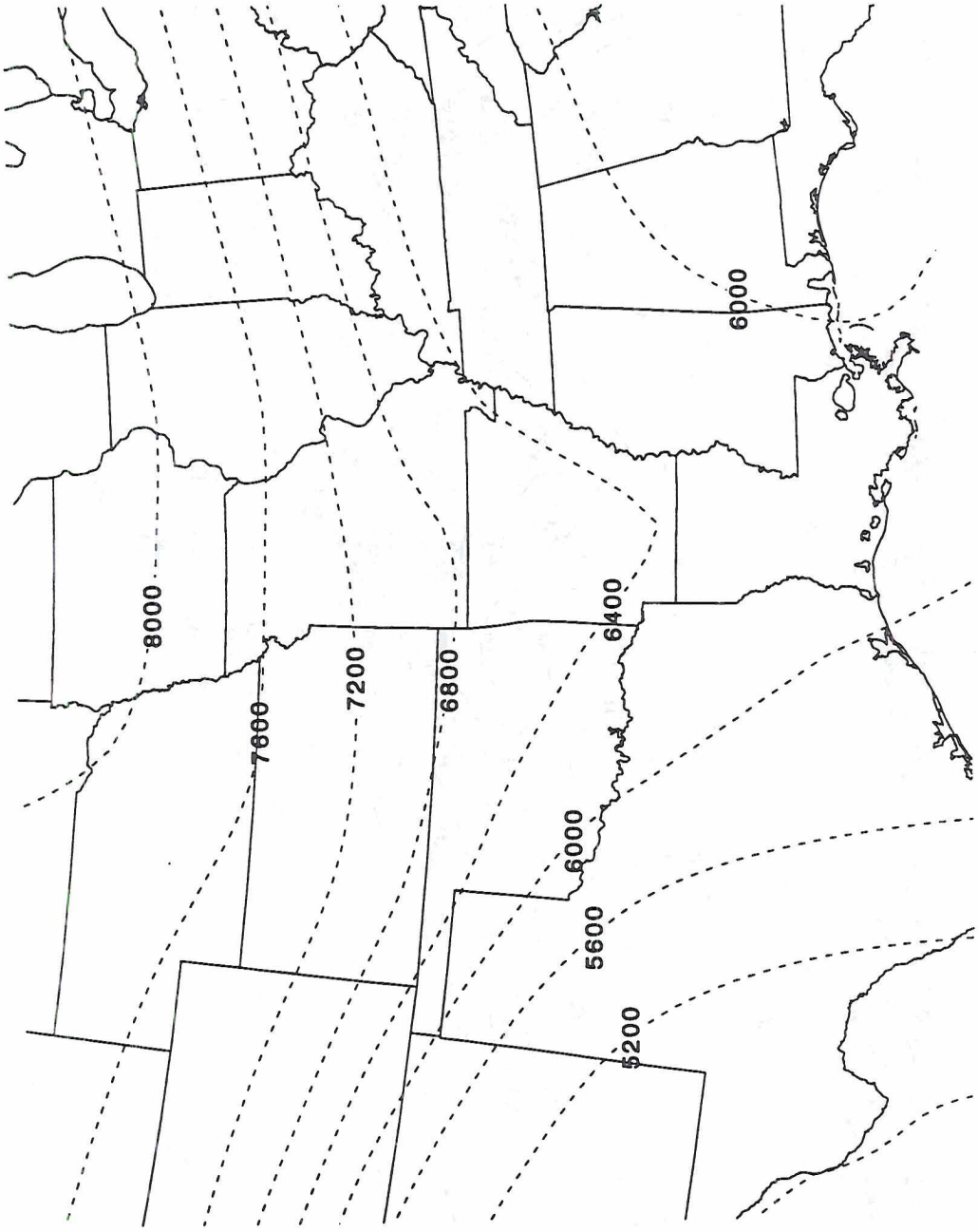

Figure 2.5 - 1800 UTC 25 November 310 Degree Isentropic Height (meters)

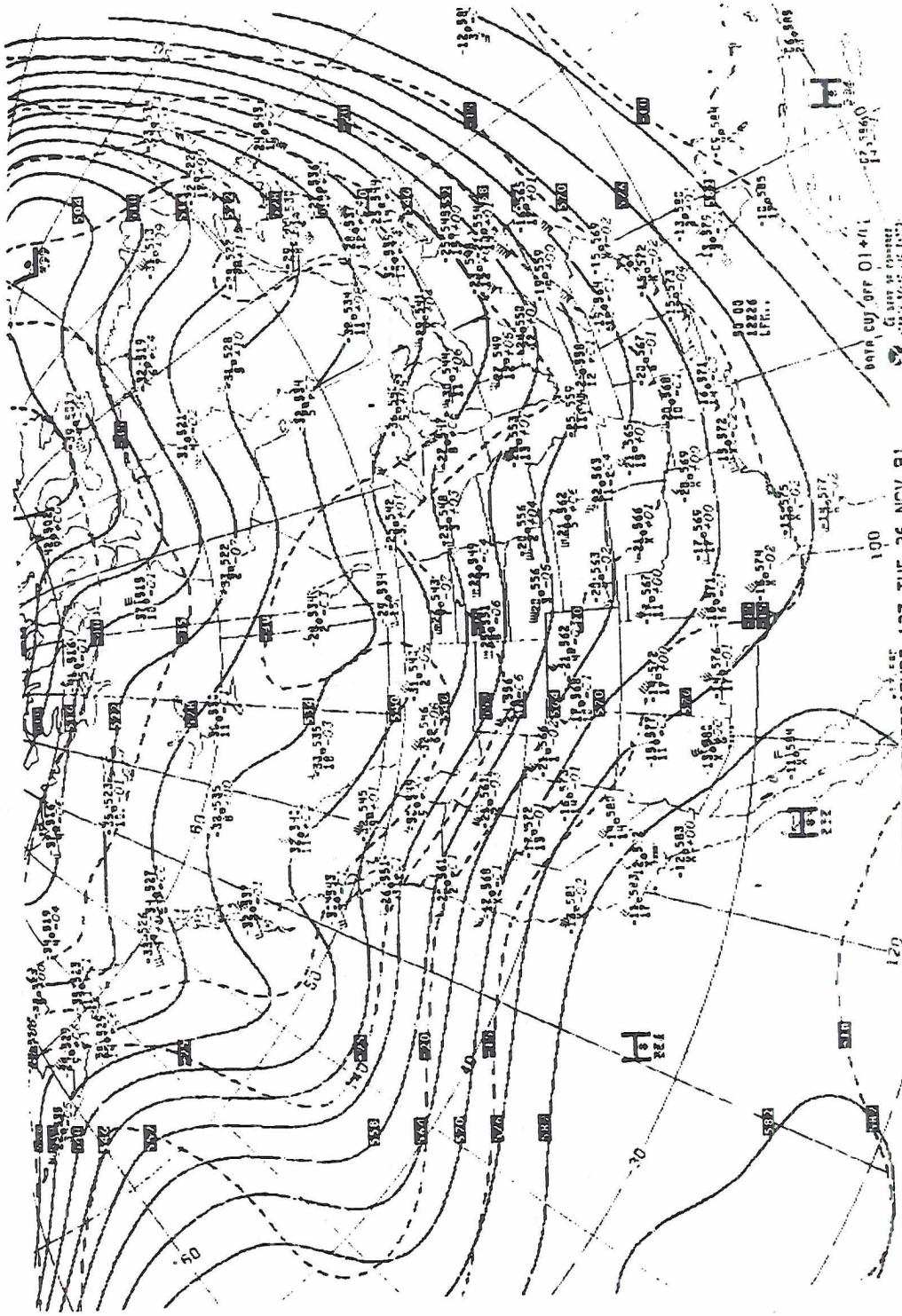

Figure 2.6 - 1200 UTC 26 November 500 mb Analysis

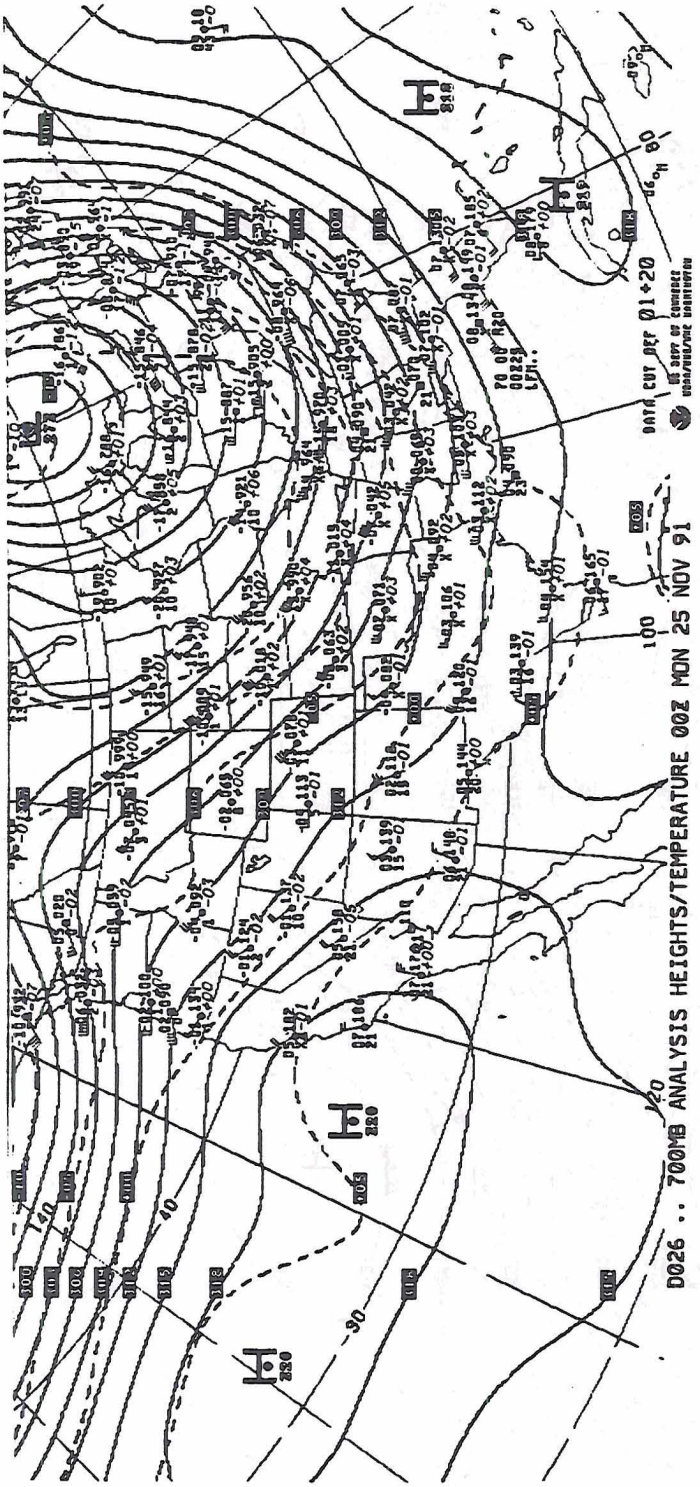

Figure 2.7 - 0000 UTC 25 November 700 mb Analysis

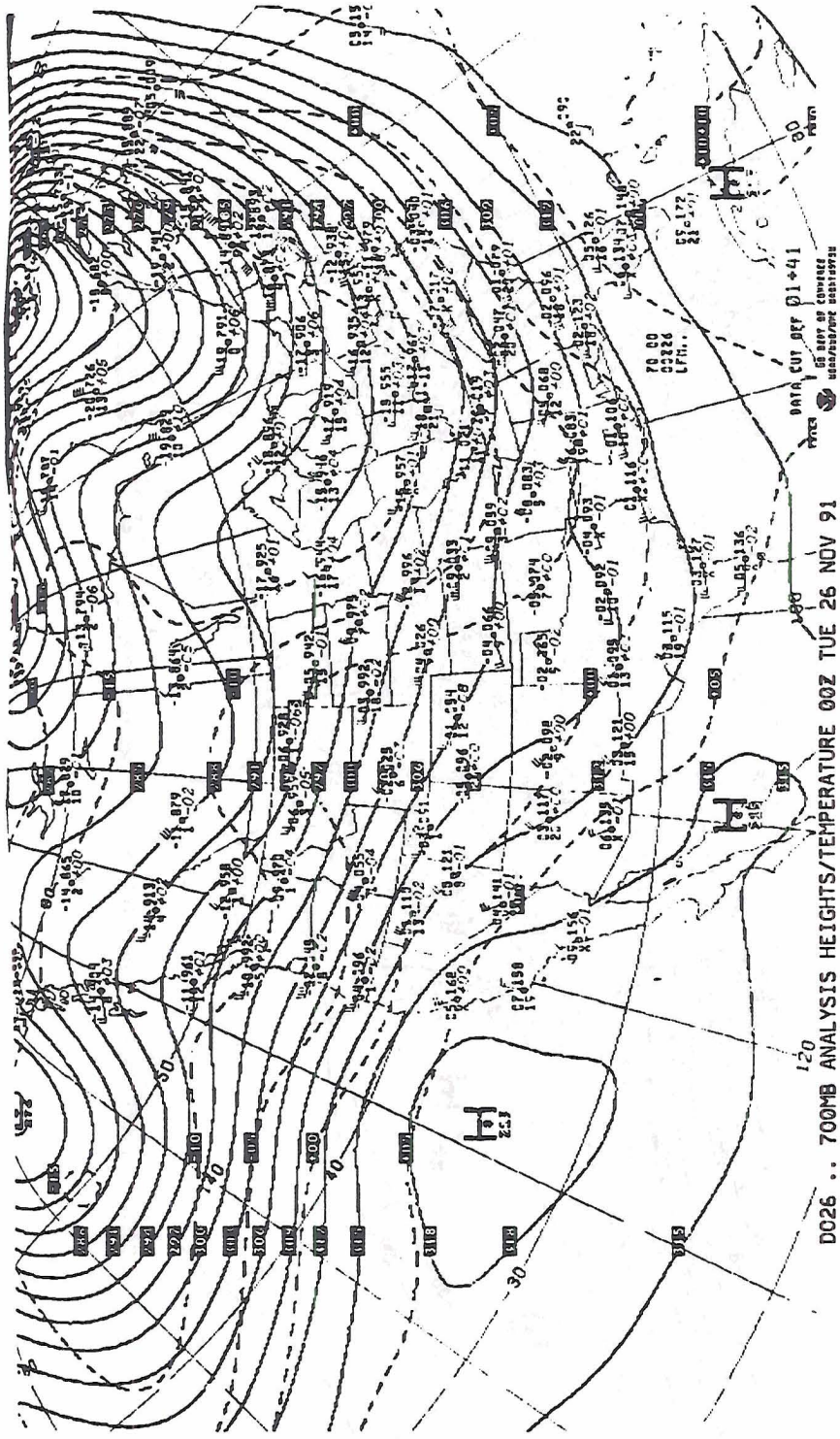

Figure 2.8 - 0000 UTC 26 November 700 mb Analysis

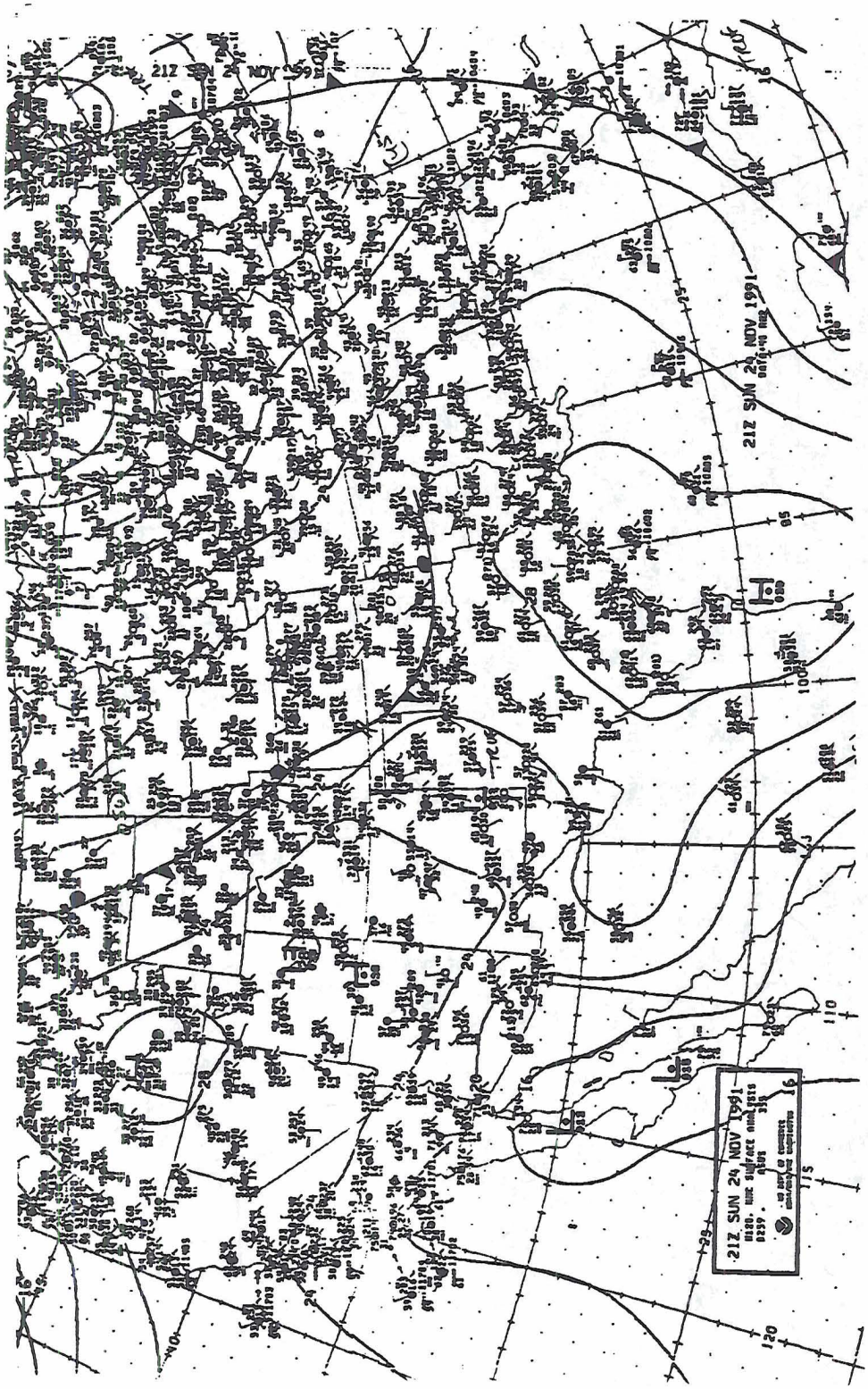

Figure 2.9 - 2100 UTC 24 November Surface Analysis

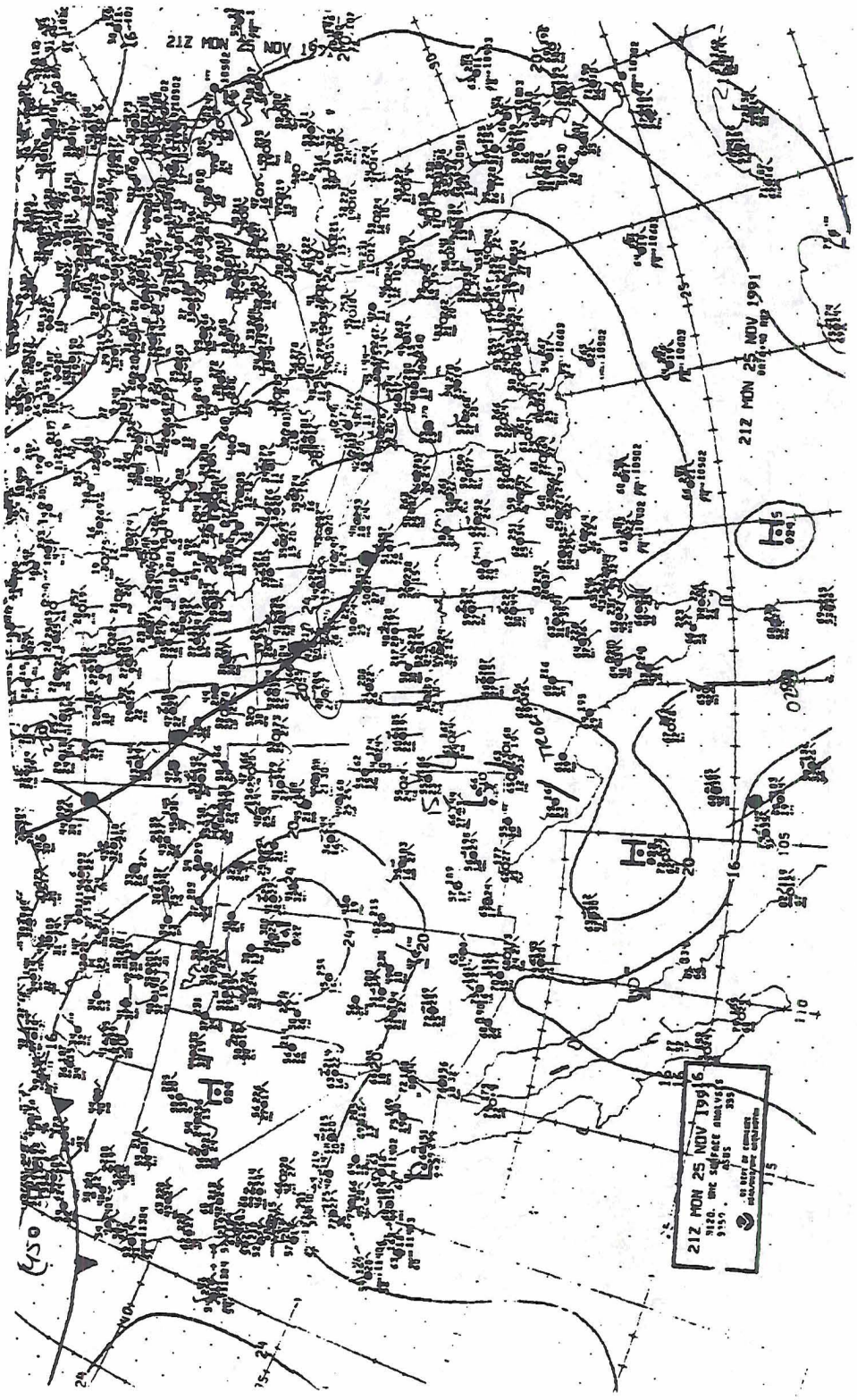

Figure 2.10 - 2100 UTC 25 November Surface Analysis

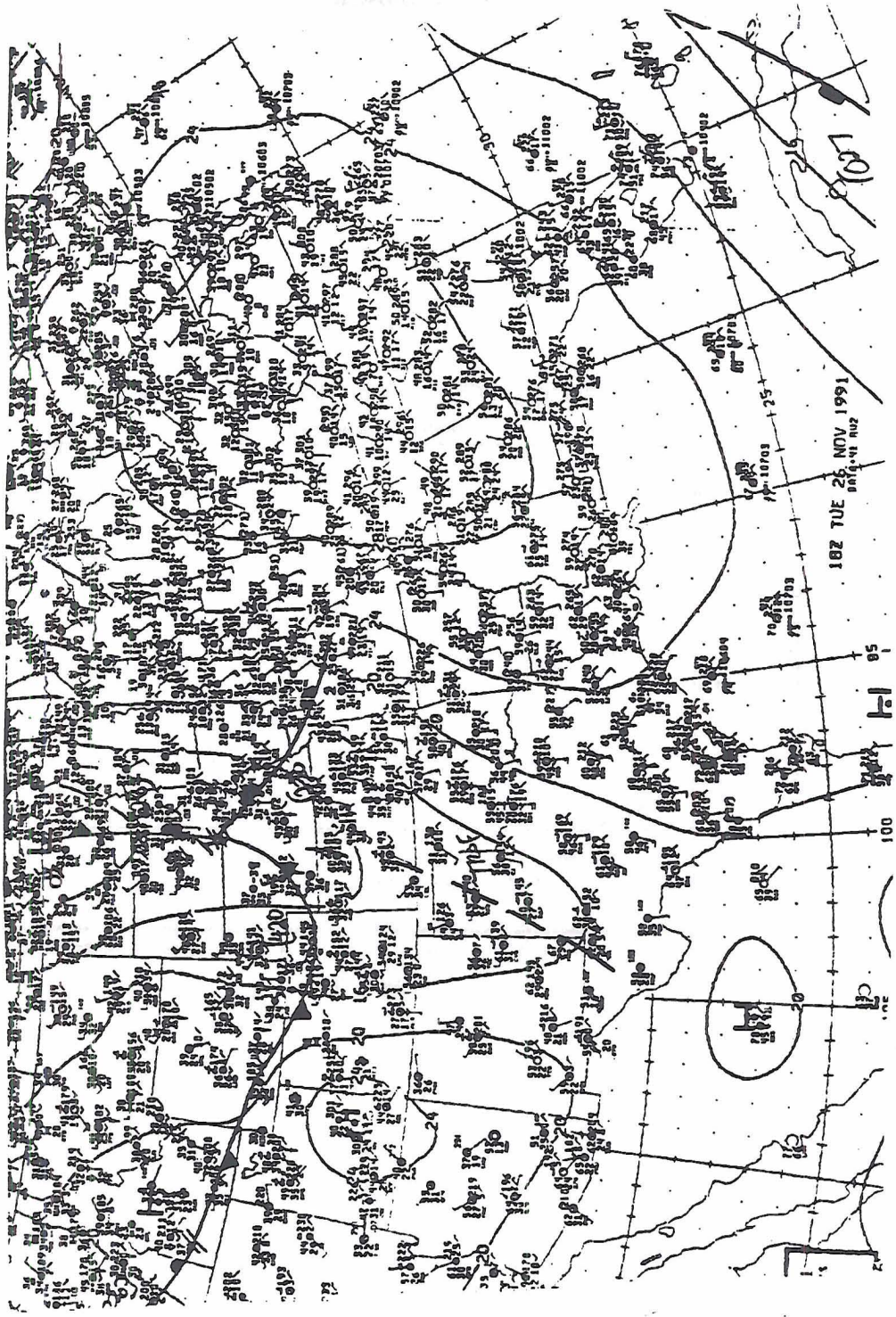

Figure 2.11 - 1800 UTC 26 November Surface Analysis

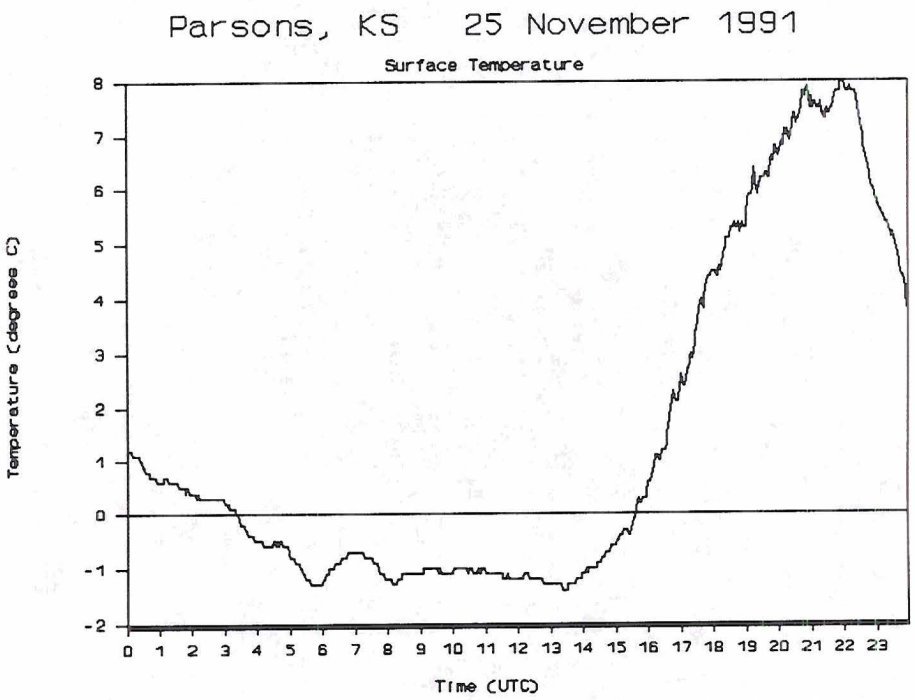

Figure 2.12 - 25 November Parsons KS Surface Temperature

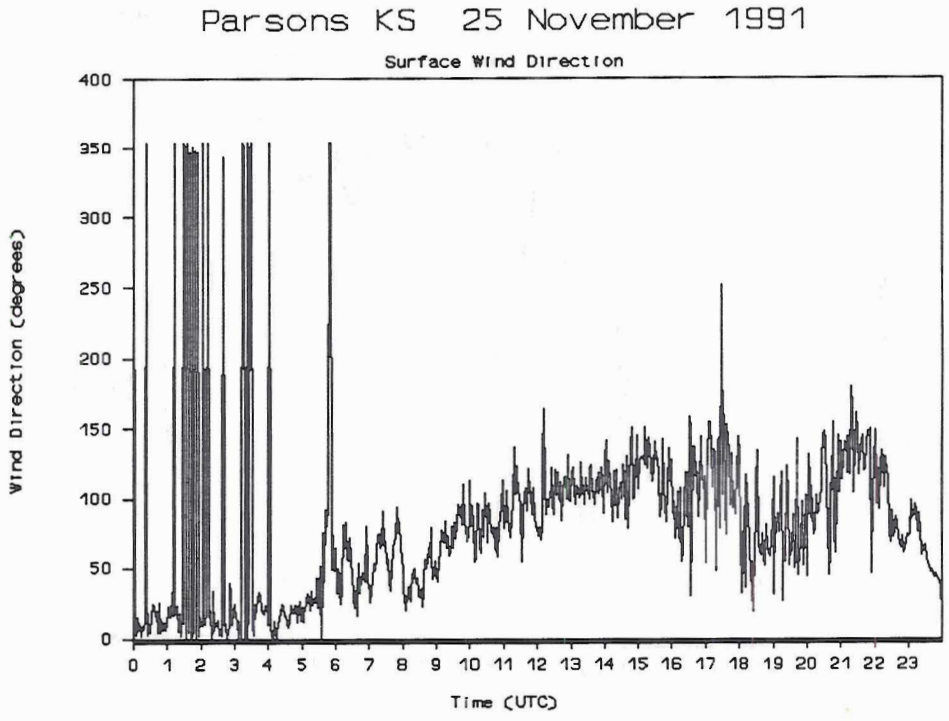

Figure 2.13 - 25 November Parsons KS Wind Direction

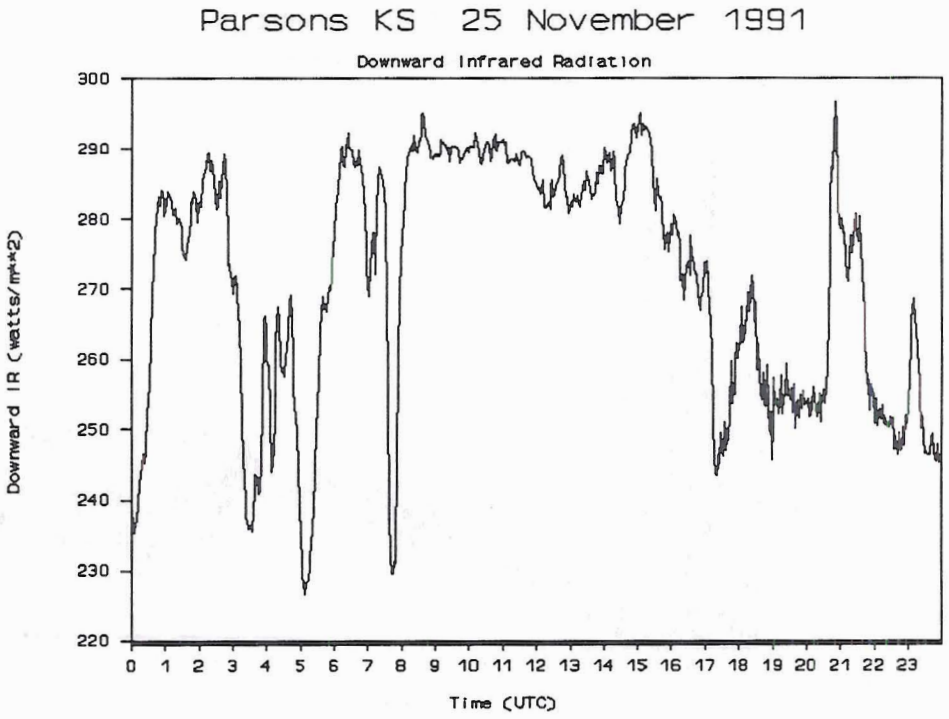

Figure 2.14 - 25 November Parsons KS Downward Infrared Radiation

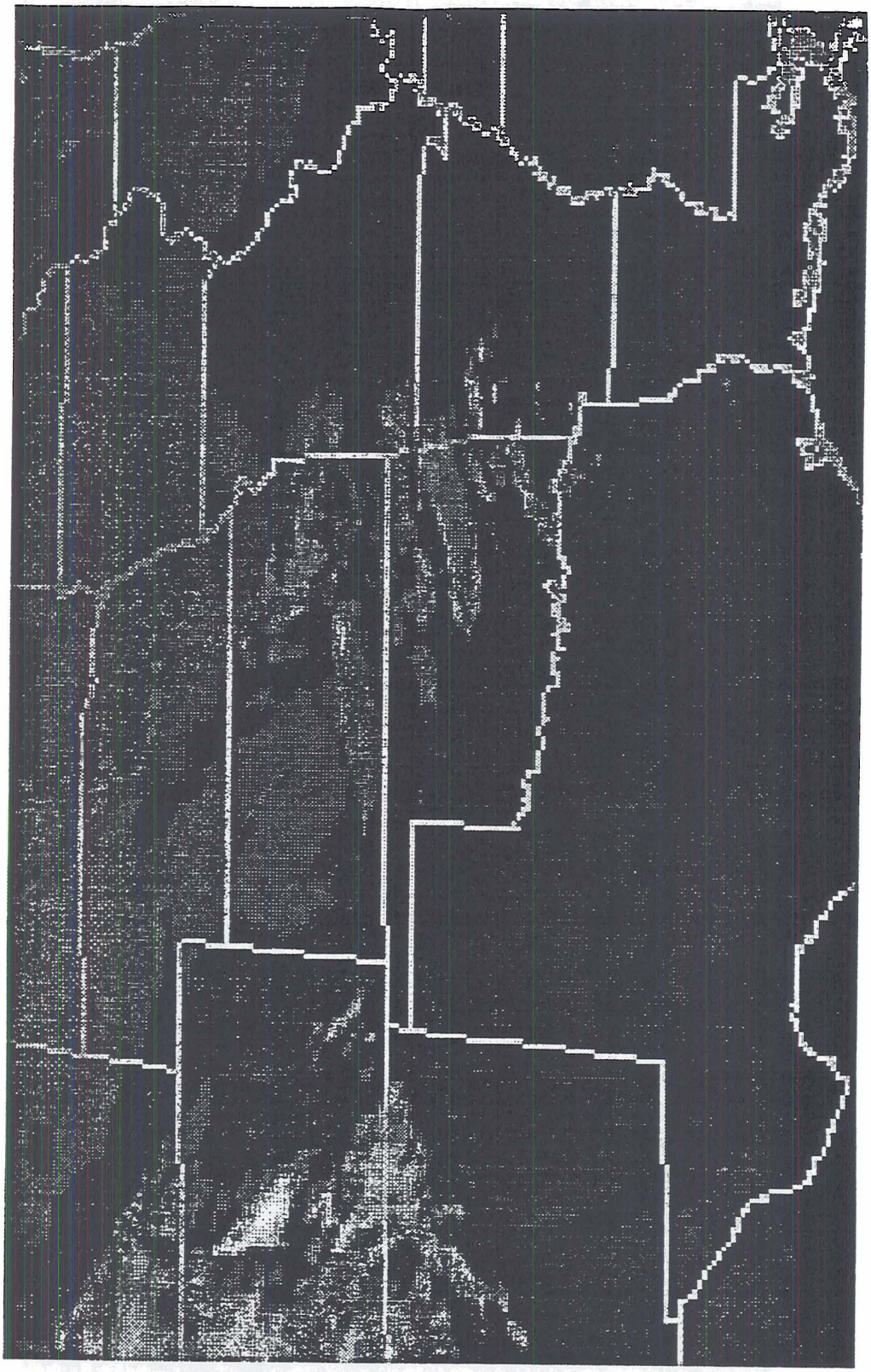

Figure 2.15 - 0300 UTC 25 November Satellite Infrared Image

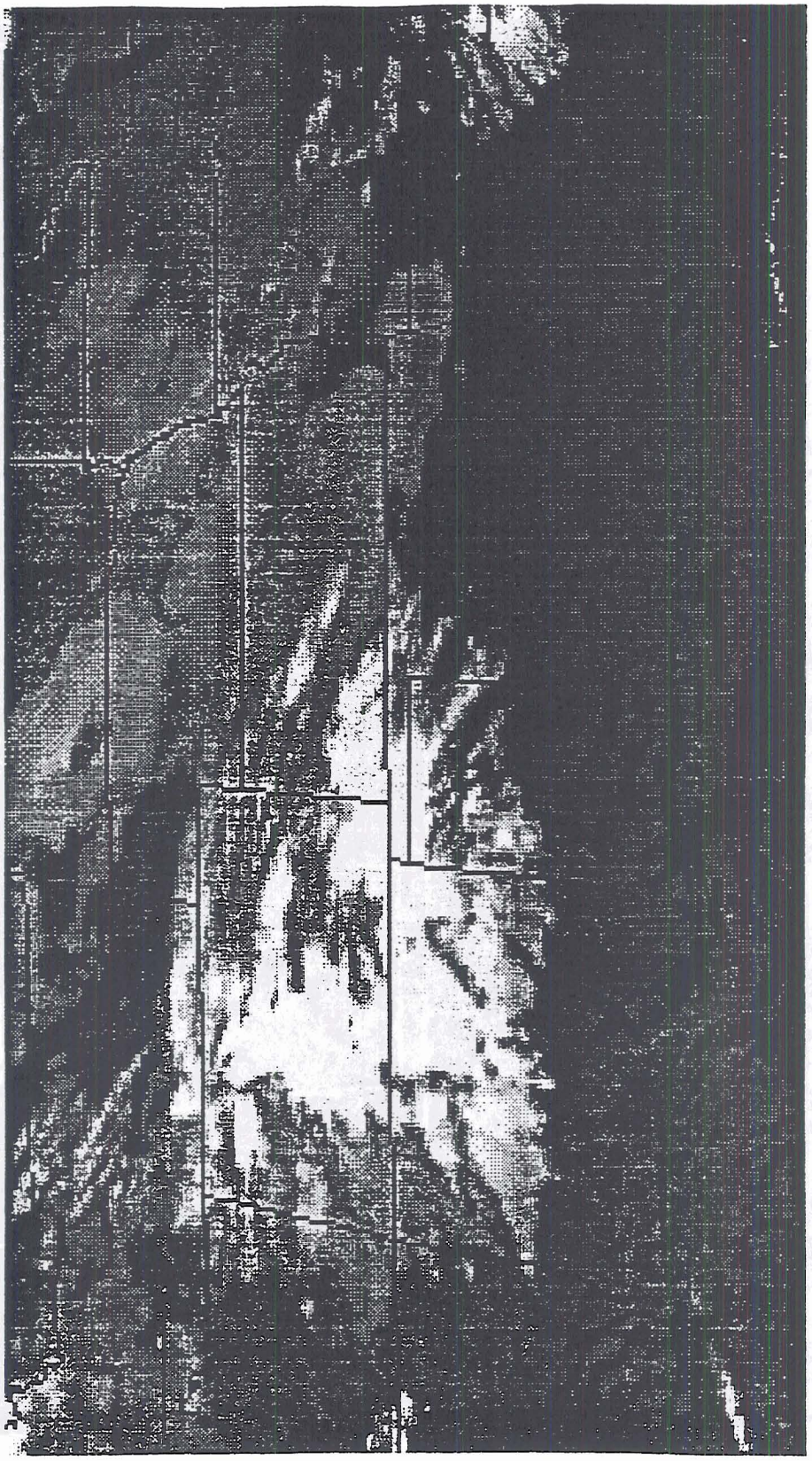

Figure 2.16 - 0900 UTC 25 November Satellite Infrared Image

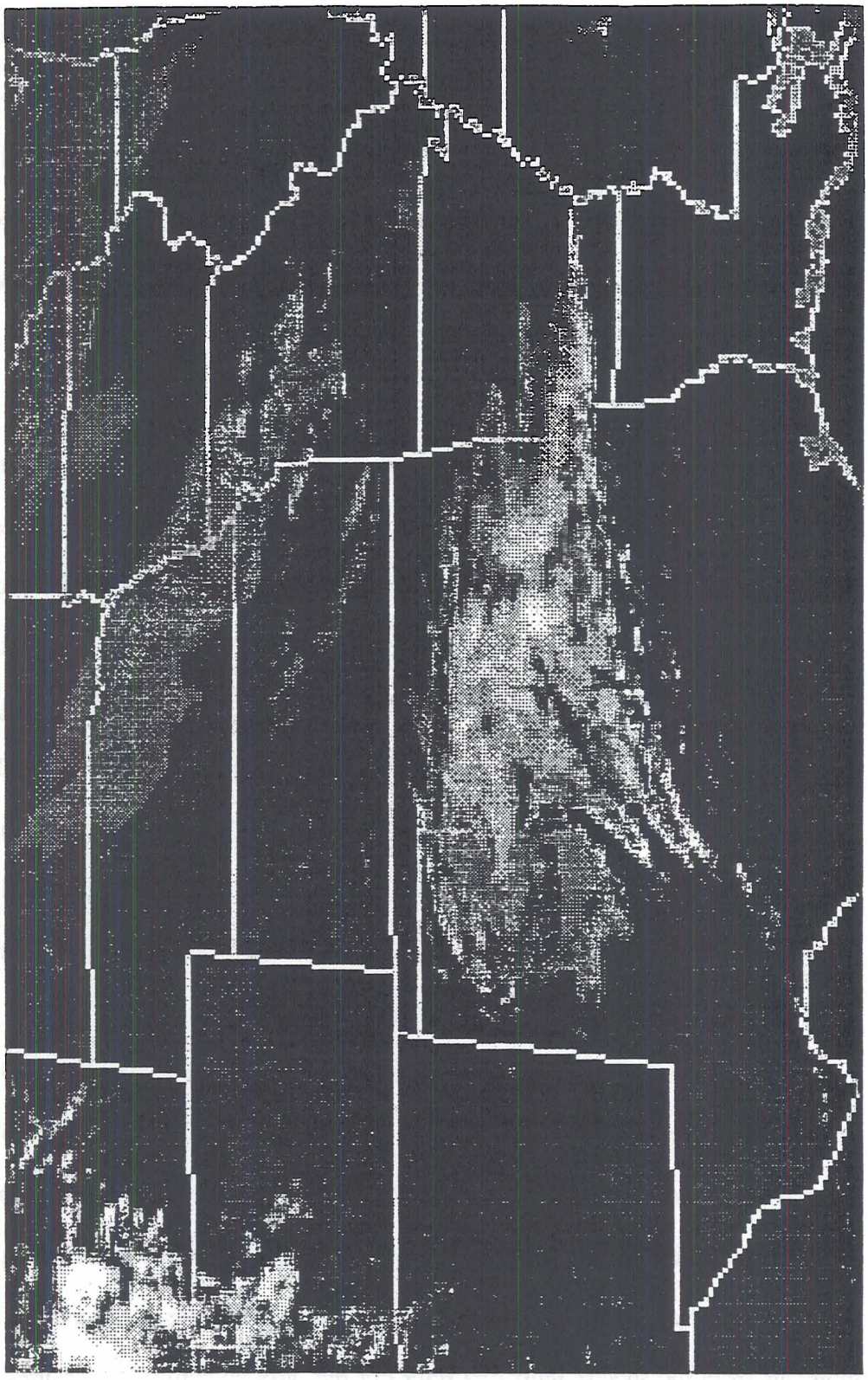

Figure 2.17 - 2100 UTC 25 November Satellite Infrared Image

3 WIND PROFILER OBSERVATIONS, PROCESSING AND ANALYSIS

This section describes the processing and analysis of the 25 November 1991 CSU wind profiler data. The processing of the wind profiler data involved the synthesis of quality-controlled, hourly, wind field averages derived from 6-minute radial velocity and frequency spectrum samples. The analysis of the processed data was used to spatially and temporally locate the warm front.

3.1 Wind Profiler Data Processing

The CSU wind profiler (Tycho Technologies Model 400) was in operation in Parsons, KS from 13 November 1991 until 7 December 1991. The wind profiler output consists of 6-minute averaged spectra and spectral moments for each beam and range gate. The 6-minute averaged spectra contain the signal power in 256 frequency bands around the transmitted frequency, f_o, from f_o-128Δf to f_o+128Δf. The 6-minute averaged spectra can be viewed as the raw data from which the spectral moments are derived. Each spectral moment is derived from the averaged doppler-shifted echo returns, and contains the signal power in the peak of the spectra, the average radial velocity derived from the doppler shift at the spectra peak, the variance of the radial velocity around the spectral peak, and the average noise power away from the spectral peak.

The imperfect antenna pattern of any wind profiler, including the CSU wind profiler, results in many sidelobes that transmit pulses and receive echos. In particular, there are sidelobes present at very low horizon angles that receive strong echos from stationary, or near-stationary objects near the ground. The resulting frequency spectra has a very strong peak near the transmitted frequency, f_o. Any attempt to extract the spectral moments from the spectra must first filter out the "ground clutter" that caused this "central

peak". Filtering out the signal power in frequency bands near the central peak can result in the loss of information on very low wind speeds.

To derive the vertical wind speed in the high-resolution, low height mode, the unfiltered 6-minute frequency spectra was used. The spectral moments were derived, with only the ground clutter filtered out. The derived vertical radial velocity moments were found to either be less than 1 m/s, or very large (typically greater than 10 m/s). The large velocities always had large variances, and low signal-to-noise ratios. These large values were probably indicative of very low vertical velocities that were perceived as ground clutter by the wind profiler filtering algorithm. Therefore, any derived vertical velocity of greater than 1.2 m/s was set to 0 m/s. The derived vertical wind speeds were averaged over three adjacent height levels.

For the low-resolution, high height mode, an inspection of the unfiltered 6-minute frequency spectra typically did not show a discernable power peak. Therefore, the high mode vertical velocities were assumed to be zero. The error introduced by this assumption should be negligible, since the non-vertical beam radial velocities in the high mode were large.

The derived vertical beam spectral moments were merged with the non-vertical beam spectral moments to create a composite spectral moment data set.

The quality control algorithms described in Section 1.1.1.1 were studied in relation to the composite spectral moment data set. The following quality control algorithms were applied to the 6-minute spectral moment data sets:

- All data during the 6-minute cycles that RASS sound waves were generated were marked as bad.

- Shear checking was used to remove wind vectors that differed significantly from their spatial and temporal neighbors.
- Radial velocity variance was checked. Radial velocity variance moments that did not exceed a minimum variance were removed.
- Horizontal homogeneity of the wind field was tested by deriving four wind velocities from the 5 beams. If the four derived wind velocities varied significantly, all radial velocities for that time and height were marked as bad.

Hourly averaged radial velocities were obtained from the post-quality control 6-minute radial velocity moments using the following procedure:

- For hours in which there were two or more 6-minute spectral moment data sets, the radial velocity spectral moments at each height level were averaged, provided there were two or more valid radial velocity spectral moments at that height. When there was only a single valid spectral moment at a height level, that height level was not included in the hourly average.
- For hours in which there was only a single set of 6-minute spectral moments (1800 UTC and 1900 UTC), this single 6-minute spectral moment became the hourly average.

The following quality control algorithms, used by other researchers, were *not* applied to the Parsons wind profiler data:

- Consensus averaging was not used to obtain hourly averages. For the 25 November time period, each hour contained from one to six 6-minute spectral moment data sets, rather than the 10 data sets per hour available from the NOAA profiler demonstration network. For hours when there are very few data sets available, the credibility of the consensus averaging technique is questionable.
- The continuity technique is a more mathematically rigorous method of shear checking. The additional complexity of the continuity technique did not seem warranted vs. the Hein (1991) shear checking technique that was applied.

3.2 Warm Front Placement Using Wind Profiler Data

The quality controlled, hourly averaged, radial velocity data from the Parsons wind profiler for 25 November were used to plot the time series of wind velocity shown in Figure 3.1, Figure 3.2, and Figure 3.3.

Warm advection, as indicated by veering winds, is first notable at 0600 UTC near 3 km (point "a" in Figure 3.1). The base of the layer of veering winds remains at the same height, but widens from 0700 UTC until 1000 UTC (point "b" in Figure 3.2). From 1100 UTC until 1400 UTC, the veering wind layer continues to broaden and lower. After 1500 UTC, the base of the veering wind layer is below the lowest profiler range gate. Based on the convention of Hobbs, et al. (1987), the warm frontal zone is defined as the layer of veering winds, with the warm front located at the top of the warm frontal zone. The 25 November warm front appears to be confined to the lower troposphere. This is made particularly apparent by the study of the temperature advection profile in Section 3.3.

Overlaying the warm frontal zone is a narrow band of backing winds, indicative of cold air advection. This band is most pronounced between 0700 UTC and 1400 UTC (point "c" in Figure 3.2). The interaction between the warm frontal zone and the cold advection will be studied in greater detail in subsequent sections of this paper.

3.2.1 Verification

Other wind profiler data and rawindsondes were used for verification of the Parsons wind profiler results. The other wind profilers were part of the NOAA wind profiler demonstration network, and the rawindsondes were launched by NWS.

The nearest NOAA wind profiler was located in Neodesha, KS, approximately 30 km west of Parsons, KS. The Neodesha, KS profiler was not in operation during the most interesting time period, from 0600 UTC until 1600 UTC. However, as shown in Figure 3.4, a narrow layer of veering winds, overlaid by backing winds was clearly evident at 0500 UTC (points "d" and "e" in Figure 3.4). By 1600 UTC, veering of wind was present from near the surface to 3.5 km.

Rawindsondes were launched from Monett, MO on 25 November at 0000 UTC, 1200 UTC and 1800 UTC and 26 November at 0000 UTC, as shown in Figure 3.5. The 1200 UTC sounding shows some veering of winds with height (point "f" in Figure 3.5), as well as a "cap" of backing winds (point "g" in Figure 3.5). By 1800 UTC, veering of wind extended downward to the surface (point "h" in Figure 3.5).

3.3 Warm Front Thermal Advection

The height-time profile of the horizontal wind field derived from the Parsons wind profiler clearly shows layers of warm and cold temperature advection. The magnitude of this thermal advection was diagnosed using the geostrophic thermal wind equation (Holton, 1979)

$$\frac{\partial V}{\partial p} - \frac{\partial V_g}{\partial p} = -\frac{R}{fp} k \times \nabla T \tag{3}$$

where R is the gas constant, f the Coriolis parameter, k the vertical unit vector, and ∇T is the horizontal temperature gradient on an isobaric surface. The retrieved temperature gradient $\nabla_r T$ can be determined by taking vertical finite centered differences (Neiman, et al., 1989)

$$\nabla_r T(z,t) = \frac{\bar{fp}}{R} k \times \frac{V[p(z + \Delta z,t),t] - V[p(z - \Delta z,t),t]}{p(z + \Delta z,t) - p(z - \Delta z,t)} \tag{4}$$

where

$$\bar{p} = \frac{[p(z + \Delta z,t) + p(z - \Delta z,t)]}{2}$$

Using the retrieved temperature gradient, $\nabla_r T$, the derived temperature advection is given by

$$-\bar{V} \cdot \nabla_r T(z,t) \tag{6}$$

where

$$\bar{V} = \frac{V[p(z + \Delta z,t),t] + V[p(z - \Delta z,t),t]}{2}$$

This approximate thermal advection diagnostic is most applicable to cases of nearly straight flow, small changes in trajectory curvature with height, and minimal accelerations. The northwest-southeast oriented warm front system of 25 November should closely satisfy these constraints.

The wind fields derived using the Parsons wind profiler data were used in equations (4) and (6). The pressure profile used in equation (4) was obtained by linear

interpolation of the Monett, MO rawindsonde soundings at 0000 UTC, 1200 UTC and 1800 UTC. The diagnosed temperature advection profile for 25 November is shown in Figure 3.6. At 0000 UTC, cold advection is present from the surface to 2.1 km. From 2 km to 2.6 km is a narrow layer of warm advection. Above 2.6 km, cold advection is prevalent. With the passage of time, the lower boundary of warm advection drops in height, while the upper boundary of warm advection lifts. After 1100 UTC, the lower boundary of warm advection is below the lowest profiler range gate. Between 0500 UTC and 2300 UTC, there are pockets of strong warm advection (> 20° C/day) between 2 km and 3.5 km. Above the warm advection layer, there are pockets of strong cold advection (< -20° C/day). From 0700 UTC until 1300 UTC, there is only 500 m of vertical separation between layers of strong warm and strong cold advection. This boundary between strong warm and cold advection will be studied in more detail in subsequent sections of this paper.

The temperature change at a height level over a time period can be estimated by integrating the temperature advection over the time period. The advection-estimated temperature change can then be compared to the rawindsonde-measured temperature change, as shown in Figure 3.7, Figure 3.8, Figure 3.9, and Figure 3.10. The sign of the wind profiler-estimated temperature change correlates well with the rawindsonde-measured temperature change up to 6.5 km. However, over a 24 hour period (Figure 3.7), the magnitude of the wind profiler derived temperature change is 2 to 3 times greater than the measured temperature change. Over shorter time intervals, such as 1200 UTC to 1800 UTC (Figure 3.9), the wind profiler and rawindsonde temperature changes correlate fairly well. Most of the disagreement between the wind profiler and rawindsonde temperature change occurred due to overestimation of warm advection at

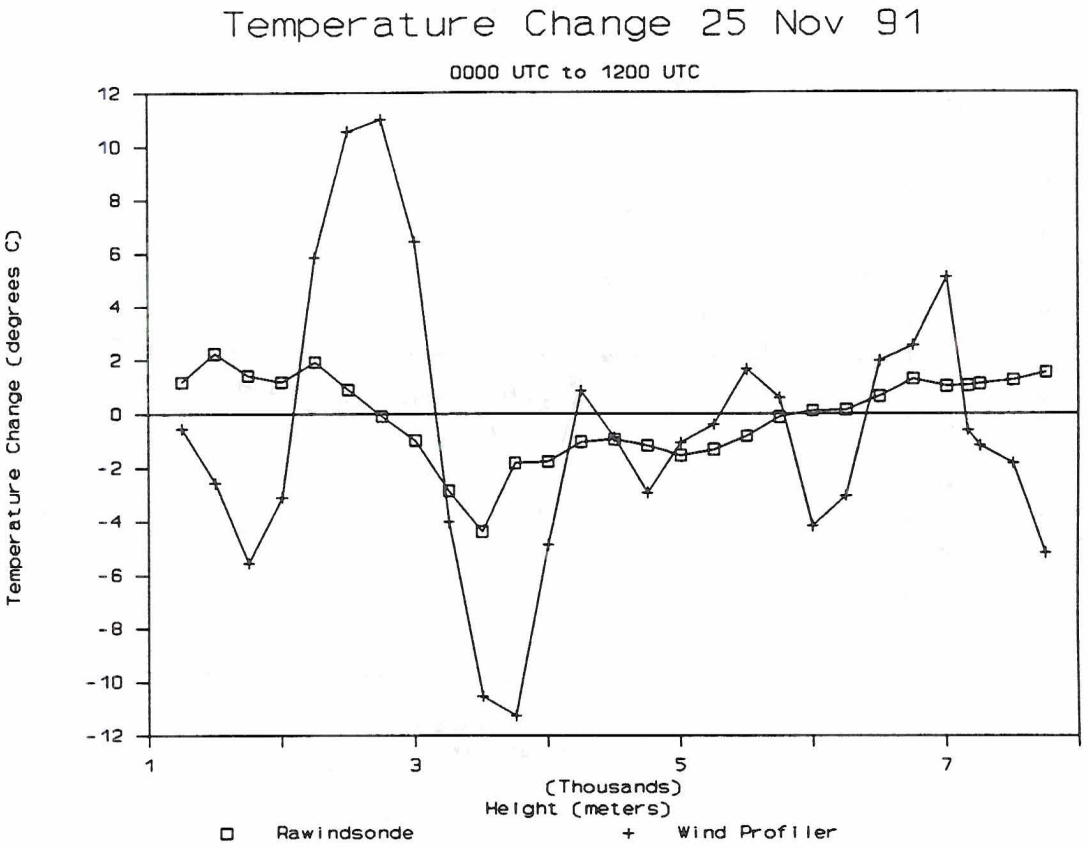

Figure 3.8 - 0000 UTC to 1200 UTC Temperature Change

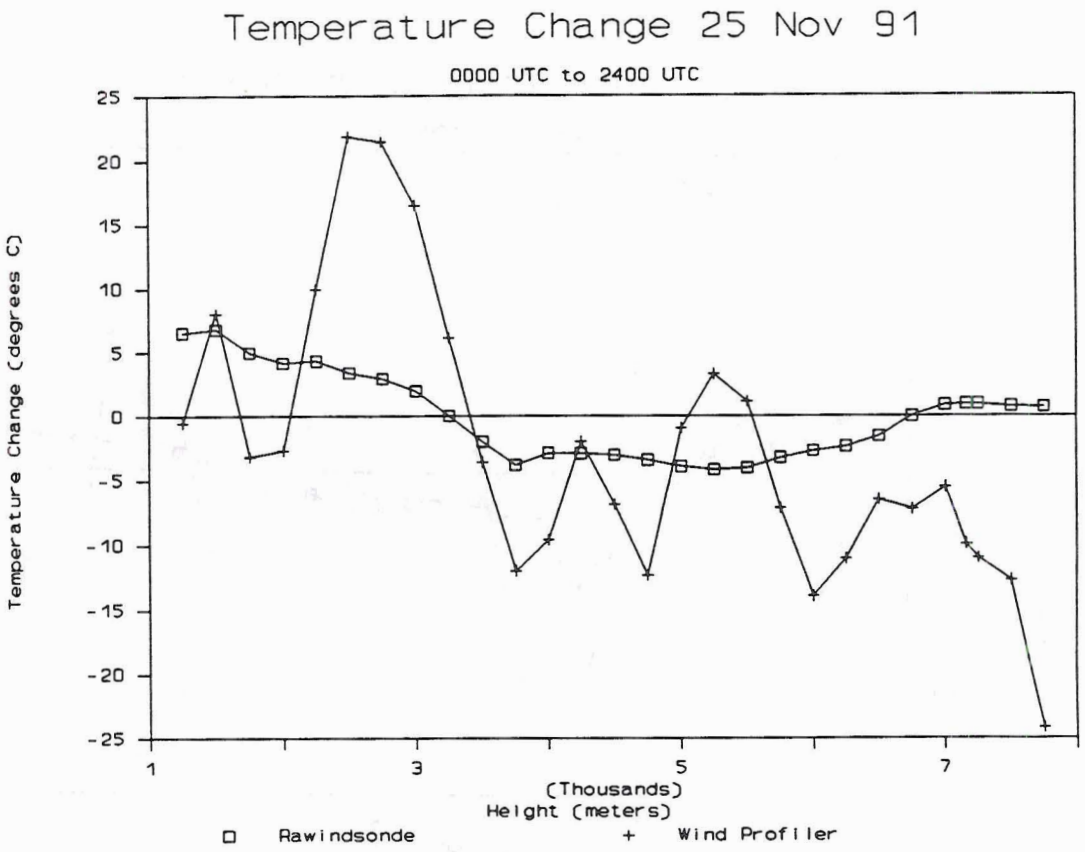

Figure 3.7 - 0000 UTC to 2400 UTC Temperature Change

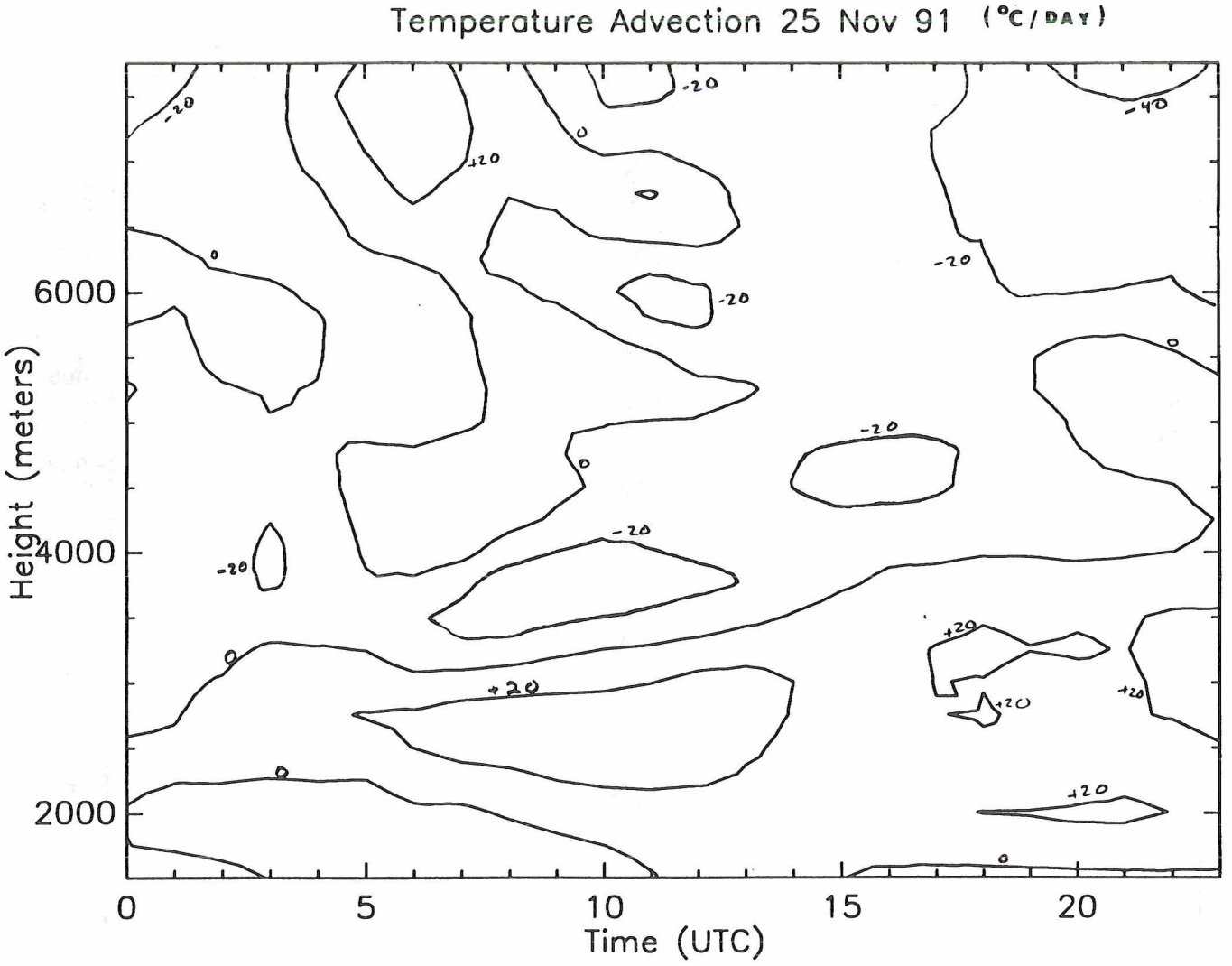

Figure 3.6 - Parsons, KS Temperature Advection

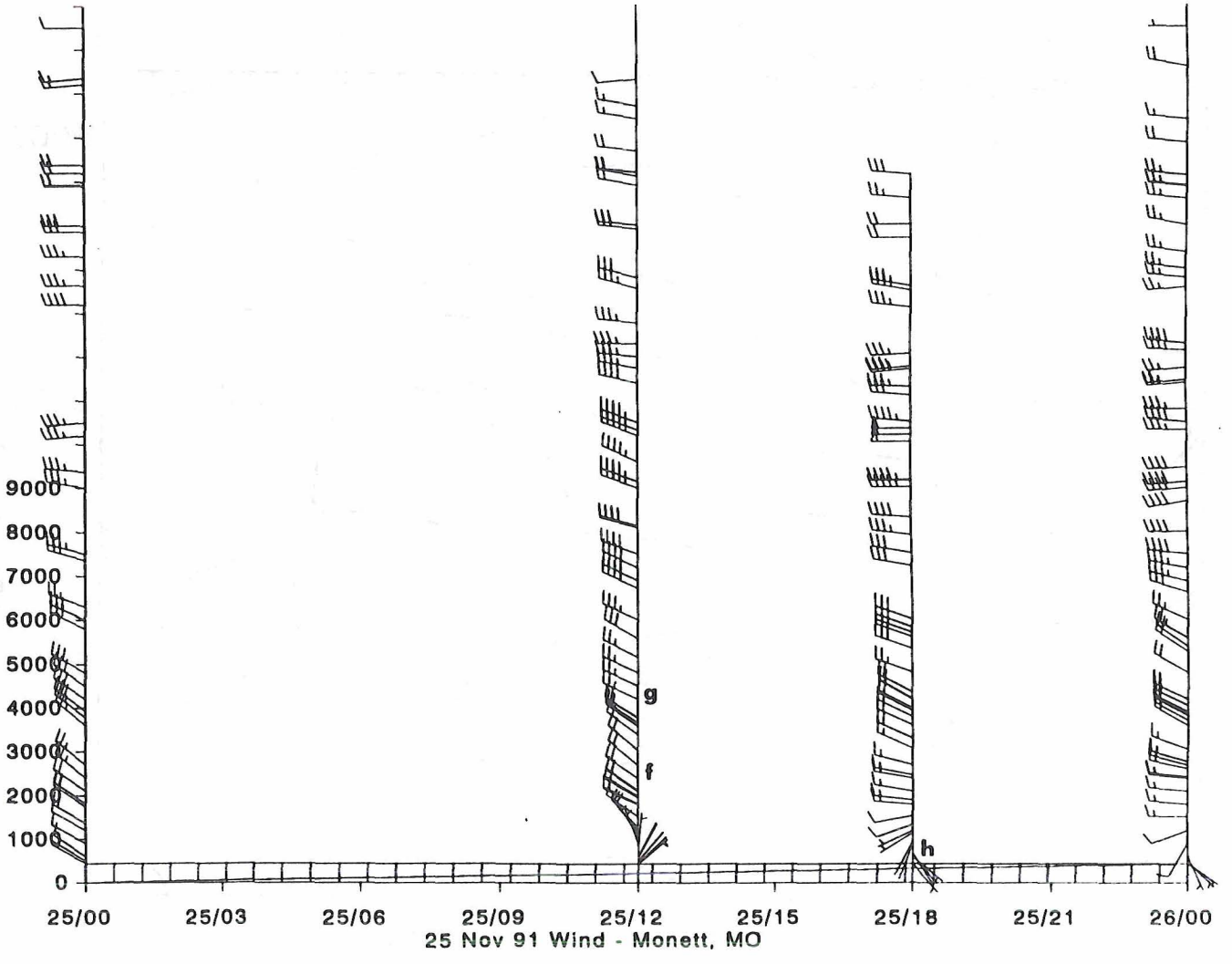

Figure 3.5 - 25 November Monett, MO Wind. Point "f" denotes veering winds. Point "g" denotes backing winds. Point "h" denotes veering winds extending to the surface.

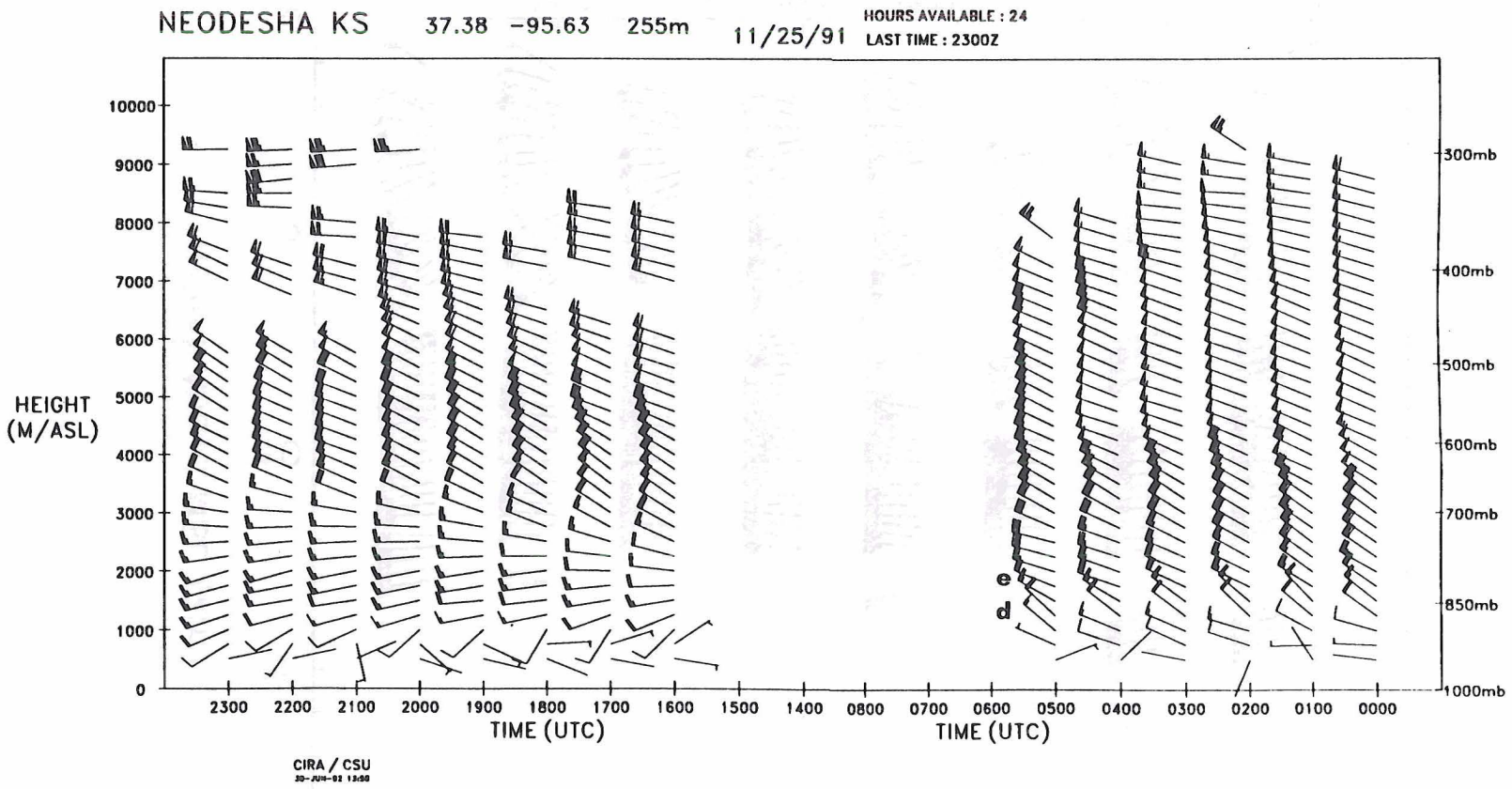

Figure 3.4 - Neodesha, KS Wind Profiler 25 November. Point "d" denotes veering winds. Point "e" denotes backing winds.

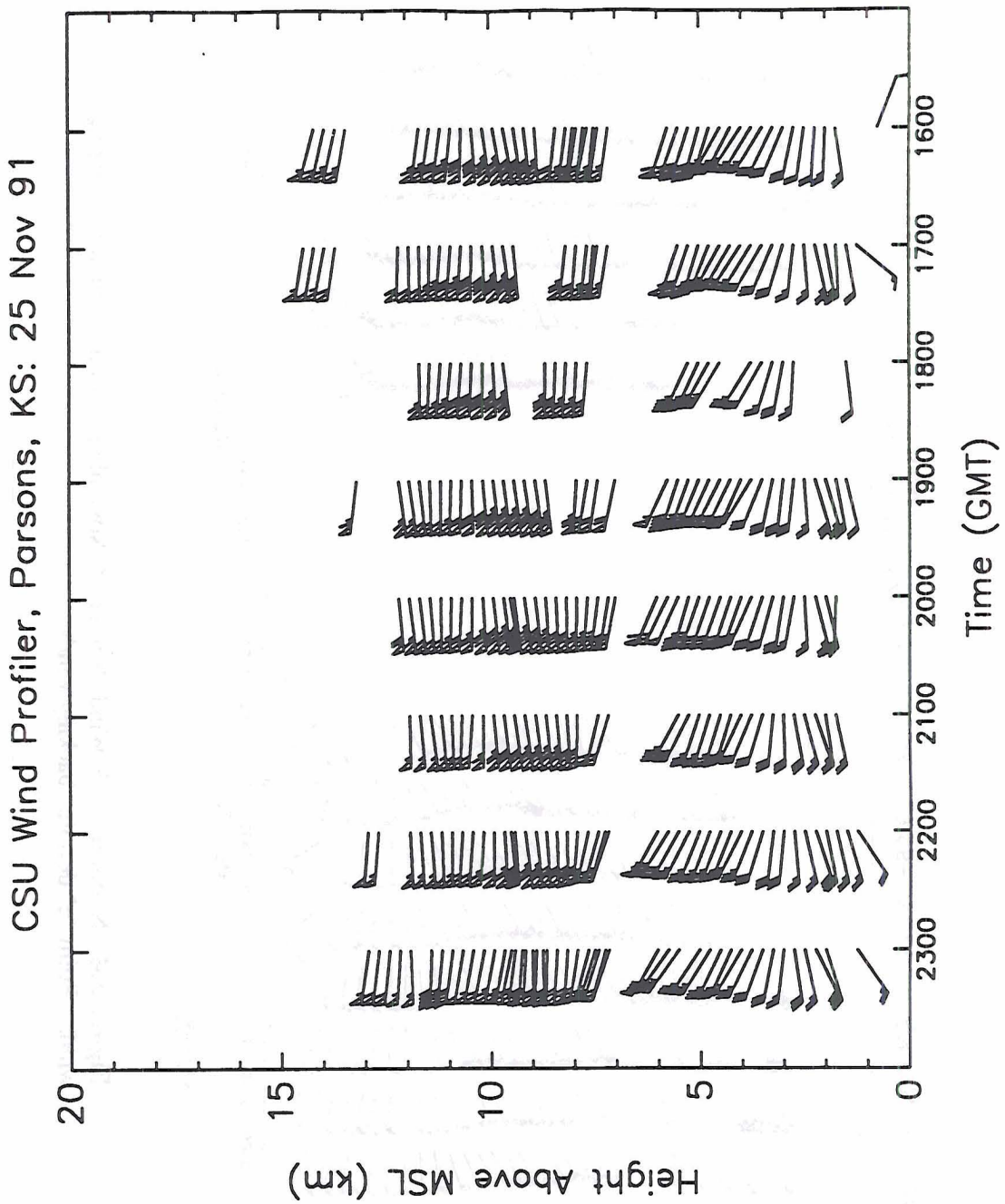

Figure 3.3 - Parsons, KS Wind 1600 UTC - 2300 UTC 25 November

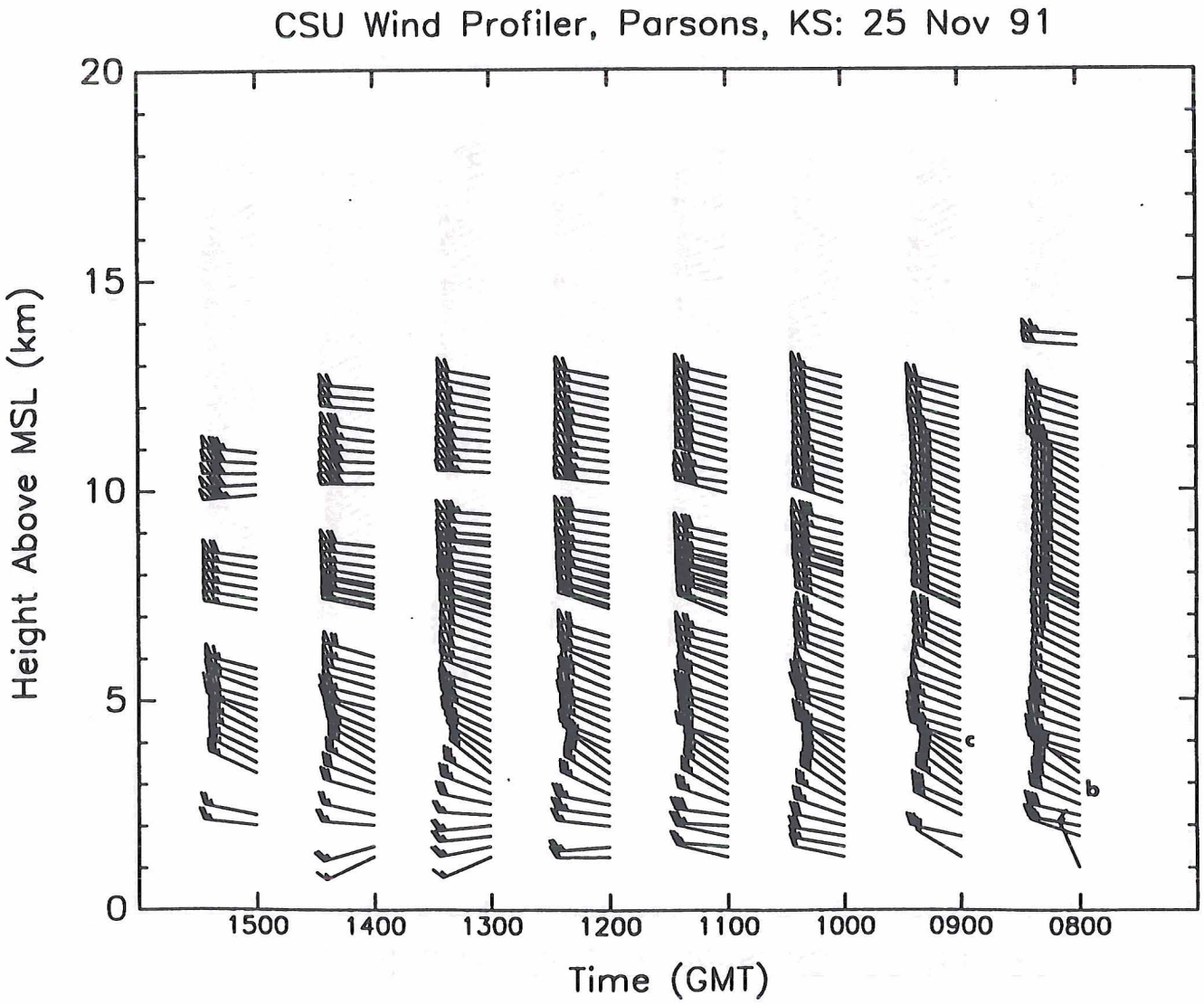

Figure 3.2 - Parsons, KS Wind 0800 UTC - 1500 UTC 25 November. Point "b" denotes widening layer of veering winds. Point "c" denotes cold advection.

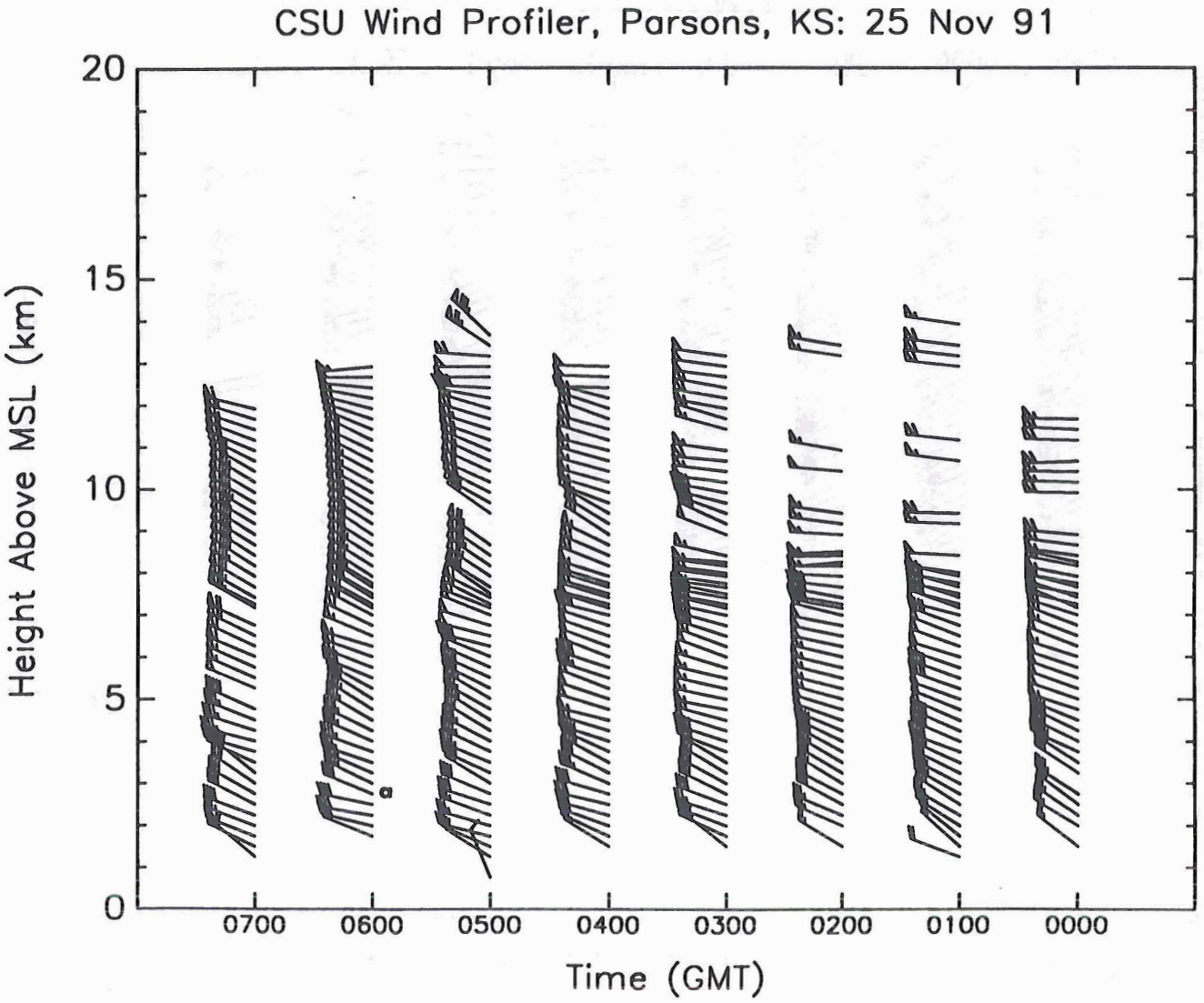

Figure 3.1 - Parsons, KS Wind 0000 UTC - 0700 UTC 25 November. Point "a" denotes warm advection.

be explained solely in terms of horizontal shear and deformation. Based on the thermal wind relationship

$$f\frac{\partial v_g}{\partial z} = \frac{g}{\theta_o} k \times \nabla\theta \qquad (20)$$

the horizontal deformation field induces a geostrophic wind, which will increase in strength as $\nabla\theta$ increases. In order to maintain geostrophic balance, an ageostrophic wind will occur. The coriolis force will deflect this ageostrophic wind, causing a secondary circulation. The secondary circulation has the characteristics of a vertical deformation field. This vertical deformation field concentrates the temperature gradient, and leads to rapid frontogenesis.

A study of frontogenesis on 25 November shows weak frontogenesis centered over eastern Kansas at 1200 UTC at 850 mb (Figure 3.23), with weak frontolysis behind the warm front in northern Texas. By 1800 UTC, the region of maximum frontogenesis at 850 mb has strengthened and moved eastward (Figure 3.24). As previously discussed, the synoptic situation leading to this warm front is dominated by the geostrophic flow around the Hudson bay cyclone, and the advection of low level, milder air from the southwest. This strongly argues for horizontal deformation to be the primary cause of warm frontogenesis. This frontogenesis is a low-level phenomena. At 700 mb, no frontogenesis is observed at 1200 UTC (Figure 3.25) or at 1800 UTC (Figure 3.26).

$$\cos 2\beta < \pm\frac{\delta}{D} \tag{17}$$

In synoptic situations, the deformation is an order of magnitude greater than the divergence, so (17) reduces to

$$\beta < \pm 45^{o} \tag{18}$$

Using quasigeostrophic theory, Equation (15) can also be expressed in terms of Q-vectors (Hoskins and Pedder, 1980)

$$F = \frac{\theta_o}{g}\frac{1}{|\nabla_p \theta|}(\nabla_p \theta \cdot Q) \tag{19}$$

where θ_o = *reference potential temperature*

This implies we have a frontogenetic condition when the Q-vector field and the temperature gradient are aligned in the same direction.

Hoskins and Bretherton (1972) identified four basic flow configurations which can increase horizontal temperature gradients in the atmosphere, and therefore lead to frontogenesis: (1) horizontal deformation, (2) horizontal shear, (3) vertical deformation, (4) differential vertical motion.

Horizontal deformation at low levels is an important mechanism for the development of warm fronts (Hoskins and Bretherton, 1972). For idealized warm frontogenesis, this is shown in Figure 3.22. There is a deformation field centered near point A with an axis of contraction nearly orthogonal to the isotherms. This deformation field causes strong warm advection south of point A, and weak warm advection north of point A. Therefore, the temperature gradient is concentrated in the vicinity of point A.

The rapid frontogenesis observed in extratropical, synoptic scale systems often results in a temperature gradient concentrated in a zone of ~50 km. This cannot usually

trajectory is shown in Figure 3.21. A vertical velocity averaging 0.9 cm/s occurred along this trajectory. This cold advected air trajectory correlates well with the cyclonic geostrophic wind around the strong upper level low located near Hudson Bay.

In summary, the air in the warm and cold advection zones originated in distinctly different geographic areas. The rising motion in the low level, warm advection zone, coupled with rising motion in the mid-level, cold advection zone caused a lifting of the warm advection - cold advection boundary with time. This is consistent with the wind profiler derived temperature advection profile, shown in Figure 3.6.

3.7 Frontogenesis

Frontogenesis is defined as the time rate of change of the magnitude of the temperature gradient on an isobaric surface:

$$F = \frac{d}{dt} |\nabla_p \theta| \tag{15}$$

Assuming adiabatic motion, such that the local variation in θ is entirely due to advection, it can be shown that (Petterssen, 1956)

$$F = \frac{1}{2}|\nabla_p \theta|(D \cos 2\beta - \delta) \tag{16}$$

where D = *deformation*

β = *angle between the axis of dilation and the isotherms*

δ = *divergence*

Positive values of F are indicative of frontogenesis. This implies we have a frontogenetic condition when

approximately 1.4 km over Parsons, KS (Figure 3.18). For the isentropic surface representative of cold advection, the 300 K surface was chosen. At 1800 UTC, this 300 K surface was at approximately 4.5 km over Parsons, KS (Figure 3.19).

The trajectory of air on these isentropic surfaces between 1200 UTC and 1800 UTC 25 November was calculated using the procedure summarized below. The details of the trajectory calculations are given in Appendix A. The 1800 UTC Parsons, KS wind velocities and Montgomery stream function values are used as the "final values". Moving "upstream", on the isentropic surface along the streamlines for three hours, the location of the air at 1500 UTC was calculated. The air is then followed upstream for three more hours, using the Montgomery streamlines from the 1200 UTC isentropic analyses (Figure 3.20 and Figure 3.21) resulting in a hypothesized origin for the Parsons, KS 1800 UTC air six hours earlier. The wind velocities and Montgomery stream function values at the hypothesized origin are interpolated from nearby 1200 UTC soundings. The hypothesized origin is tested, and modified as necessary by assuring that equations (13) and (14) are satisfied. The trajectory is further tested by verifying that potential vorticity and mixing ratio are conserved between the origin at 1200 UTC and Parsons, KS at 1800 UTC.

Using the 285 K isentropic surface, the air in the warm advection zone moved from approximately 193 km WSW of Parsons at 1200 UTC, to Parsons at 1800 UTC. This trajectory is shown in Figure 3.20. An upward motion averaging 0.9 cm/s occurred along this trajectory. This warm advected air trajectory closely corresponds with the motion of air associated with the movement of the warm front from southwest to northeast.

Using the 300 K isentropic surface, the air in the cold advection zone moved from approximately 402 km WNW of Parsons at 1200 UTC, to Parsons at 1800 UTC. This

$$\int \left.\frac{\partial M}{\partial t}\right|_\theta dt = (M_2 - M_1)|_\theta + \left.\left(\frac{V_2^2 - V_1^2}{2}\right)\right|_\theta + \overline{\frac{\partial}{\partial \theta}\left(\frac{V^2}{2}\right)}(\theta_2 - \theta_1) \quad (11)$$

where subscript 1 indicates the initial values and 2 indicates the final values. The first term represents that portion of the change in enthalpy and potential energy of the system that is not converted into kinetic energy. The second and third terms express the total change in kinetic energy of the horizontal wind. The left hand side can be approximated by

$$\int \left.\frac{\partial M}{\partial t}\right|_\theta dt = \frac{\Delta M_1 + \Delta M_2 + 2\Delta M_{mid}}{4} \quad (12)$$

where $\Delta \equiv$ *N-hour difference at a fixed point*

$M_{mid} \equiv$ *Montgomery stream function midway between the initial and final points*

The third term is negligible when the amount of water vapor condensed out is small.

Therefore, a trajectory is constructed, starting with known values of M_2 and V_2, by "working upstream" to an initial point such that the following equations are satisfied:

$$M_2 - M_1 + \frac{V_2^2}{2} - \frac{V_1^2}{2} \simeq \frac{\Delta M_2 + \Delta M_1 + 2\Delta M_{mid}}{4} \quad (13)$$

$$D \simeq \frac{V_2 + V_1}{2}\Delta t \quad (14)$$

where D is the distance traveled in time Δt and all values are on a constant θ surface.

Using Danielsen's (1961) method, isentropic surfaces in the warm and cold advection layers were chosen. For the isentropic surface representative of warm advection, the 285 K surface was chosen. At 1800 UTC, this 285 K surface was at

3.6 Isentropic Trajectory Analysis

Isentropic analysis is a useful technique for analyzing air trajectories when atmospheric processes are overwhelmingly adiabatic, and there is positive static stability along the isentropic surface. Under these conditions, isentropic surfaces are material surfaces, across which there is no exchange of mass.

As previously discussed, the 25 November 91 warm front has a distinct boundary separating low-level warm advection from mid-level cold advection. The presence of these two layers suggests two different air mass source regions.

The method of Danielsen (1961) was used to trace the trajectory history of these two air layers over Parsons, KS. Tracing the trajectory of the air on isentropic surfaces is equivalent to tracing the three-dimensional motion of an infinitesimal open system which has no net mass flux across its boundaries. Danielsen (1961) states that the energy equation for this system is

$$\frac{c_p T}{\theta}\frac{d\theta}{dt} + \left.\frac{\partial M}{\partial t}\right|_\theta = \frac{dM}{dt} + \frac{d}{dt}\left(\frac{V^2}{2}\right) \tag{8}$$

where $M \equiv$ *Montgomery Stream Function* $(c_p T + gz)$

Using the hydrostatic assumption

$$\frac{\partial M}{\partial \theta} = c_p\left(\frac{T}{\theta}\right) \tag{9}$$

and expanding the right hand side gives

$$\left.\frac{\partial M}{\partial t}\right|_\theta = \left.\frac{dM}{dt}\right|_\theta + \frac{d}{dt}\left(\frac{V^2}{2}\right) + \frac{\partial}{\partial \theta}\left(\frac{V^2}{2}\right)\frac{d\theta}{dt} \tag{10}$$

Integrating (10)

km (620 mb), the conditionally unstable air is near saturation. Above 4.0 km, the air is absolutely stable. The boundary between warm and cold advection is located at 4.0 km (620 mb).

Two hours later, the Parsons, KS 2008 UTC rawindsonde sounding (Figure 3.14) shows a layer of conditionally unstable air extending from 1.5 km to 3.6 km (850 to 650 mb). This layer approaches saturation at 3.6 km. A strong temperature inversion occurs above 3.6 km and extends to 4.2 km (600 mb). From 4.2 km to 5.5 km (600 to 510 mb), the air is conditionally unstable, but dry. Above 5.5 km, the air is absolutely stable. The boundary between warm and cold advection has remained at 4.0 km (620 mb).

Thus, the increase in height of the warm advection-cold advection boundary between 1200 UTC and 2000 UTC is associated with a lifting and thinning of the layer of moist, conditionally unstable air. The thinning and lifting of the moist layer can also be observed by comparing the cross section of relative humidity on the Amarillo, TX to Paducah, KY line at 1200 UTC (Figure 3.15). and 1800 UTC (Figure 3.16).

3.5 Vertical Velocity Profile

The time series of vertical motion over Parsons, KS, derived from the vertically-oriented wind profiler beam, is shown in Figure 3.17. A tongue of strong, downward motion occurs from 0000 UTC until 0400 UTC. This downward motion appears to temporarily suppress the warm advection-cold advection boundary by about 0.5 km. Several pockets of low level, upward motion occur at 0500 UTC and 0700 UTC. Strong downward motion occurs at low levels between 0800 UTC and 1500 UTC and is replaced by upward motion after 1500 UTC. Both the downward and upward motion occur entirely within the warm advection zone. At higher levels, weak upward motion occurs sporadically within the cold advection zone.

lower levels, and overestimation of cold advection at higher levels. Neither diabatic heating (or cooling) or adiabatic vertical motion are sufficient to explain this disagreement. The boundary separating warm and cold advection, rising from 3 to 4 km between 1000 UTC to 2200 UTC, is a consistent feature of both methods of observation.

3.4 Interactions Between Warm and Cold Advection Zones

The upper surface of the warm frontal zone marks the boundary between warm and cold air advection. As the temperature gradient across this interface increases, a decrease in stability would be expected to result. Thus, a change in the height of the warm advection-cold advection boundary should be associated with a change in the height of an unstable air layer.

The sounding from the Monett, MO 1200 UTC rawindsonde is shown in Figure 3.11. A layer of moist, conditionally unstable air is present from 2.0 km to 3.6 km (800 mb to 650 mb), becoming nearly saturated at 3.6 km. Above 3.6 km (650 mb), the air is absolutely stable. The boundary between warm and cold advection is at 3.3 km (680 mb).

Three hours later, the Parsons, KS 1512 UTC sounding (Figure 3.12) shows the moist, conditionally unstable air has been replaced by a layer of dry, absolutely unstable air from 2.3 km to 2.8 km (780 mb to 720 mb). A moist, stable layer now exists from 2.8 km to 3.0 km (720 to 700 mb). A layer of near-saturated, conditionally unstable air extends from 3.0 to 3.6 km (700 to 650 mb). Just above 3.6 km (650 mb), the air becomes absolutely stable. The boundary between warm and cold advection has risen to 3.7 km (640 mb).

By 1800 UTC, the Monett, MO 1800 UTC sounding (Figure 3.13) shows dry, conditionally unstable air from 1.8 km to 2.7 km (810 to 720 mb). Above 2.7 km, to 4.0

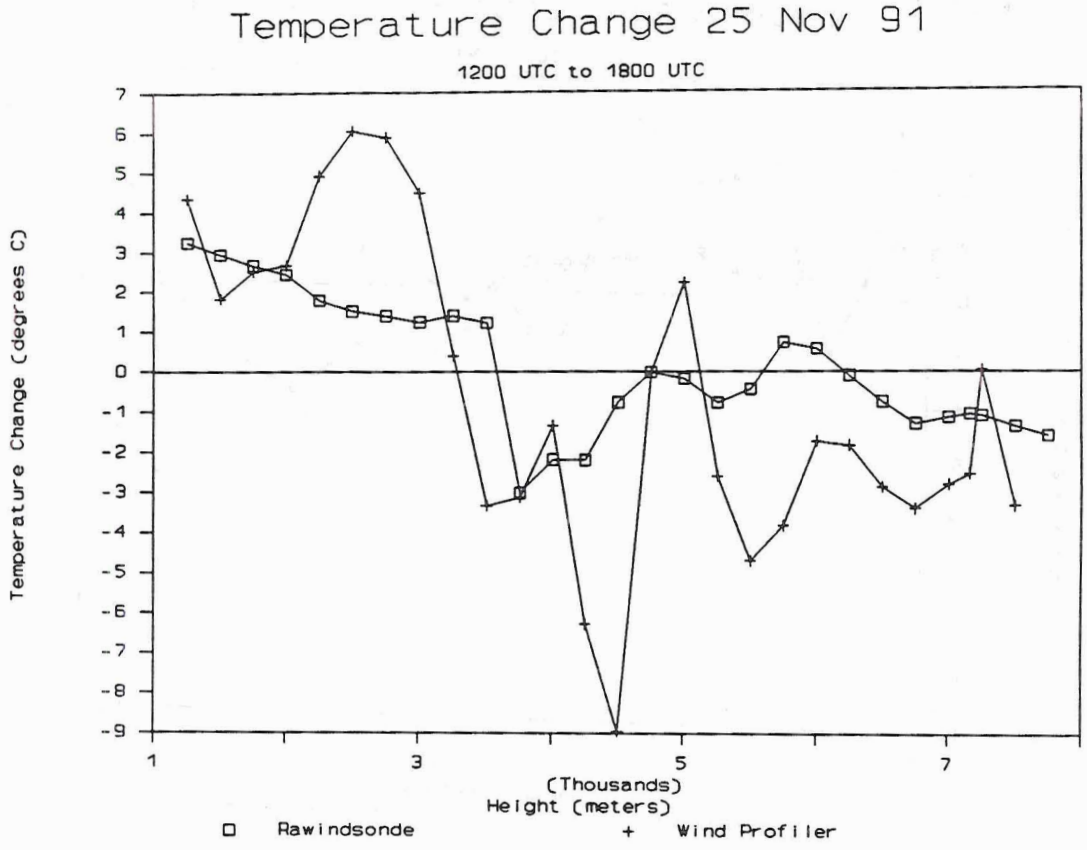

Figure 3.9 - 1200 UTC to 1800 UTC Temperature Change

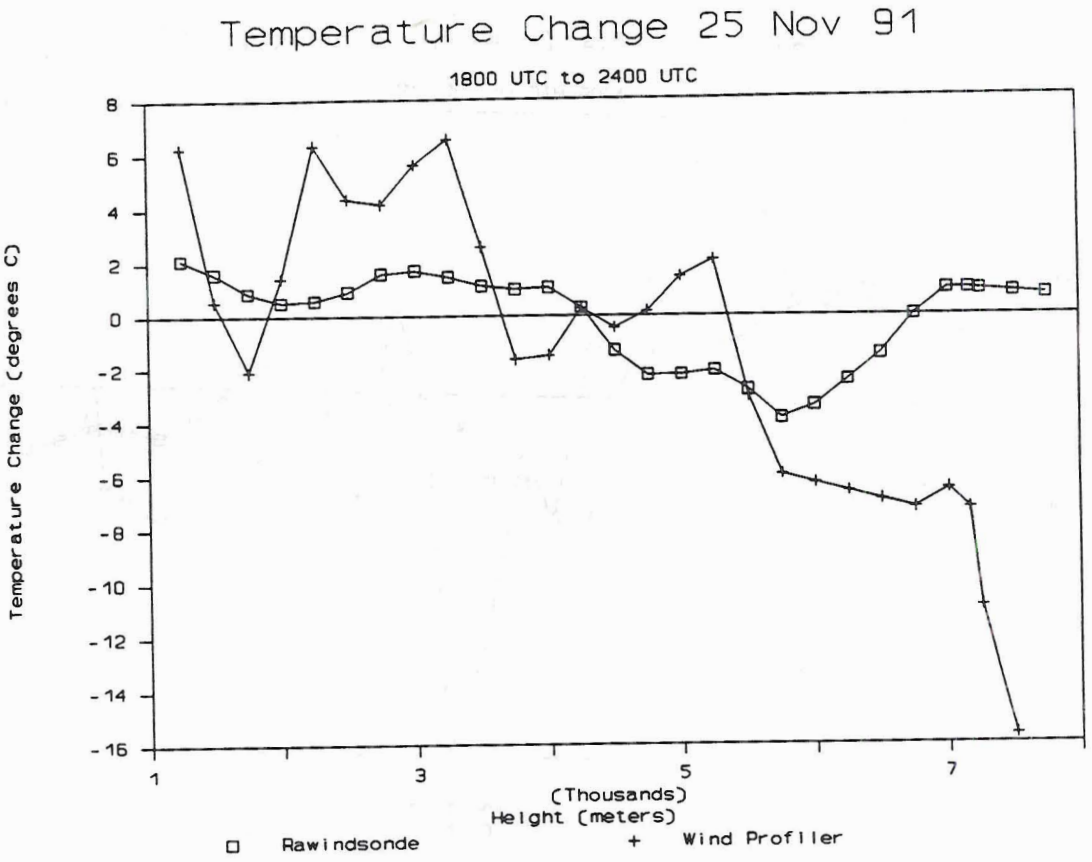

Figure 3.10 - 1800 UTC to 2400 UTC Temperature Change

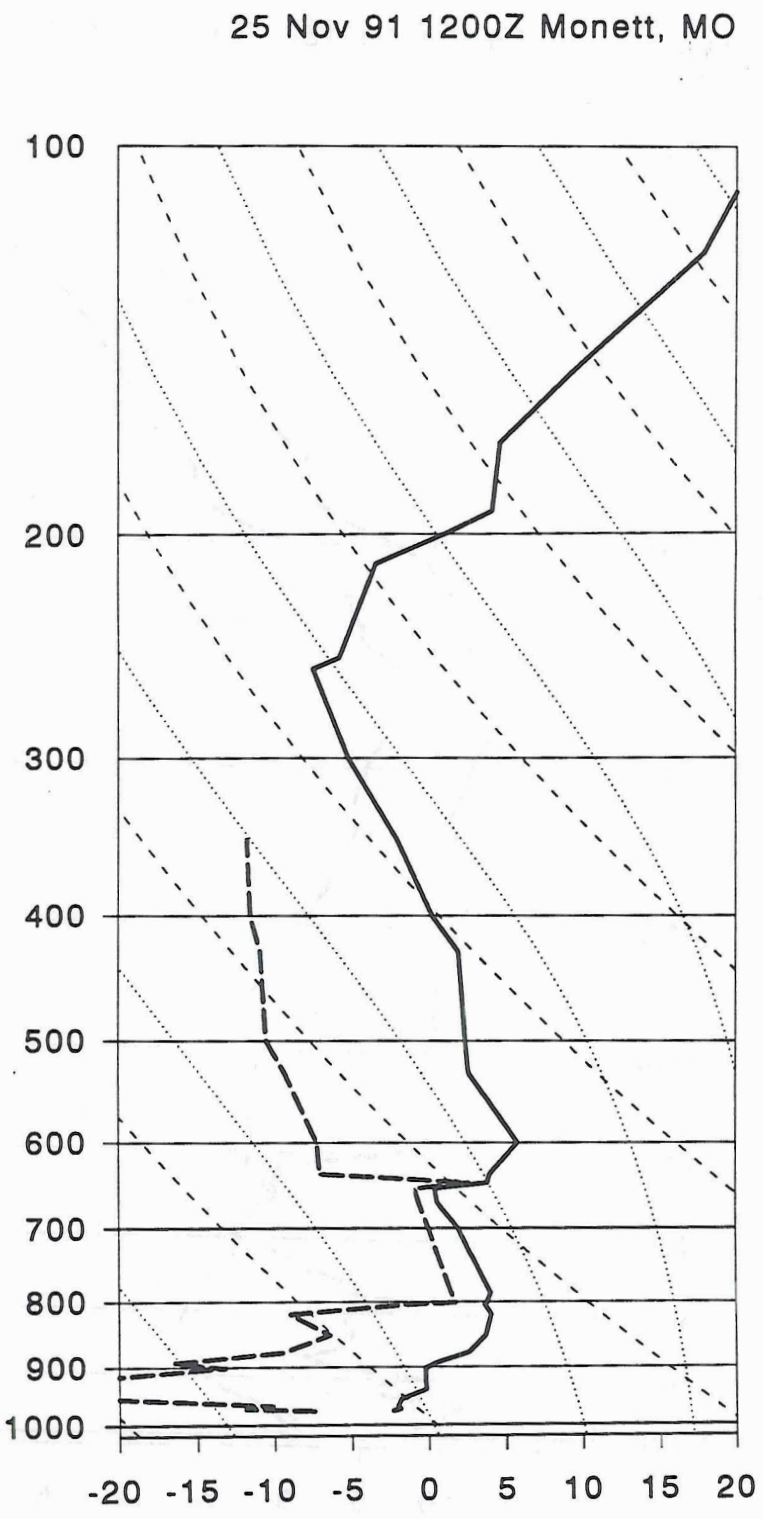

Figure 3.11 - Monett, MO Sounding 1200 UTC

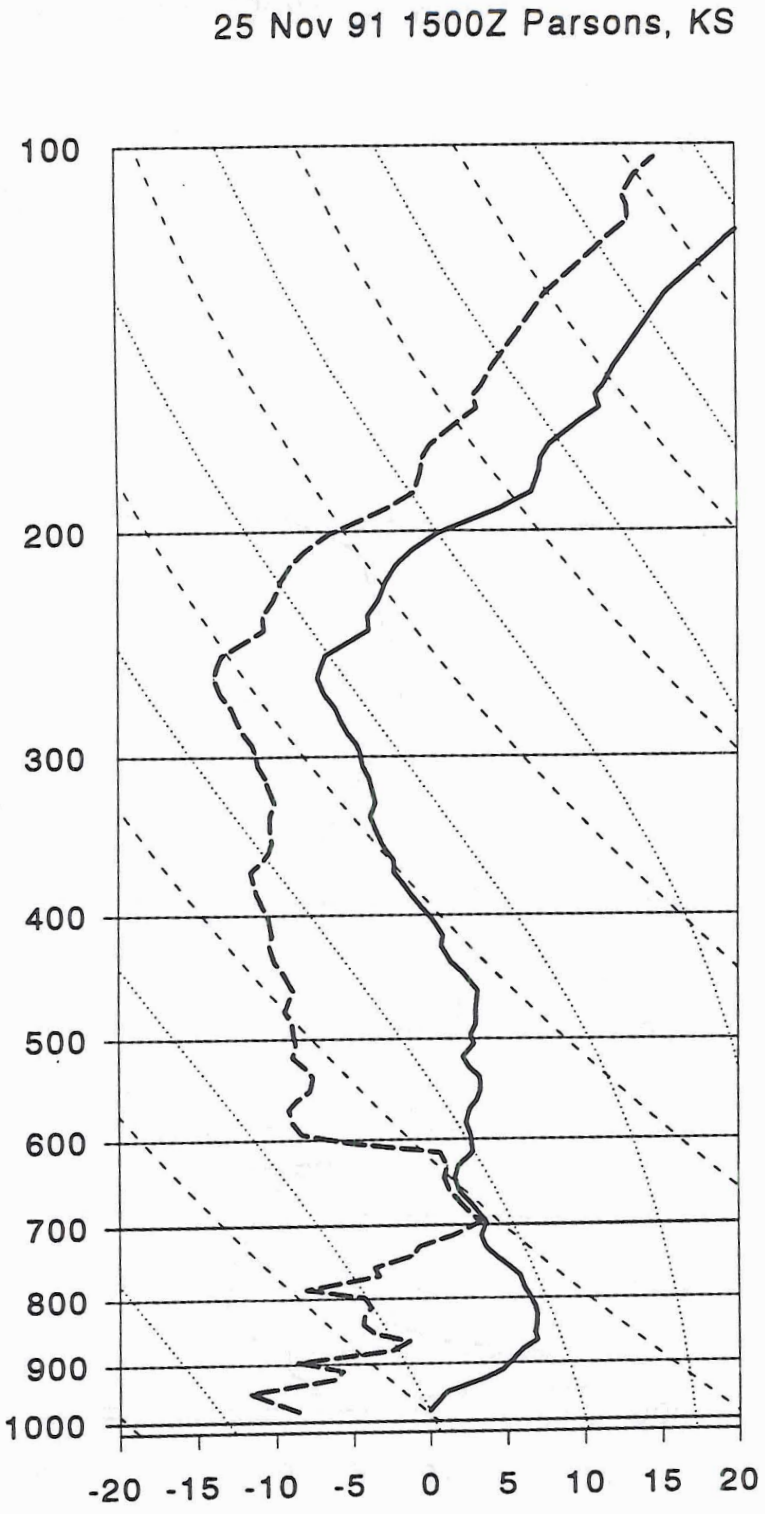

Figure 3.12 - Parsons, KS Sounding 1512 UTC

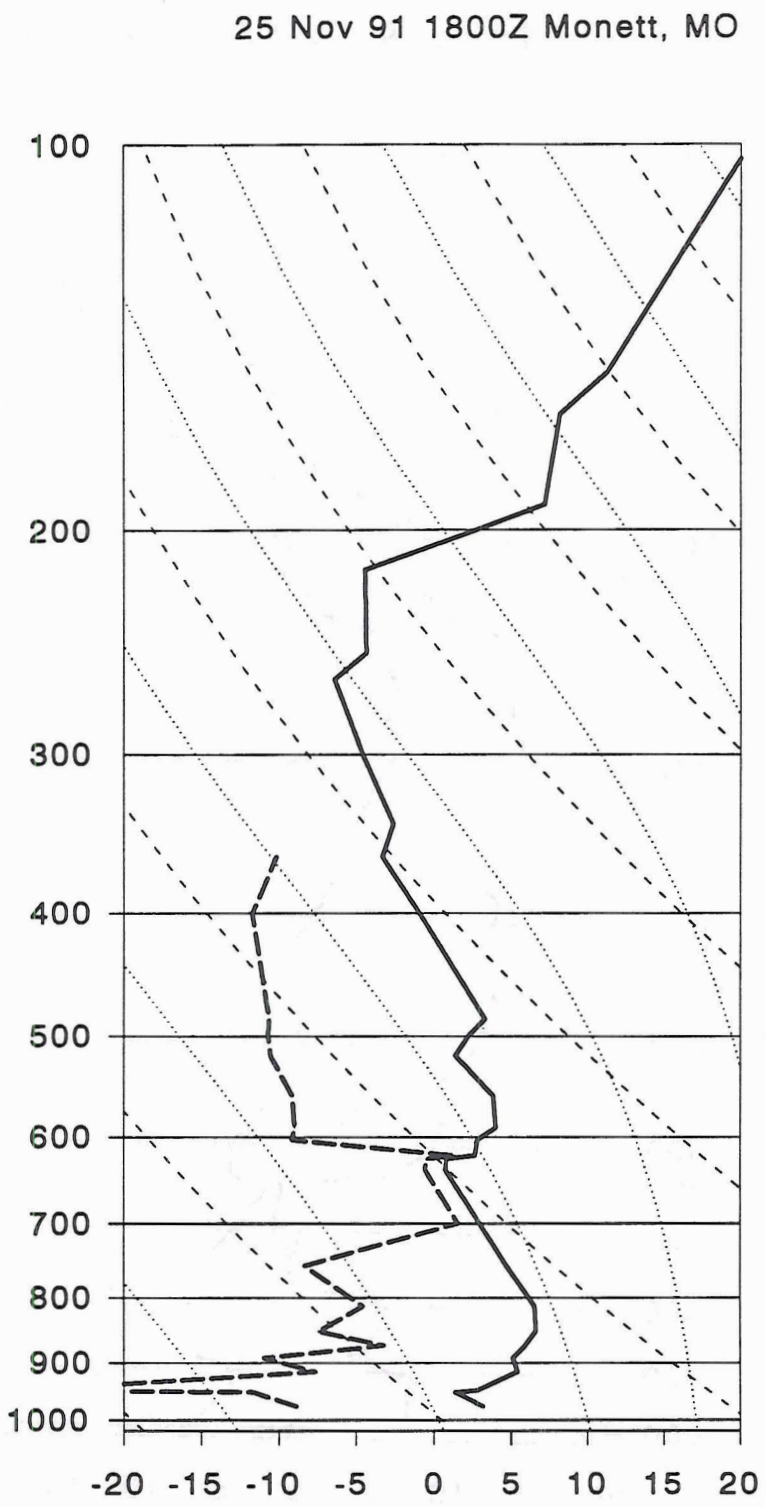

Figure 3.13 - Monett, MO Sounding 1800 UTC

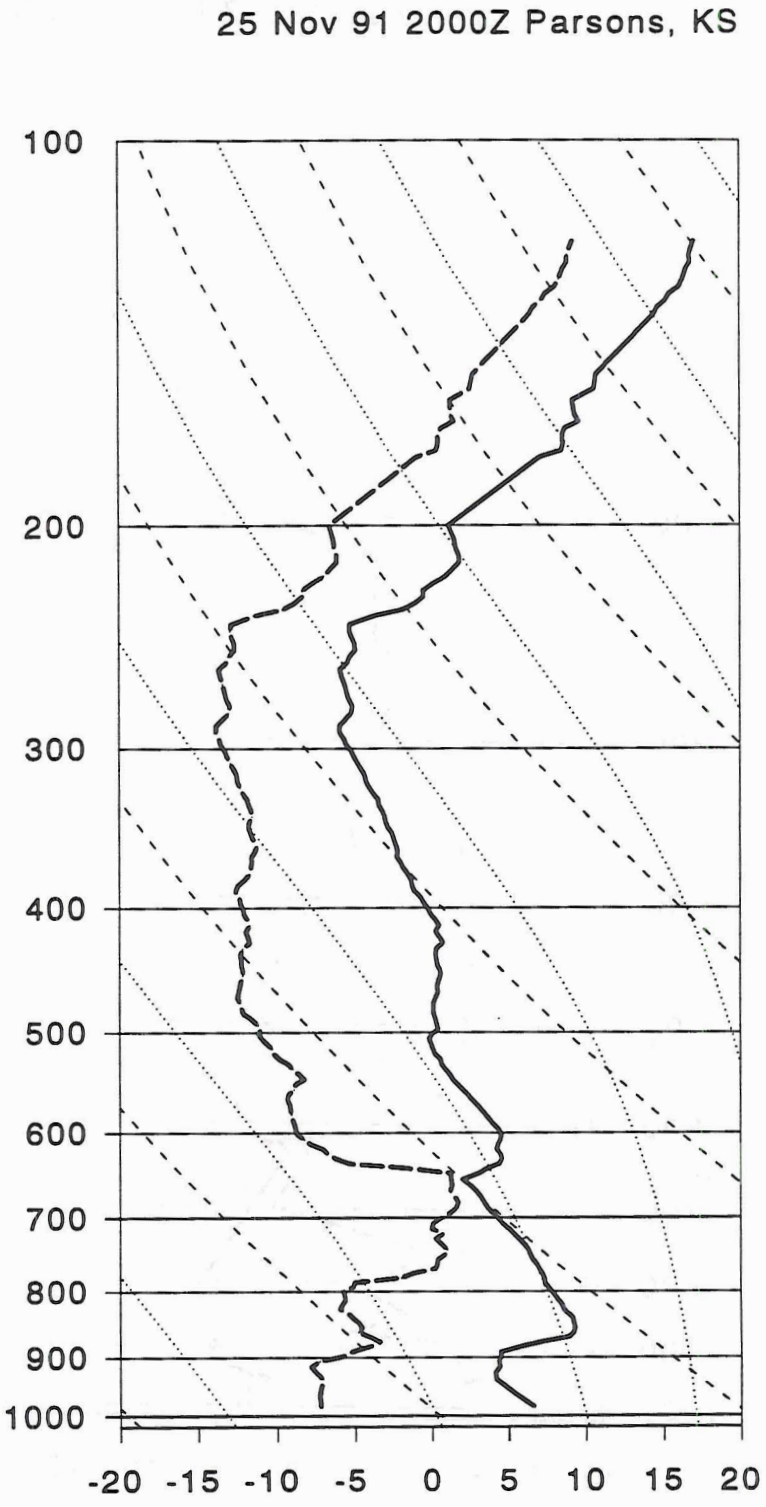

Figure 3.14 - Parsons, KS Sounding 2008 UTC

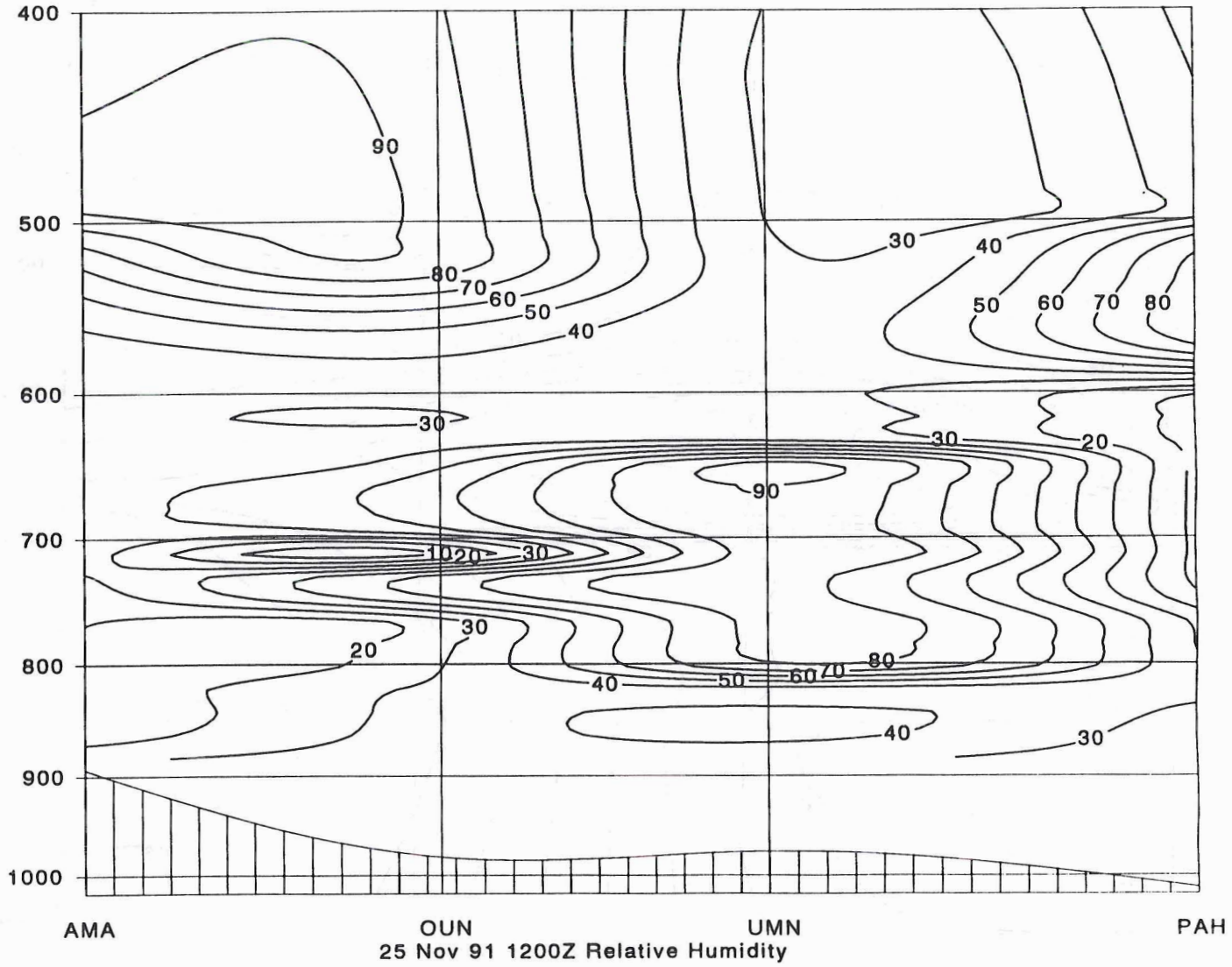

Figure 3.15 - Relative Humidity Cross Section 1200 UTC

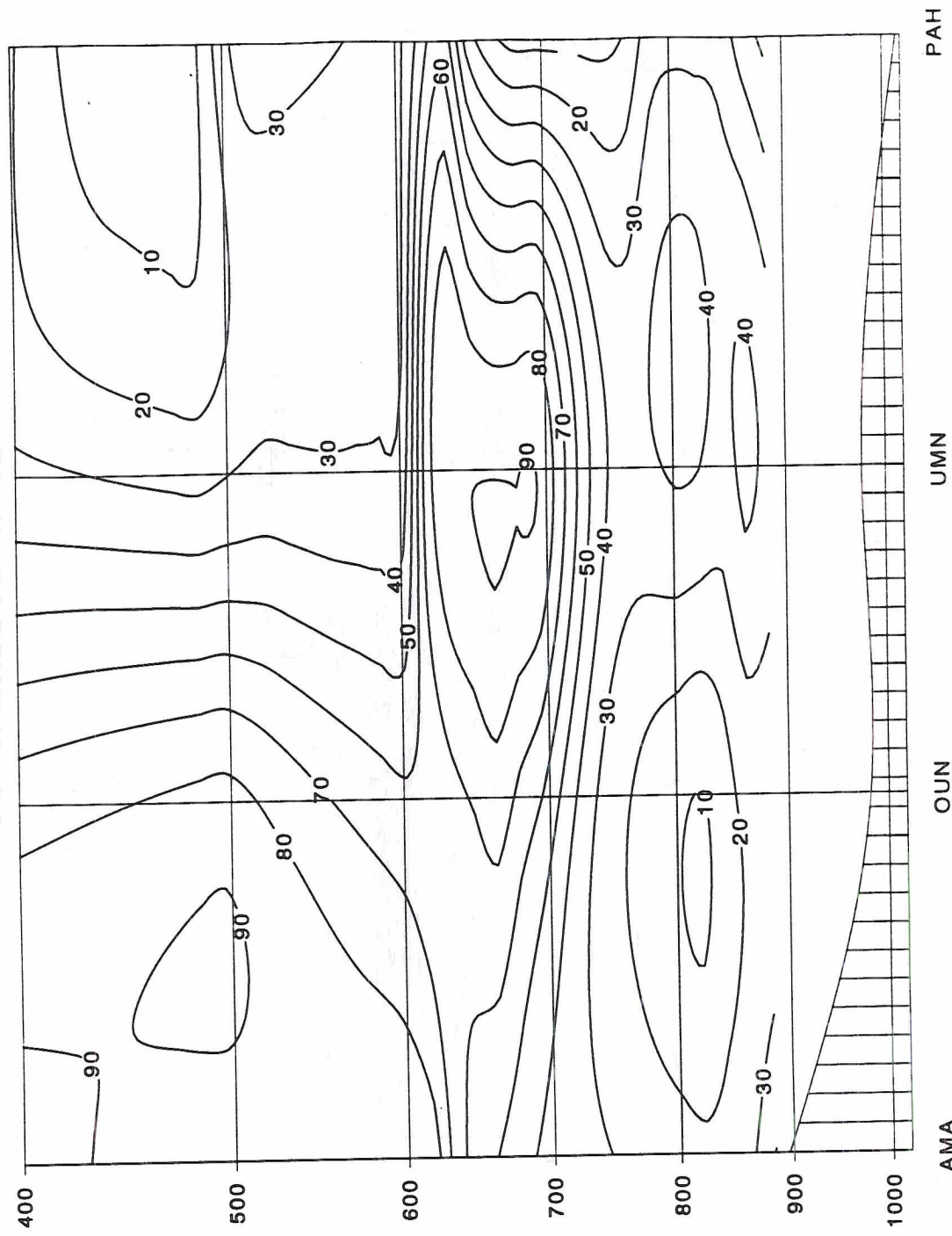

Figure 3.16 - Relative Humidity Cross Section 1800 UTC

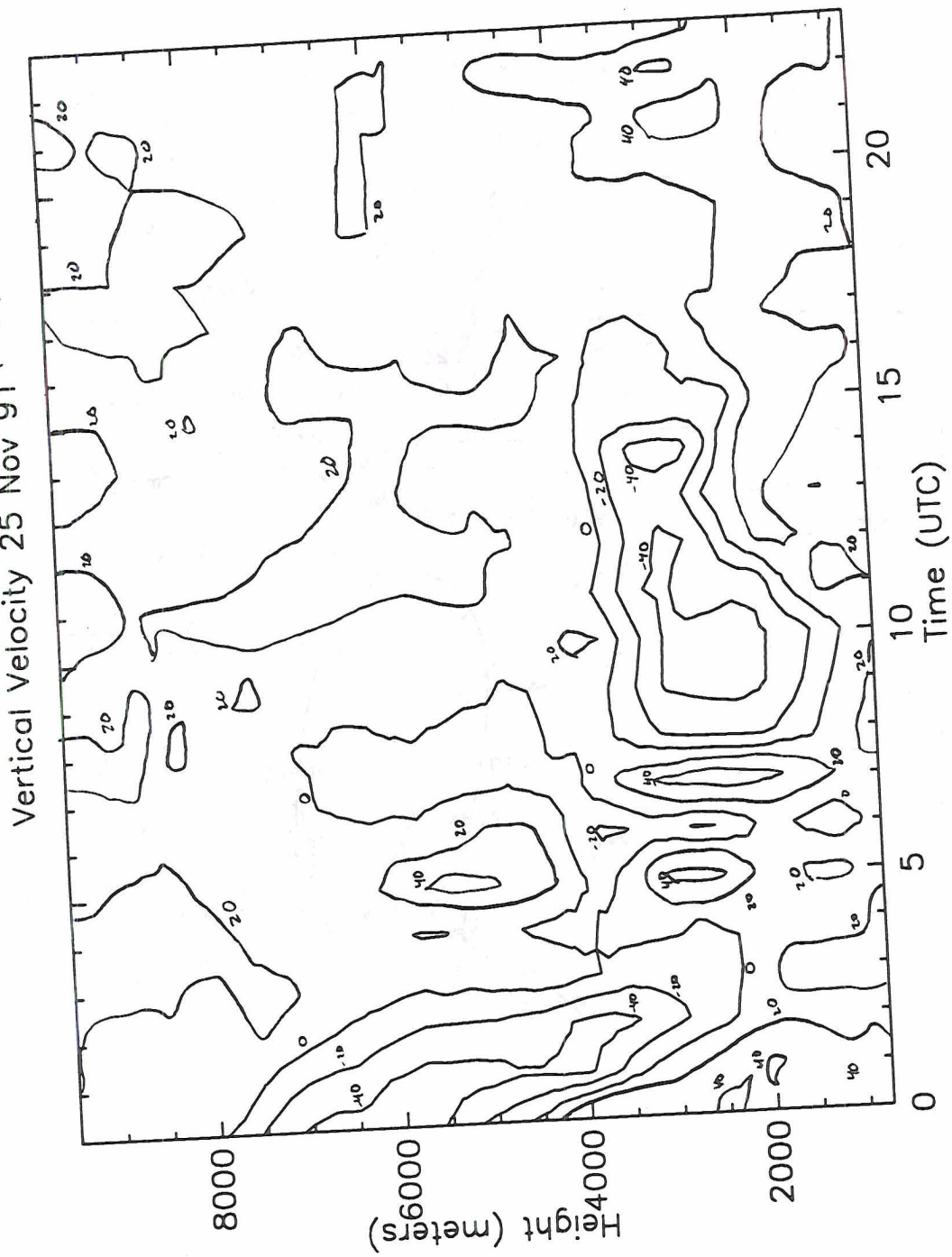

Figure 3.17 - Parsons, KS Vertical Velocity (cm s^{-1})

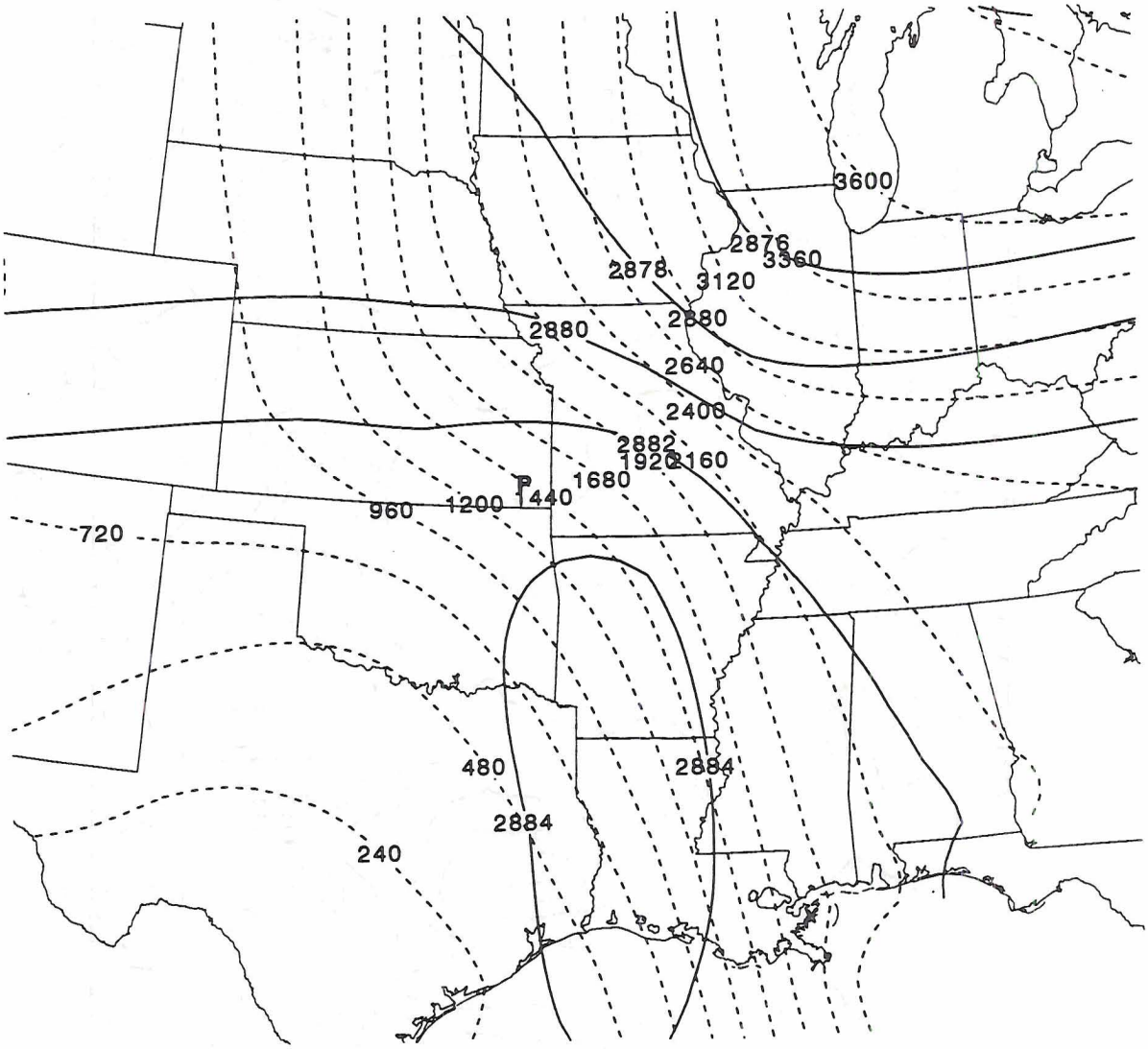

Figure 3.18 - 1800 UTC 25 November 285 K Isentropic Analysis. Solid lines are Montgomery stream function in 10^2 m^2s^{-2}. Dashed lines are height in meters. Point "P" is Parsons, KS.

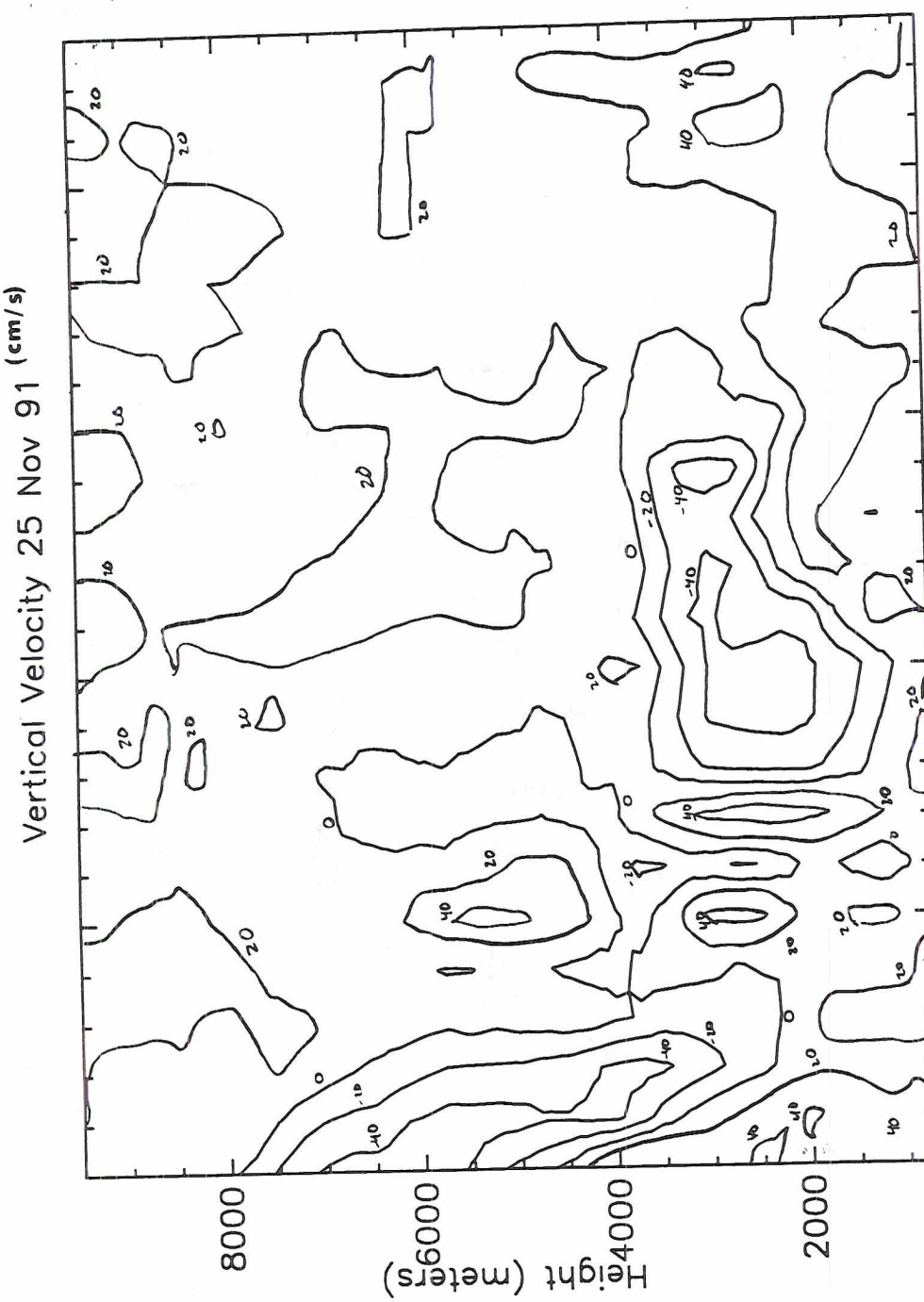

Figure 3.17 - Parsons, KS Vertical Velocity (cm s^{-1})

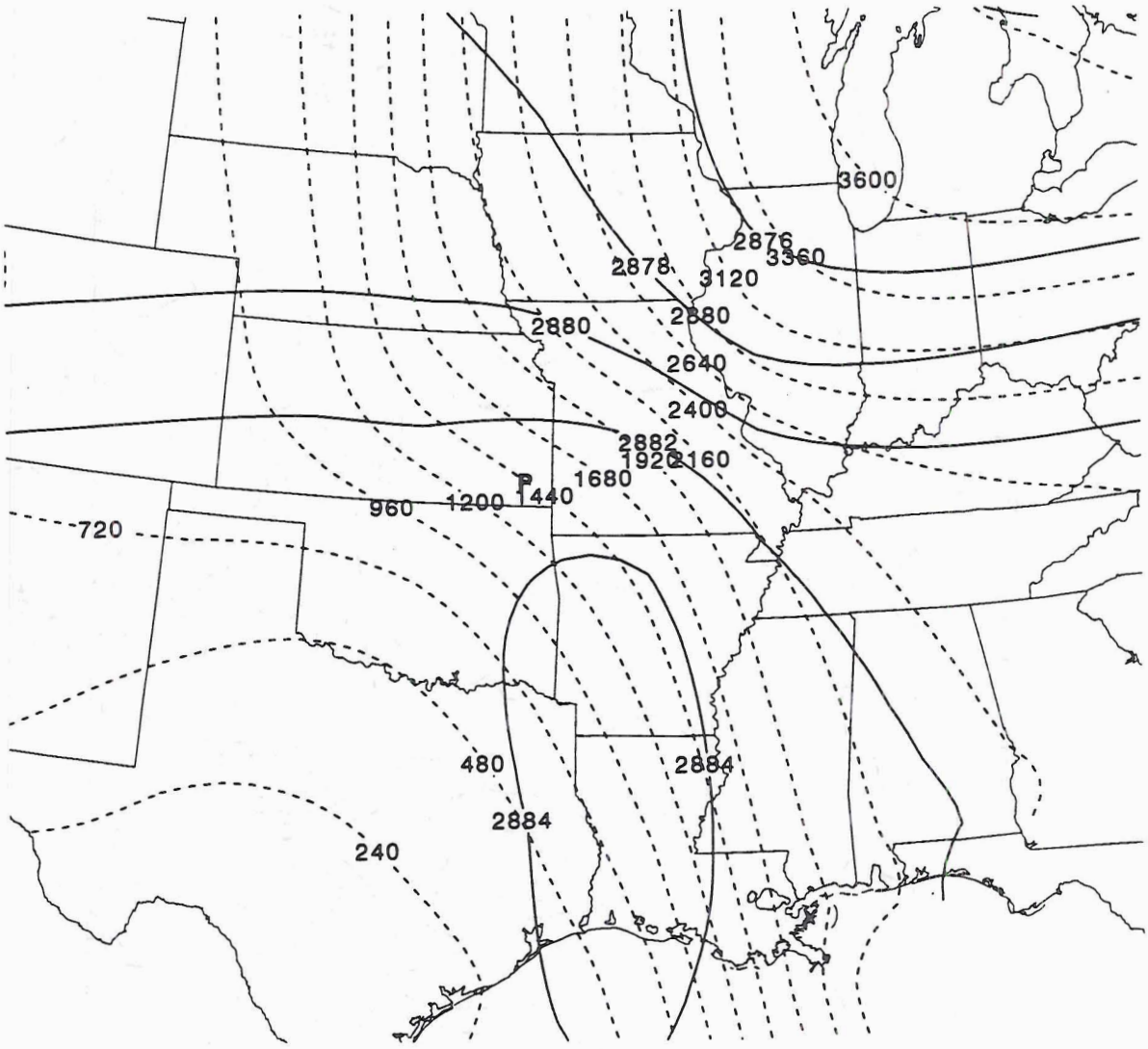

Figure 3.18 - 1800 UTC 25 November 285 K Isentropic Analysis. Solid lines are Montgomery stream function in 10^2 m^2s^{-2}. Dashed lines are height in meters. Point "P" is Parsons, KS.

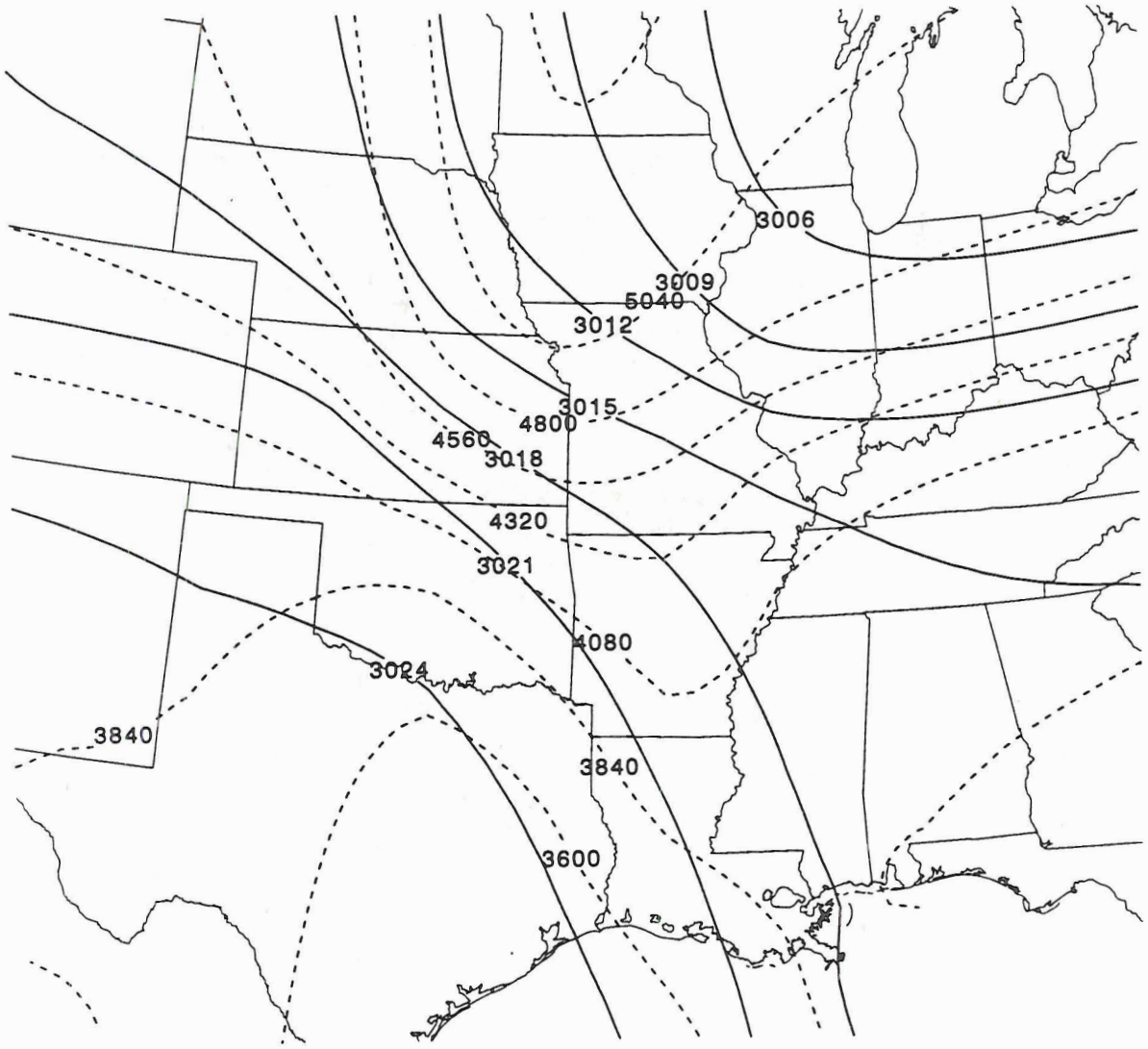

Figure 3.19 - 1800 UTC 25 November 300 K Isentropic Analysis. Solid lines are Montgomery stream function in 10^2 m^2s^{-2}. Dashed lines are height in meters.

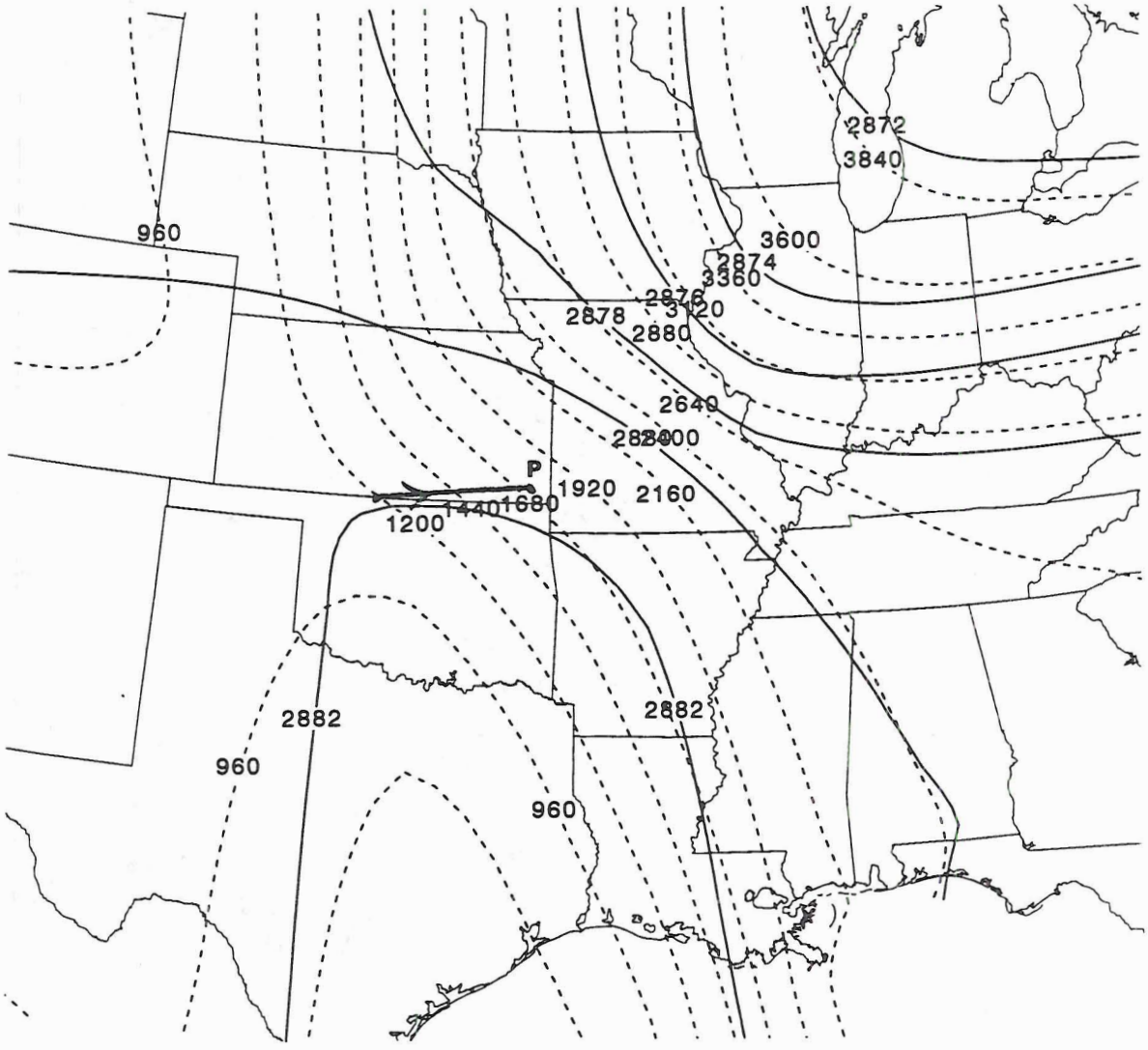

Figure 3.20 - 1200 UTC 25 November 285 K Isentropic Analysis. Solid lines are Montgomery stream function in 10^2 m^2s^{-2}. Dashed lines are height in meters. Point "P" is Parsons, KS.

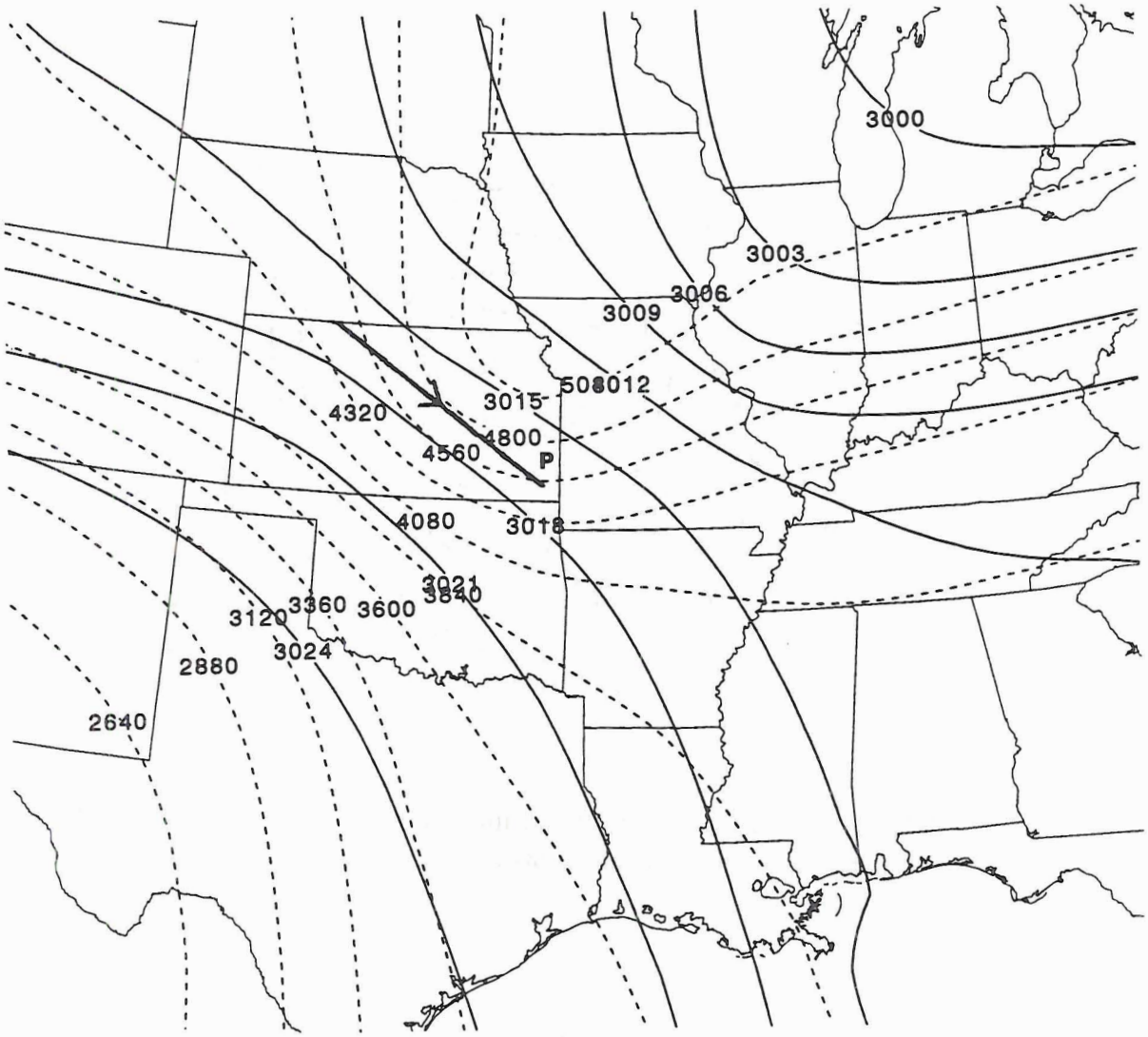

Figure 3.21 - 1200 UTC 25 November 300 K Isentropic Analysis. Solid lines are Montgomery stream function in 10^2 m^2s^{-2}. Dashed lines are height in meters. Point "P" is Parsons, KS.

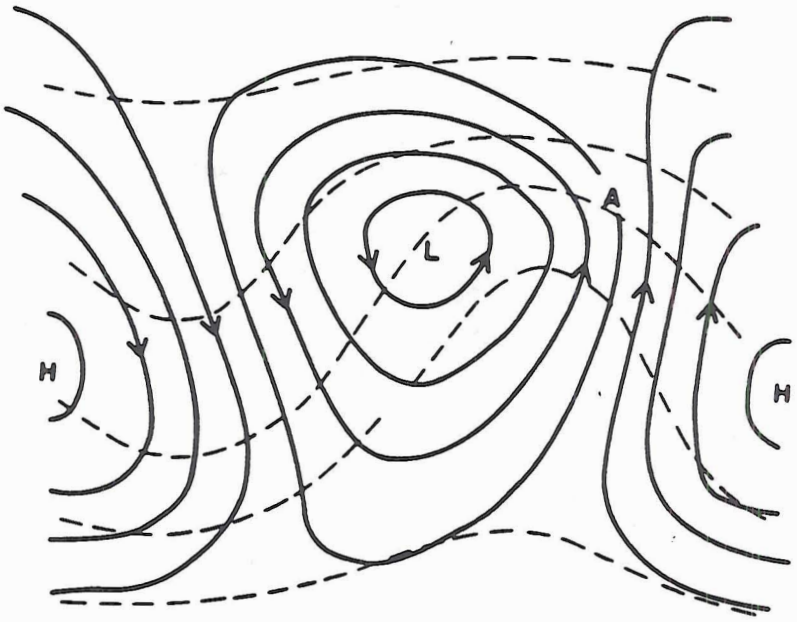

Schematic surface isobars (solid lines) and isotherms (dashed lines) for a baroclinic wave disturbance.

Figure 3.22 - Idealized Warm Frontogenesis. Point "A" denotes area of warm frontogenesis. (from Hoskins and Bretherton, 1972)

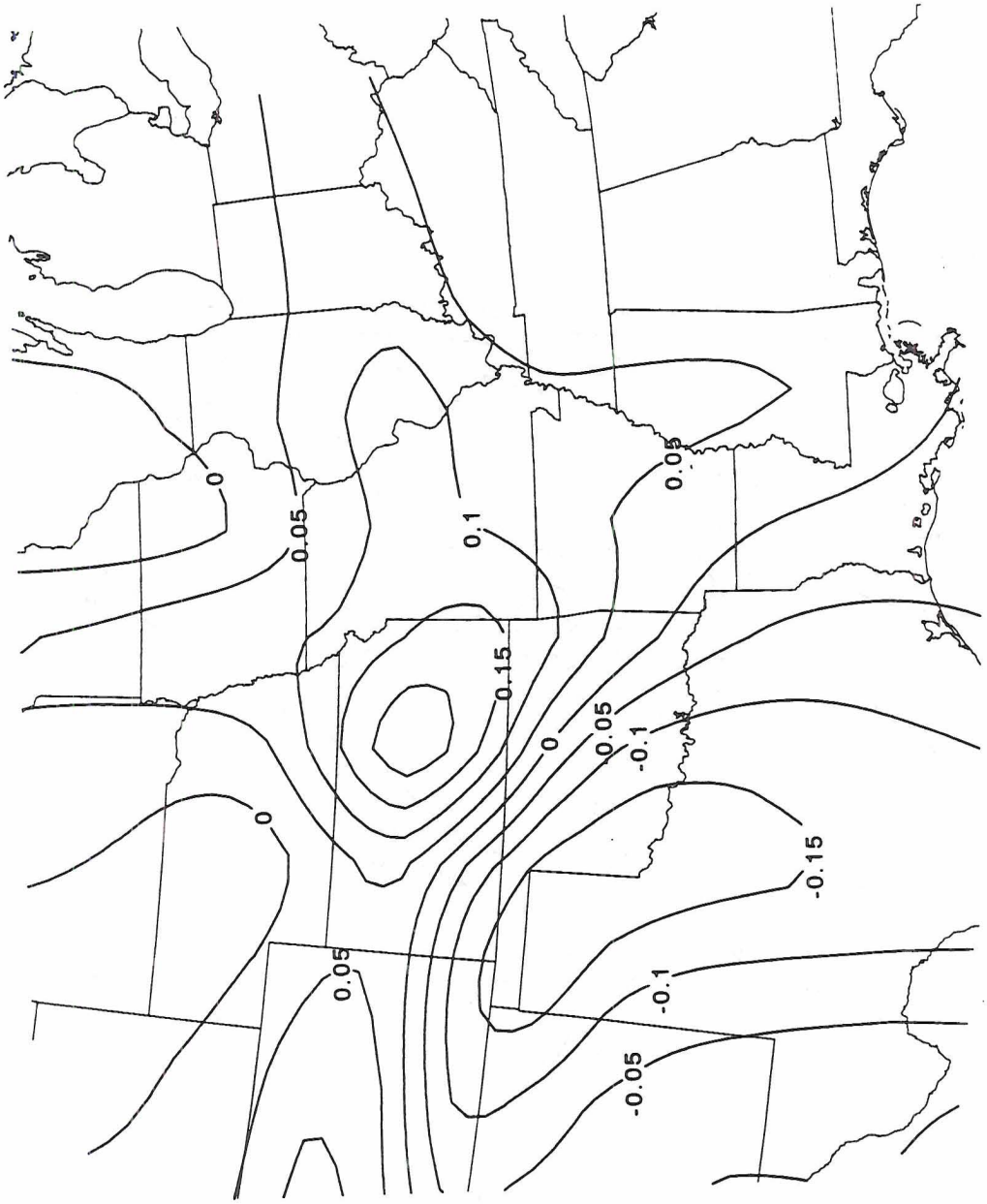

Figure 3.23 - 1200 UTC 25 November 850 mb Frontogenesis. Solid lines are frontogenesis in °C/100 km/3 hours.

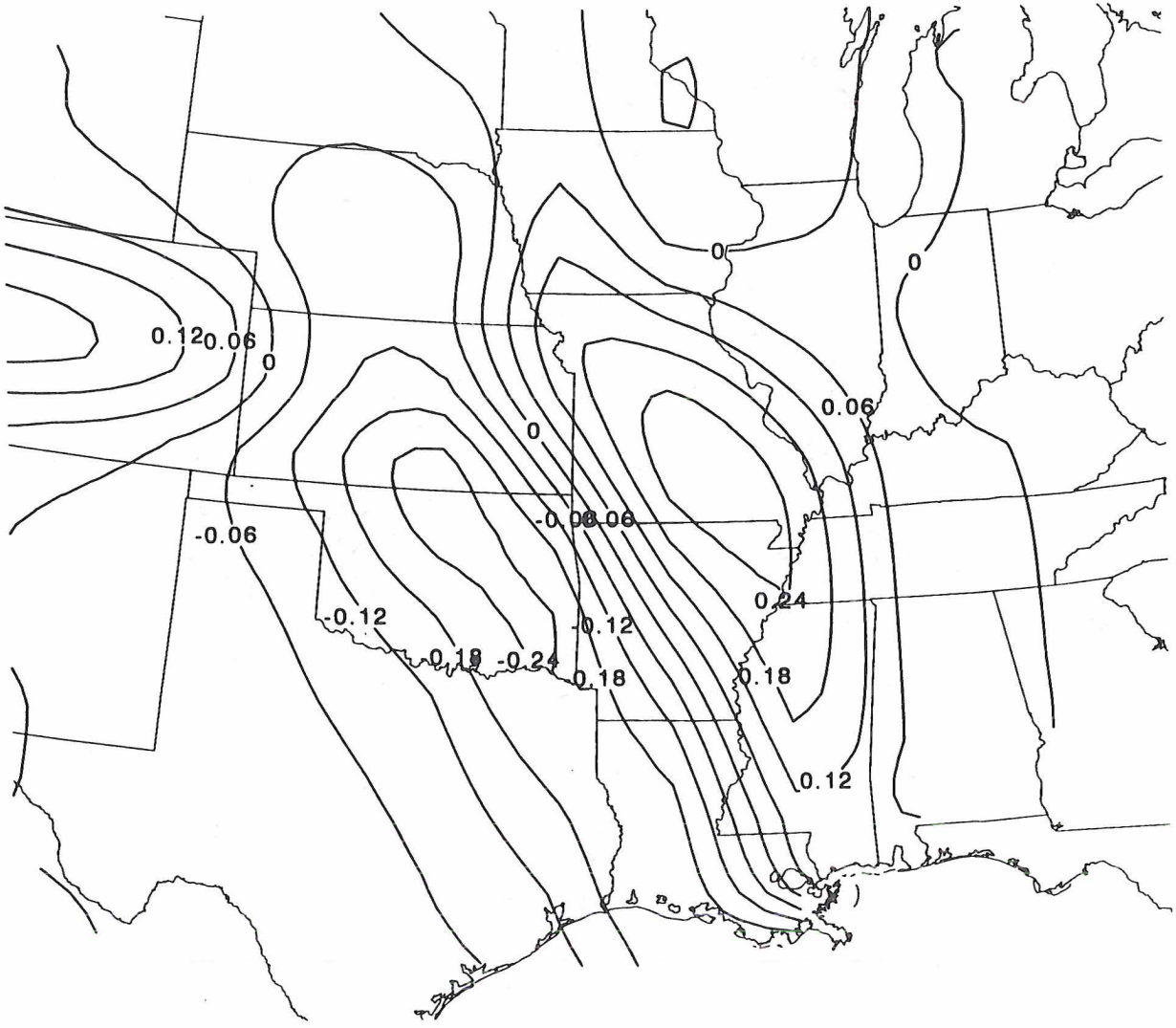

Figure 3.24 - 1800 UTC 25 November 850 mb Frontogenesis. Solid lines are frontogenesis in °C/100 km/3 hours.

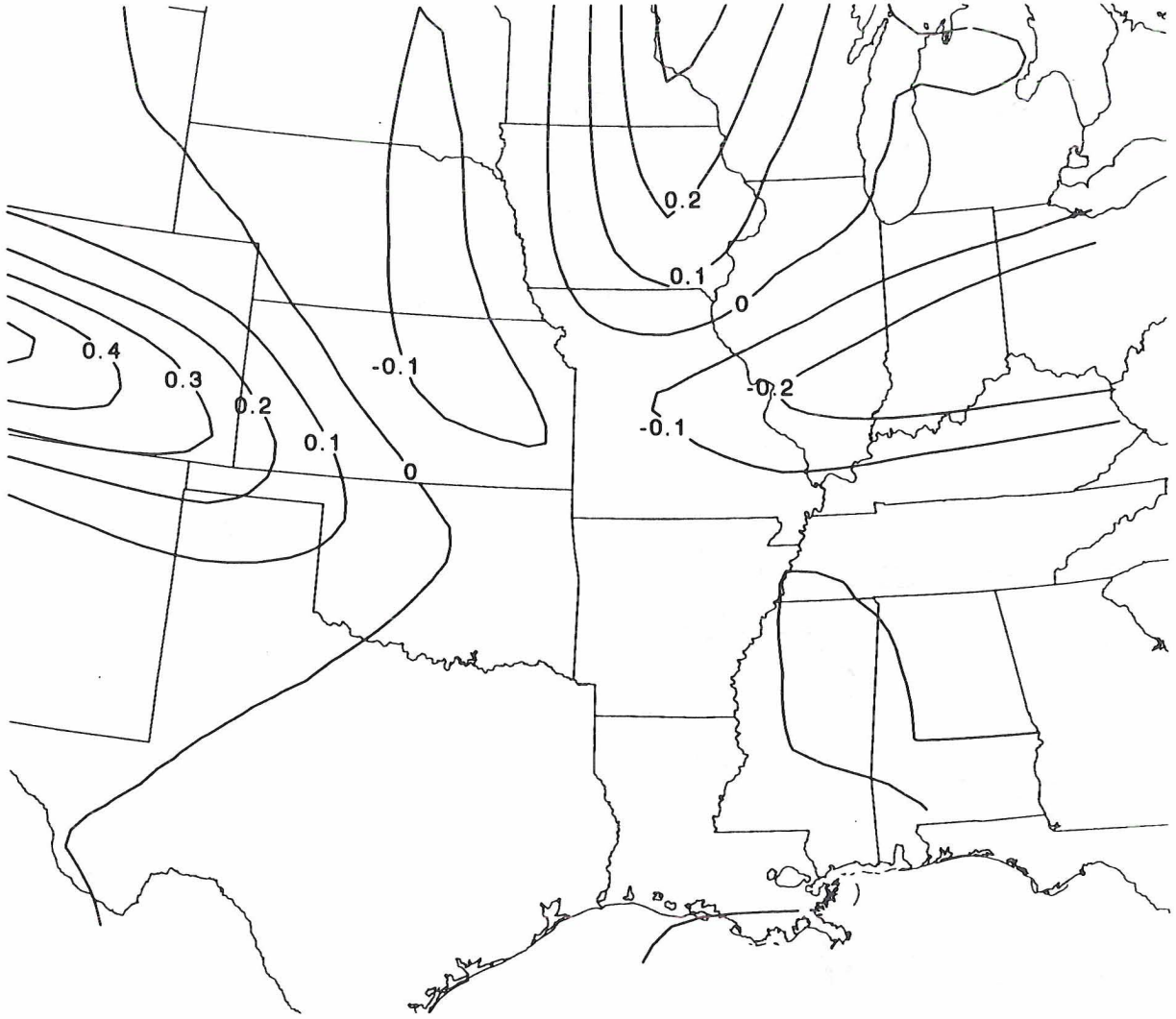

Figure 3.25 - 1200 UTC 25 November 700 mb Frontogenesis. Solid lines are frontogenesis in °C/100 km/3 hours.

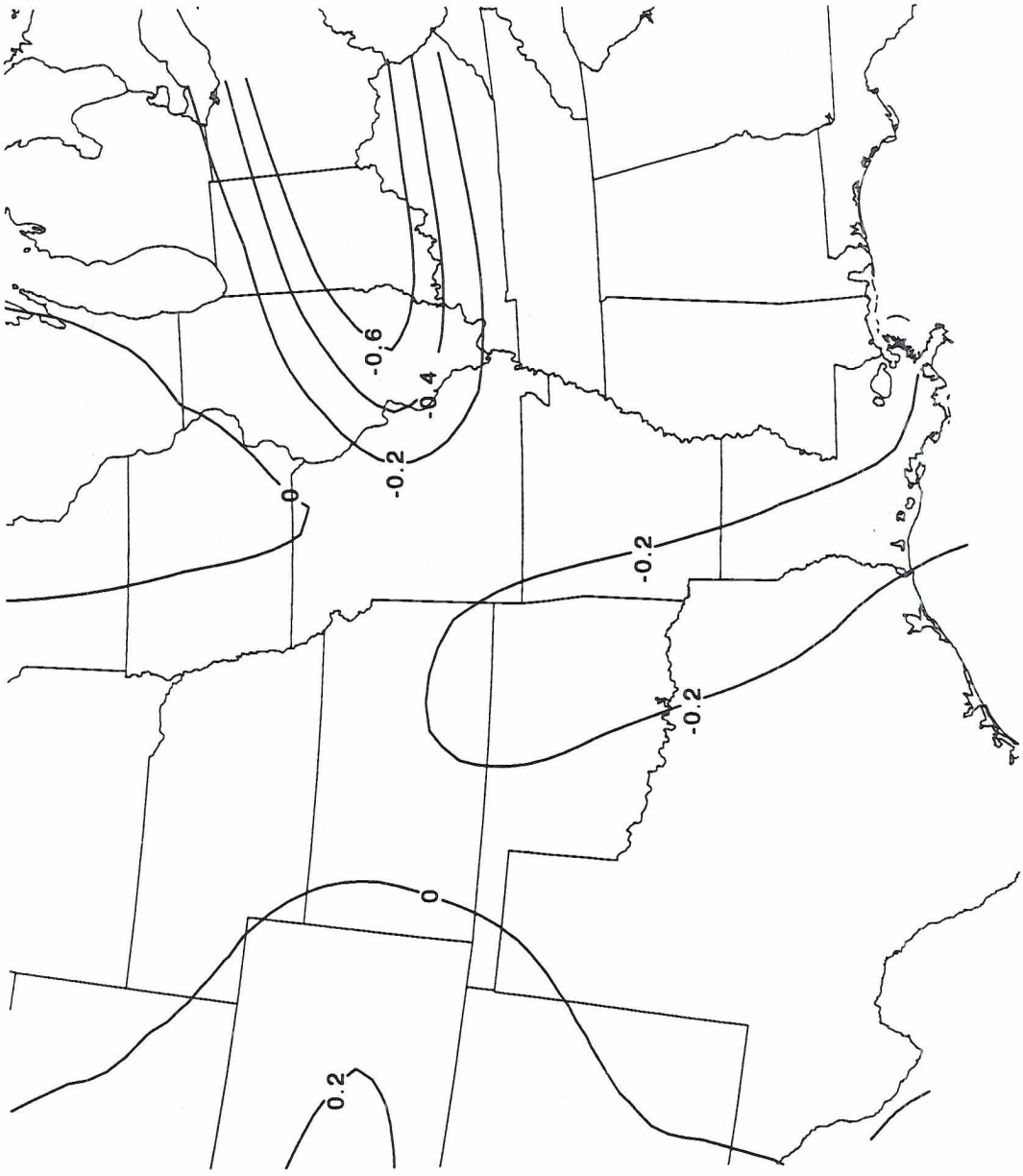

Figure 3.26 - 1800 UTC 25 November 700 mb Frontogenesis. Solid lines are frontogenesis in °C/100 km/3 hours.

4 DISCUSSION AND CONCLUSIONS

4.1 Three-Dimensional Structure of the Parsons, KS Warm Front

Using the analysis described in Section 3, it is now possible to develop a picture of the 25 November 91 Parsons, KS warm front.

A deep cyclonic system, centered over Hudson Bay, was dominating the northcentral region of the United States, north of Parsons, KS, at all levels of the atmosphere. The strong geostrophic flow around the low cyclonically advected cold air into the region. A trough developing over west Texas cyclonically advected milder air from the southwest United States northward, towards Parsons, KS. Over Parsons, the warm air advection first appeared around 0000 UTC 25 November as a "tongue" of warm advection at 2.4 km. With the passage of time, the warm air "tongue" moved northward, thickening. In addition, the warm advection increased in magnitude. The top of the warm advection tongue did not exceed 4 km until 2000 UTC. Above 4 km, the cold advection induced by the Hudson Bay low continued to dominate. The interaction between the warm advection tongue and the overlaying cold advection caused a layer of instability and cloudiness. Rising motion in both the warm and cold advection layers caused a pronounced lifting of the boundary between the layers after 2000 UTC.

Lower in the atmosphere, the northward moving warm advection tongue was being forced upward by the colder air near the surface. As the origin of the warm advection air was west-southwest of Parsons, it was not surprising that there was insufficient moisture in the warm air to cause precipitation stimulated by the overriding of warm air over the cold air. Moister air, possibly originating in the Gulf of Mexico, would be required for precipitation.

4.2 Comparison With Other Warm Front Observational Studies

This section compares the results of the Parsons, KS warm front study with two previous observational studies. Heymsfield (1979) used a dual-Doppler radar system, rawindsondes, and surface observations to study the structure of a precipitating, warm frontal zone near Chicago, IL. Hobbs and Locatelli (1987) used doppler radars, rawindsondes, aircraft and surface observations to study a precipitating, maritime warm front approaching the Washington coast.

4.2.1 Comparison with Chicago Warm Front (Heymsfield, 1979)

Heymsfield (1979) conducted a case study of the structure of a warm frontal region near Chicago, IL. The high resolution of the doppler radar data allows reflectivity and three-dimensional wind fields to be calculated on a grid with horizontal grid spacings of 1.5 km, and vertical grid spacing of 0.7 km. From these wind fields, high resolution time series of reflectivity, horizontal velocity, vertical velocity, divergence, relative vorticity, deformation and vertical shear were constructed. The resolution of these time series is significantly greater than obtainable using the CSU wind profiler.

The sloping surface of the warm frontal zone, characteristic of the Parsons, KS warm front, was clearly present in the Chicago, IL warm front, based on a zone of veering winds. The Chicago warm front had a distinct low level jet, with winds in excess of 30 ms^{-1}, coincident with the warm frontal zone. No evidence of a low level jet was evident from the Parsons warm front observations.

The Chicago warm front showed highly organized vertical circulations, on a horizontal scale of 50 km, present in a 2.5 km thick layer just above the warm frontal zone. The areas of upward motion were strongly correlated with precipitation bands. The Parsons warm front showed no organized vertical circulation above the warm frontal zone,

and much larger scale vertical motion within the warm advection region. There was far less moisture associated with the Parsons warm front, with dry air extending from the surface to a 1 km thick cloud layer at 3 km. No precipitation was associated with the Parsons warm front. In contrast, ahead of the Chicago warm front, nearly saturated air extended from the surface to heights in excess of 6 km. The overriding cold advection present in the Parsons warm front was not present in the Chicago warm front, where the wind continued to veer with height up to 6 km.

4.2.2 Comparison with Washington Warm Front (Hobbs and Locatelli, 1987)

Hobbs and Locatelli (1987) studied the structure of a warm frontal region as it approached the Washington coast. The frontal structure was deduced using two Doppler radars, rawindsondes, aircraft and surface observations. High resolution maps of reflectivity near the surface were constructed from the Doppler radars, as well as time-height cross sections of horizontal wind fields and reflectivity. Time-height temperature cross sections were constructed by interpolation of rawindsonde observations. The time-height cross section of wind velocity had resolution comparable to that obtained using the Parsons wind profiler.

Rather than the smoothly sloping warm front surface exhibited by the Chicago and Parsons wind profiler studies, the Washington warm frontal zone had a "staircase" profile, with some segments nearly horizontal, and other segments with steep slopes. These steps were thought to increase convergence across the frontal zone.

The overriding cold advection layer present in the Parsons warm front was not present in the Washington warm front. In the Washington warm front, above the warm advection layer, there was little vertical wind shear.

4.3 Conclusions

This study exploited the capabilities of a single wind profiler to examine the structure of a nonprecipitating warm front over the central United States. The characteristics of this particular set of wind profiler data were studied to determine satisfactory algorithms for generating a quality-controlled data set. Surface measurements, NWS rawindsonde soundings, and special rawindsonde soundings were used to supplement the wind profiler data to gain a better understanding of the structure of the warm front.

The wind profiler data used in this study consisted of time-averaged spectra, and spectral moments derived from the time-averaged spectra. Several techniques were used to produce a quality-controlled data set. The spectra and spectral moments during the 6-minute time intervals when RASS sound waves were being generated were removed from the data set. For all other wind profiler 6-minute time intervals, the application of "RASS parameters" required that the vertical beam spectral moments be rederived from the time-averaged spectra.

Wind vectors that differed significantly from their spatial and temporal neighbors were removed from the data set. Radial velocity variance moments that were too small were also removed from the data set.

The CSU wind profiler uses five beams, rather than the more common three beams. This allowed the uniformity of the wind field to be tested over the profiler site. For a site far from a mountain barrier, and a warm front synoptic event, an indication of nonhomogeneous winds is suspect. Therefore, nonuniform winds were removed from the data set.

Using the quality-controlled wind profiler data set, a low level, descending layer of veering winds over Parsons, KS was tracked in high temporal resolution. This layer of

veering winds, implying warm advection, defined the warm frontal zone. The warm frontal zone exhibited a relatively smooth surface, without the apparent height discontinuities observed by other researchers.

Above the layer of warm advection, the wind profiler observations indicated an abrupt transition to a layer of cold advection. The temperature gradient across this warm advection-cold advection boundary resulted in a layer of decreased stability. The air in this layer was conditionally unstable. Continued lifting of the air to saturation resulted in a cloud layer, capped by stable air within the cold advection zone.

The origin of the air within the warm and cold advection layers was studied. The warm advection originated west-southwest of Parsons, in a region of warmer, but dry air. The cold advection was from geostrophic flow around a strong cyclone far to the northeast of Parsons.

Frontogenesis was clearly observed over Kansas. The origin of this frontogenesis was thought to be horizontal deformation caused by the interaction of the warm advection west-southwest of Parsons with the geostrophic flow around the Hudson Bay cyclone.

4.4 Suggestions for Future Research

While many useful observations of the structure of a synoptic scale front can be made using a single wind profiler, other tools are available that could greatly increase the amount, and utility of information available.

The three-dimensional wind structure over a mesoscale horizontal region can be deduced from Doppler radar observations. In addition to the wind fields obtainable from a wind profiler, the Doppler radar would allow a researcher to determine kinematic quantities such as divergence, vorticity and deformation on a small spatial and temporal

scale. For a precipitating warm front, the Doppler radar has obvious advantages for studying the intensity of precipitation.

Alternatively, a triangular network of wind profilers would allow a researcher to determine the same kinematic quantities as obtainable with Doppler radar. However, the assumption of linearity between the largely-spaced wind profiler sites decreases the horizontal resolution, compared to Doppler radar.

The use of a lower frequency wind profiler (i.e. 50 Mhz) in conjunction with RASS would allow the study of the thermal structure of warm fronts into the middle troposphere with the same spatial and temporal resolution as the frontal wind fields.

The study of the structure of a precipitating warm front in conjunction with a lower frequency wind profiler and RASS would allow further research into the mechanisms causing embedded bands of intense precipitation within a larger scale region. Conditional symmetric instability (CSI) has been proposed as a mechanism for these bands (Bennett and Hoskins, 1979), but has not been studied with the resolution obtainable with wind profilers.

REFERENCES

Bennetts, D.A. and Hoskins, B.J., 1979: Conditional symmetric instability - a possible explanation for frontal rainbands, *Quart. J. Roy. Meteor. Soc.*, **105**, 945-962.

Bjerknes, J., 1918: On the structure of moving cyclones, *Geofys. Publikasjoner*, Norske Videnskaps - Akad. Oslo 3, **1**, 1-18.

Bjerknes, J. and Solberg, H., 1922: Life cycle of cyclones and the polar front theory of atmospheric circulation, *Geofys. Publikasjoner*, Norske Videnskaps - Akad. Oslo 3, **1**, 1-18.

Brewster, K.A., 1989: Profiler Training Manual #2, Quality Control of Wind Profiler Data, NOAA/ERL, Boulder, CO.

Brewster, K.A. and Schlatter, T.W., 1986: Automated quality control of profiler data, *11th Conf. on Weather Forecasting and Analysis*, Kansas City, Mo., June 17-20, AMS, Boston, Mass., 171-176.

Brewster, K.A. and Schlatter, T.W., 1988: Recent progress in automated quality control of wind profiler data, *8th Conf. on Numerical Weather Prediction*, Baltimore, Md., Feb. 22-26, AMS, Boston, Mass., 331-338.

Danielsen, E.F., 1961: Trajectories: isobaric, isentropic and actual, *J. Meteor.*, **18**, 479-486.

Forsythe, G.E., 1945: A generalization of the thermal wind equation to arbitrary horizontal flow. *Bull. Amer. Meteor. Soc.*, **26**, 371-375.

Harrold, T.W., 1973: Mechanisms influencing the distribution of precipitation within baroclinic disturbances, *Quart. J. Roy. Meteor. Soc.*, **99**, 232-251.

Herzegh, P.H. and Hobbs, P.V., 1980: The mesoscale and microscale structure and organization of clouds and precipitation in midlatitude cyclones. II: Warm frontal clouds, *J. Atmos. Sci.*, **37**, 597-611.

Hein, P.F., et al., 1991: Quality control of the CSU wind profiler data, Lower Tropospheric Profiling: Needs and Technologies, 131-132.

Hertzman, O., et al., 1988: The mesoscale and microscale structure and organization of clouds and precipitation in midlatitude cyclones. XVI: Three-dimensional airflow and vertical vorticity budget, *J. Atmos. Sci.*, **45**, 3650-3666.

Heymsfield, G.M., 1979: Doppler radar study of a warm frontal region, *J. Atmos. Sci.*, **36**, 2093-2107.

Hobbs, P.V. and Locatelli, J.D., 1987: The mesoscale and microscale structure and organization of clouds and precipitation in midlatitude cyclones. XIII: Structure of a warm front, *J. Atmos. Sci.*, **44**, 2290-2309.

Holton, J.R., 1979: An Introduction to Dynamic Meteorology, Academic Press.

Hoskins, B.J. and Bretherton, F.P., 1972: Atmospheric frontogenesis models: Mathematical formulation and solution, *J. Atmos. Sci.*, **29**, 11-37.

Hoskins, B.J. and Heckley, W.A., 1981: Cold and warm fronts in baroclinic waves, *Quart. J. Roy. Meteor. Soc.*, **107**, 79-90.

Hoskins, B.J. and Pedder, M.A., 1980: The diagnosis of middle latitude synoptic development, *Quart. J. Roy. Meteor. Soc.*, **106**, 707-719.

Hoskins, B.J. and West, N.V., 1979: Baroclinic waves and frontogenesis. Part II: Uniform potential vorticity jet flows - cold and warm fronts, *J. Atmos. Sci.*, **36**, 1663-1680.

Houze, R.A., et al., 1981: The mesoscale and microscale structure and organization of clouds and precipitation in midlatitude cyclones. III: Air motions and precipitation growth in a warm-frontal rainband, *J. Atmos. Sci.*, **38**, 639-649.

Kuo, Y.H., et al., 1987: Retrieving temperature and geopotential fields from a network of wind profiler observations, *Mon. Wea. Rev*, **115**, 3146-3165.

Larsen, M.F., and Rottger, J., 1983: Comparison of tropopause height and frontal boundary locations based on radar and radiosonde data, *Geo. Res. Letters*, **10**, 325-328.

Neiman, P.J. and Shapiro, M.A., 1989: Retrieving horizontal temperature gradients and advections from single-station wind profiler observations, *Wea. Forecasting*, **4**, 222-233.

Petterssen, S., 1956: Weather Analysis and Forecasting, McGraw-Hill, 201-203.

Rottger, J., 1979: VHF radar observations of a frontal passage, *J. Appl. Meteor.*, **18**, 85-91.

Rutledge, S.A. and Hobbs, P.V., 1983: The mesoscale and microscale structure and organization of clouds and precipitation in midlatitude cyclones. VIII: A model for the seeder-feeder process in warm-frontal rainbands, *J. Atmos. Sci.*, **40**, 1185-1206.

Shapiro, M.A., et al., 1984: Radar wind profiler observations of fronts an jet streams, *Mon. Wea. Rev*, **112**, 1263-1266.

Strauch, R.G., et al., 1987: The precision and relative accuracy of profiler wind measurements, *J. Atmos. Oceanic Technol.*, **4**, 563-571.

Tycho Technology, Inc., 1988: Wind Profiling, The History, Principles, and Applications of Clear-Air Doppler Radar, Tycho Technology, Inc.

Van de Kamp, D.W., 1988: Profiler Training Manual #1, Principles of Wind Profiler Operation, NOAA/ERL, Boulder, CO.

Weber. B.L., et al., 1992: Effects of small-scale vertical motion on radar measurements of wind and temperature profiles., *J. Atmos. Oceanic Technol.*, **9**, 193-209.

Wuertz, D.B., et al., 1988: Effects of precipitation on UHF wind profiler measurements. *J. Atmos. Oceanic Technol.*, **5**, 450-465.

Wuertz, D.B. and Weber, B.L., 1989: Editing Wind Profiler Measurements, NOAA Technical Report ERL 438-WPL 62, Boulder, Co.

Zamora, R.J., et al., 1987: The diagnosis of upper tropospheric divergence and ageostrophic wind using profiler wind observations, *Mon. Wea. Rev*, **115**, 871-884.

APPENDIX A

Isentropic Trajectory Calculations

Parsons, KS: θ = 285 K, z_2 = 1400 m, V_2 = 9 ms^{-1} @ 267°

	1800 UTC	1200 UTC
M_2	2883 x 10^2 m^2s^{-2}	2881 x 10^2 m^2s^{-2}

For θ = 285 K, extrapolating upstream for 3 hours along M = 2883 x 10^2 m^2s^{-2} at 9 ms^{-1}. Extrapolate 3 more hours along M = 2882 x 10^2 m^2s^{-2} to approximately 193 km WSW of Parsons. Nearest rawindsonde station is Oklahoma City.

Oklahoma City, OK: z_1 = 1200 m, V_1 = 9 ms^{-1}

	1800 UTC	1200 UTC
M_1	2882.6 x 10^2 m^2s^{-2}	2882 x 10^2 m^2s^{-2}

ΔM_2 = 2 x 10^2 m^2s^{-2}

ΔM_1 = 0.6 x 10^2 m^2s^{-2}

ΔM_{mid} = 1 x 10^2 m^2s^{-2}

$\therefore$ Equations (13) and (14) are satisfied.

Potential Vorticity:

Parsons, KS 1800 UTC: -1.4 x 10^{-7} $s^{-1}m^{-1}$

Oklahoma City, OK 1200 UTC: -1.1 x 10^{-7} $s^{-1}m^{-1}$

$\therefore$ potential vorticity is approximately conserved.

Mixing Ratio:

Parsons, KS 1800 UTC: 2.4 g/kg

Oklahoma City, OK 1200 UTC: 2.2 g/kg

$\therefore$ mixing ratio is approximately conserved.

Parsons, KS: θ = 300 K, z_2 = 4500 m, V_2 = 22 ms^{-1} @ 301°

	1800 UTC	1200 UTC
M_2	3019 x 10^2 m^2s^{-2}	3017 x 10^2 m^2s^{-2}

For θ = 300 K, extrapolating upstream for 3 hours along M = 3019 x 10^2 m^2s^{-2} at 22 ms^{-1}. Extrapolate 3 more hours along M = 3017 x 10^2 m^2s^{-2} to approximately 402 km WNW of Parsons. Nearest rawindsonde station is North Platte, NE.

North Platte, NE: z_1 = 4300 m, V_1 = 25 ms^{-1}

	1800 UTC	1200 UTC
M_1	3019 x 10^2 m^2s^{-2}	3017 x 10^2 m^2s^{-2}

ΔM_2 = 2 x 10^2 m^2s^{-2}

ΔM_1 = 2 x 10^2 m^2s^{-2}

ΔM_{mid} = 2 x 10^2 m^2s^{-2}

To satisfy equation (13), M_1 at 1200 UTC needs to be 3016 x 10^2 m^2s^{-2}. Therefore, actual trajectory is slightly north of the 3017 x 10^2 m^2s^{-2} streamline.

Potential Vorticity:

Parsons, KS 1800 UTC: -3.2 x 10^{-7} $s^{-1}m^{-1}$

North Platte, NE 1200 UTC: $-3.3 \times 10^{-7}\ s^{-1}m^{-1}$

$\therefore$ potential vorticity is approximately conserved.

Mixing Ratio:

Parsons, KS 1800 UTC: 0.8 g/kg

North Platte, NE 1200 UTC: 0.8 g/kg

$\therefore$ mixing ratio is approximately conserved.